2019

Drive-By Bridge Monitoring And Damage Detection

Chengjun Tan
University of Alabama at Birmingham

DRIVE-BY BRIDGE MONITORING AND DAMAGE DETECTION

by

CHENGJUN TAN

NASIM UDDIN, CHAIR
CHRISTOPHER WALDRON
MOHAMMAD HAIDER
IAN HOSCH
ASHRAF Z. AL-HAMDAN

A DISSERTATION

Submitted to the graduate faculty of The University of Alabama at Birmingham,
in partial fulfillment of the requirements for the degree of
Doctor of Philosophy

BIRMINGHAM, ALABAMA

2019

DRIVE-BY BRIDGE MONITORING AND DAMAGE DETECTION

CHENGJUN TAN

CIVIL CONSTRUCTION AND ENVIROMENT ENGINEERING

ABSTRACT

Bridges are key components of the transportation network, and their safety is essential to maintain effective and safe operation of the transportation facilities. To maintain the structural integrity of the bridges, it is essential to estimate the extent and location of the structural damage through periodic monitoring. Therefore, there is considerable interest in bridge damage detection and considerable progress has been made in recent years. The traditional bridge health monitoring requires many sensors installed on the bridge to collect vibration data for damage assessment, which is expensive, time-consuming, and even dangerous in-site. Compared with traditional ways, the concept of indirect measurement has received increasing attention. One can extract bridge dynamic properties from the responses of a passing vehicle, which is known as 'drive-by' inspection. This indirect measurement way shows many advantages of effectiveness, economic, and safety, etc. However, in most cases, the bridge dynamic properties information contained by measured vehicle responses is too faint to be extracted, or contaminated by noises.

To solve it, this dissertation develops algorithms to improve the performance in 'drive-by' inspection, based on robust signal processing tools such as wavelet transform and Hilbert transform. Because of its sensitivity to signal discontinuity, wavelet analysis has been frequently used to detect structural damage. Hilbert transform associated with

band-pass filter can extract information of bridge damping or mode shapes from a passing vehicle acceleration.

With the rapid development of technology, the performance of unmanned aerial vehicles (UAVs) has been exceedingly improved including its battery life and wireless communication. It gains wide application for many fields including bridge health monitoring. UAVs allow remote imaging which can be used for bridges visual inspection, especially for where a man cannot reach. In addition, UAVs have many other functions of wireless charging sensor installed on the bridges, data transmission with sensors (on the bridges) and cloud, and working as fly-sensor. This dissertation takes the advantages of 'drive-by', UAVs techniques and others to present a 'fly-by' bridge monitoring system, which is designed to monitor the bridge's health, controls the loads imposed on bridges by heavy trucks, and provides visual inspectors with quantitative information.

Keywords: damage detection, drive-by, bridge health monitoring, deep learning, unmanned aerial vehicle (UAV), signal processing

TABLE OF CONTENTS

Page

LIST OF TABLES

Tables *Page*

"DRIVE-BY'' BRIDGE FREQUENCY BASED MONITORING UTILIZING WAVELET TRANSFORM

HILBERT TRANSFORM BASED APPROACH TO IMPROVE EXTRACTION OF "DRIVE-BY" BRIDGE FREQUENCY

EXTRACTION OF BRIDGE MODAL PARAMETERS USING PASSING VEHICLE RESPONSE

STRUCTURAL HEALTH MONITORING OF BRIDGES – THE CONFLICTING CHALLENGES OF DETECTING GLOBAL AND LOCAL DAMAGE

WAVELET-ENTROPY APPROACH FOR DETECTION OF BRIDGE DAMAGES USING DIRECT AND INDIRECT BRIDGE RECORDS

LIST OF FIGURES

Figure *Page*

INTRODUCTION

"DRIVE-BY'' BRIDGE FREQUENCY BASED MONITORING UTILIZING WAVELET TRANSFORM

HILBERT TRANSFORM BASED APPROACH TO IMPROVE EXTRACTION OF "DRIVE-BY" BRIDGE FREQUENCY

EXTRACTION OF BRIDGE MODAL PARAMETERS USING PASSING VEHICLE RESPONSE

STRUCTURAL HEALTH MONITORING OF BRIDGES – THE CONFLICTING CHALLENGES OF DETECTING GLOBAL AND LOCAL DAMAGE

WAVELET-ENTROPY APPROACH FOR DETECTION OF BRIDGE DAMAGES USING DIRECT AND INDIRECT BRIDGE RECORDS

DEVELOPING A REAL-TIME CRACK DETECTOR USING MASK R-CNN TECHNIQUE

LIST OF ABBREVIATIONS

SHM	structural health monitoring
UAV	unmanned aerial vehicle
HT	Hilbert transform
WT	wavelet transform
CWT	continuous wavelet transform
DWT	discrete wavelet transform
WET	Wavelet Entropy Theory
FT	Fourier transform
FFT	fast Fourier transform
VBI	vehicle-bridge interaction
FE	finite element
MOSS	mode shape squares
MAC	modal assurance criterion
DI	damage index
BWIM	bridge weigh in motion
CNN	convolution neural network
R-CNN	region with convolution neural network

INTRODUCTION

Problem Statement

Bridges are an integrated part of the transportation network and represents the most expensive elements of this network. The cost of repairing faults in a large structure once the fault starts to approach criticality, is enormous. If damage is prevented at an early stage, maintenance works will be carried out in a planned way and before the bridge can become damaged beyond repair (Uddin et al. 2004, 2006). However, without monitoring, there is no easy way to predict how infrastructure will deteriorate over time.

Traditionally, visual inspection is regarded as one of the most common methods to inspect bridges, however, it only provides a qualitative measure of the bridge health index (Malekjafarian, McGetrick, and Obrien 2015). In addition, the human factor reduces the credibility of the method, where a number of bridges collapsed catastrophically, whereas, however, they had been visually inspected just before the disaster. Infrastructure needs to be more 'smarter', i.e., to incorporate more sensors and algorithms that will monitor its condition and communicate this information to the infrastructure manager.

The last decades, Structural Health Monitoring (SHM) technologies, which rely on automatic detection of anomalous structural behavior, have evolved dramatically. There are four distinguish levels of SHM (Carden 2004, Rytter 1993) 1) Identify whether the damage exists, 2) Locate the damage, 3) Determine the damage level and 4) calculate the remaining service life of the structure. Conventional SHM methods require a large number of sensors on the structure, which is called as direct approach of SHM. This approach is

expensive, time-consuming, and even dangerous, limiting the expansion of the approach to a large number of bridges (Malekjafarian, McGetrick, and Obrien 2015).

Recently, the idea of an indirect approach, or what has been known as “drive-by” bridge inspection, are based on extracting the dynamic properties of the bridge structures from the dynamic response of a passing vehicle over the bridge, which is first proposed by (Yang and Chang 2009, Yang, Lin, and Yau 2004). To some extents, it has demonstrated that “drive-by” bridge inspection system gives a better screening for the bridge degrees of freedom than the direct measurements from an installed sensors on the bridge structure. Compared with the direct methods, the indirect methods show many advantages in term of equipment need, specialist personnel on-site, economy, simplicity, efficiency, and mobility (Malekjafarian, McGetrick, and Obrien 2015). However, there is no doubt that the indirect approach is more difficult to assess the bridge structural condition and detect the structure damage effectively and practically. Current research efforts on drive-by monitoring systems with an efficacy still remain to be demonstrated in the field.

In nowadays mature and commercial SHM system, as a consequence of continuous monitoring of structural health, the monitoring systems generate vast quantities of sensor measurements that must be processed to assess the current state of the structural health. Due to continuous monitoring, extremely large volume of data accumulates in a short period of time, e.g., a single sensor channel sampled at 200 Hz generates 34 MB of data in one day or 12.6 GB of data in one year. The sensor data processing problem is exacerbated by the fact that infrastructure owners already have a burden of large inventory of structures requiring SHM technologies let alone the data processing in a traditional way. Another challenge is the requirement of a continuous power supply on every bridge in the network.

While this is feasible for larger structures, it constitutes a prohibitive cost for the smaller bridges that make up more than 90% of the total stock. It also gets around with very expensive road closures with associated extra staffs, hiring of raised platforms and other equipment, costly installation of power supplies and mobile network towers in remote no-network-coverage bridge sites, etc. Moreover, the SHM systems are only telling half of the story. A road bridge is only safe if the stresses caused by the passing traffic are less than the capacity of the bridge. The solution to the bridge safety problem is, therefore, two-fold: control of overloaded trucks, and safety assessment/monitoring of bridges and their loads.

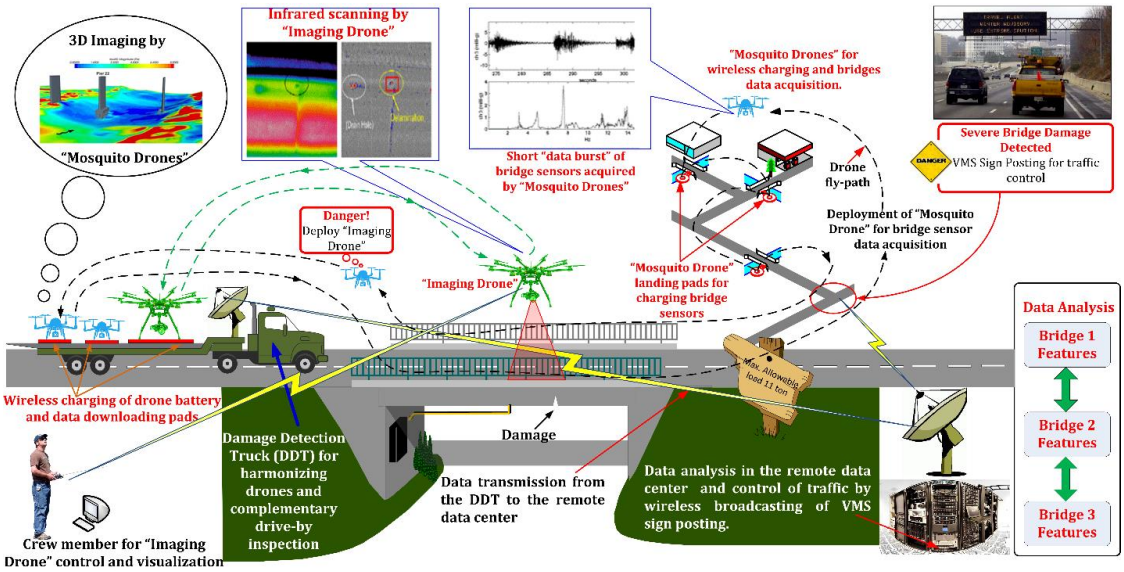

Figure 1. Fly-by bridge monitoring system concept

Proposed Solution

This dissertation will introduce a newly innovative cyber-physical system called "Mobile Automated Rovers Fly-by" to monitor the health of highway bridges, control the

loads imposed on bridges by heavy trucks, and provide visual inspectors with quantitative information for data-driven bridge health assessments.

The “fly-by” bridge monitoring system can be considered as combining “drive-by” bridge monitoring system and traditional bridge SHM system. In compassion to two previous system, the main difference is that the “fly-by” bridge monitoring system utilizes small unmanned aerial vehicle (drones) to collect all of numerical data from sensors installed on bridge structure or inspection vehicle, which is the core of that. As a result, the infrastructure manager can dominate inspection time to automatically monitor bridge serving condition and save a ton of electric power. In addition, bridge weigh in motion (BWIM) system will be embedded into “fly-by” bridge monitoring system that can be better manage traffic flow of highway road network and control load of heavy trucks.

As shown in Figure 1, a damage detection “drive-by” vehicle will be equipped with a swarm of small drones, a large size drone, drone charging and communication pads, vehicle mounted sensors (e.g. accelerometers) and on-board computers, wireless antenna, etc. for continuous bridge network monitoring, inspection, assessment, and control of traffic flow, and to avert potential threats of impending failures of transportation network, and catastrophes of the nation’s trade and commerce.

Specifically, intelligent collaborative teams (herein simply referred to as swarms of “Mosquito Drones”) of small-drones equipped with lightweight navigation, imaging, and other sensors can be harmonized on one platform, and utilized effectively to collect sensor data and 3D image on the fly, and inform about the health of essential transportation components within the highway bridge network. Next, the inspection by swarms of “Mosquito Drones” will be followed by a large size drone called “Imaging Drone”, which

can be perched and deployed upon identification of a threshold (user defined trigger of movement for example) by the "Mosquito Drones", along with crews to offer unprecedented promise to support detail investigation based on systems' requirements. Furthermore, infrared (IR) cameras will be incorporated in larger "imaging drones" for inspection and detection of delamination of concrete bridges even before it becomes visible to the human eye.

Wireless charging is one of the main challenges in "fly-by" bridge monitoring system. To overcome the long time working, drones employed in this system obtain power from the inspection vehicle or nearby national grid lines using wireless charging technique. Meanwhile drones need to charge and wake up sensors installed on bridge using wireless charging technique. Another main challenges is that the collected numerical data used to analysis is low quality "data bursts" because of the operational roadway speeds leading to short time of vehicle and bridge interaction and the use of limited number of sensor channels.

There are numbers of data resources and corresponding algorithms of damage detection in "fly-by" bridge monitoring system. Detected algorithms based on short data burst from sensors installed on bridges are main approaches. "Drive-by" and BWIM are alternative/complementary approaches to "fly-by" monitoring but shares the advantage of requiring no mains electrical power source on the bridge. On the other hand, the image processing techniques can give more accurate information of detailed damage quantification.

Figure 2. Drone attached to wall or celling

Nowadays, the performance of unmanned aerial vehicles (UAVs) has been exceedingly improved including its battery life and wireless communication. These techniques further promote the feasibility and effectiveness of the “fly-by” bridge monitoring system. In addition, UAVs can attach to walls and ceiling as Figure 2. The build-in sensor with wireless communication makes a drone as a fly-sensor. It can collect some data from the bridges where a man can’t reach or there are no pre-installed sensors.

Furthermore, image processing gains a breakthrough revolution driven by the convolutional neural network (CNN). The image classification and object detection (from images or videos) have been improved exceedingly with computer visual. The development of other hardware facilities leads to achieving a high level of effectiveness and accuracy in object detection from images or videos. These application technologies are able to promote the “fly-by” bridge monitoring system developing an automatic and real-time defect detector, based on the remoting images of UAVs. For instance, a special trained model can automatically detect bridge surface cracks, corrosion and connections defect.

However, this special trained model requires a large number of database to learn the object characteristics.

This dissertation proposes some algorithms to improve extracting bridge dynamic properties and detecting bridge damage. These algorithms are suitable for either direct measurement or indirect measurement, represented by sensors installed on the bridges (or fly-sensors) and "drive-by" inspection respectively. These algorithms are verified by theoretical analysis and numerical simulation. Some of them are further verified by lab experiments. In addition, this dissertation develops an effective and fast automatic crack detector based on Mask R-CNN, which can suppress noises efficiently by learning inherent feature of cracks from a 'very deep' CNN. Comparing to only CNN based method working on small batch of images, it can detect the crack of images in a global view providing a bound box for the crack exist and location. Moreover, This Mask R-CNN based crack detector outputs mask for predicted cracks simultaneously displaying the shape of cracks.

Reference

Carden, E. P. 2004. "Vibration Based Condition Monitoring: A Review." *Structural Health Monitoring* 3 (4):355-377. doi: 10.1177/1475921704047500.

Malekjafarian, Abdollah, Patrick J. McGetrick, and Eugene J. Obrien. 2015. "A Review of Indirect Bridge Monitoring Using Passing Vehicles." *Shock and Vibration* 2015:1-16. doi: 10.1155/2015/286139.

Rytter, Anders. 1993. "Vibrational based inspection of civil engineering structures."

Yang, Y. B., and K. C. Chang. 2009. "Extraction of bridge frequencies from the dynamic

response of a passing vehicle enhanced by the EMD technique." *Journal of Sound and Vibration* 322 (4-5):718-739. doi: 10.1016/j.jsv.2008.11.028.

Yang, Y. B., C. W. Lin, and J. D. Yau. 2004. "Extracting bridge frequencies from the dynamic response of a passing vehicle." *Journal of Sound and Vibration* 272 (3-5):471-493. doi: 10.1016/s0022-460x(03)00378-x.

"DRIVE-BY'' BRIDGE FREQUENCY BASED MONITORING UTILIZING WAVELET TRANSFORM

by

CHENGJUN TAN
AHMED ELHATTAB
NASIM UDDIN

Journal of Civil Structural Health Monitoring, Volume 7, Issue 5, pp.615-625.

Format adapted [and errata corrected] for dissertation

“DRIVE-BY’’ BRIDGE FREQUENCY BASED MONITORING UTILIZING WAVELET TRANSFORM

Abstract

In recent years, the concept of bridge monitoring using indirect measurements from a passing vehicle has been rapidly developed. This concept is known as “Drive-by Bridge inspection”. Most of the methods proposed under this approach utilize the dynamic characteristics of the bridge as an indicator of damage, such as the natural frequency of the bridge. The natural frequency is often estimated using Fast Fourier Transform (FFT). However, FFT has a low frequency resolution at the condition of higher velocity of passing vehicle, therefore it is not appropriate to be used to monitor the frequency change caused by the degradation of the bridge structural integrity. This paper introduces a new frequency identification techniques based on wavelet analysis. Wavelet transform is characterized by its high-frequency resolution and can, therefore, be used to visualize the bridge damage represented as changing the fundamental frequency of the bridge. The paper will implement this approach using an implicit Vehicle-Bridge Interaction (VBI) algorithm to simulate the passage of the instrumented vehicle over the bridge. The acceleration signals are then processed using wavelet analysis to extract the bridge frequency. In addition, the study will investigate the use of a subtracted signal from a two consecutive axles. The later point has the advantage of substantially removing the effect of the road roughness from the recorded accleration history.

Keyword: wavelet transform, wavelet pseudo-frequency, bridge damage detection, drive-by bridge inspection, structural health monitoring

1. Introduction

The structural integrity of bridges, as the main component of transport infrastructure, is an integral part of the safety of transport facilities. However, bridges are subject to continuous degradation due to environmental impacts and an excessive increase in the weight of traffic over time. Therefore, bridge structures require continuous monitoring to ensure maintenance and hence their structural integrity. Traditionally, visual inspection is regarded as one of the most common methods to inspect bridges, however, it only provides a qualitative measure of the bridge health index [1]. In addition, the human factor reduces the credibility of the method, where a number of bridges collapsed catastrophically, whereas, however, they had been visually inspected just before the disaster. Thus, Chupanit and Phromsorn [2] have suggested that visual inspection alone may not be sufficient to monitor the structural health of the bridges. Recently, Structural Health Monitoring (SHM) technologies, which rely on automatic detection of anomalous structural behavior, have evolved dramatically. There are four distinguish levels of SHM [3, 4]: 1) Identify whether the damage exists, 2) Locate the damage, 3) Determine the damage level and 4) calculate the remaining service life of the structure. Conventional SHM methods require a large number of sensors on the structure [4]. This approach is expensive, time-consuming, and even dangerous, limiting the expansion of the approach to a large number of bridges [1]. From another perspective, short and medium span bridges

represent a large portion of the bridge inventory of the road network, and conventional bridge health monitoring could not be used for the aforementioned drawbacks. From another perspective, a large number of medium to short bridges operate for several years, requiring an assessment of their current structural health condition, while this cannot be achieved using traditional monitoring techniques due to the aforementioned obstacles [1]. Thus, there is a necessity to find a less expensive SHM method that could be applied to a broad number of bridges.

The idea of an indirect approach, or what has been known as ‘drive-by bridge inspection’, are based on extracting the dynamic properties of the bridge structures from the dynamic response of a passing vehicle over the bridge, which is first proposed by Yang et. al [5, 6]. The authors adopted a fast Fourier transforms (FFT) to find the bridge frequency from dynamic response of passing vehicle. It is shown that the vehicle response is dominated by four specific frequencies: the vehicle frequency, driving frequency of the moving vehicle and two shifted frequencies of the bridge. The feasibility of such indirect method in practice has been experimentally verified by Yang and Chang [7] and Lin and Yang [8] via passing an instrumented vehicle over a bridge. Yang, Li and Chang [9] constructed bridge modal shapes successfully from a passing vehicle by employing Hilbert Transform combined with band-filter technical, and pointed out that the indirect measurements from the inspection vehicle, give a better screening for the bridge degrees of freedom than the direct measurements from an installed sensor on the bridge structure.

Yang and Chang [7] decomposed acceleration history of a passing instrumented vehicle with the empirical mode decomposition (EMD) to generate the intrinsic mode functions (IMFs). Then generated IMFs were adopted by FFT to successfully extract bridge

natural frequencies of higher modes, instead of the original recorded response. Lin and Yang [8] used a two-wheel cart towed by a light truck to extract the fundamental frequency of the bridge. In this truck-cart system, truck acts as an exciter for the bridge, while accelerometers are installed in the cart making it function as a receiver for bridge responses. It has been proven that the bridge frequencies can be successfully deduced from the acceleration histories of the cart utilizing FFT.

Since the concept of the drive-by bridge inspection emerged, many studies have been conducted to investigate the limits of the approach [7, 8, 10-15]. Yang, Lin and Yau [5] showed that higher speeds provide higher visibility of the bridge frequency in the vehicle's acceleration spectrum. This study has been carried out assuming a smooth road profile. By contrast, recent research has revealed that when road roughness is taken into account, vehicle responses dominate the acceleration spectrum, and the bridge frequency cannot be extracted in this case [16]. Therefore, Lin and Yang [8], Fujino, Kitagawa, Furukawa and Ishii [17] pointed out that lower vehicle speeds provides the best accuracy for estimating the bridge frequency, due to higher spectral resolution and the smaller impact of the road surface profile on the vehicle responses.

Wavelet transform is a robust signal-processing tool, characterized by its sensitivity to the discontinuities in the signal. Therefore, it has the ability to localize bridge damage. Khorram, Bakhtiari-Nejad and Rezaeian [18] employed a wavelet based damge detection approach to estimate the location of damage in a numerical simulation beam subjected to a moving force. They use a moving sensor that calculates the displacement under the passing load. Using the sensor readings they computed the Continuous Wavelet Transform (CWT). The results revealed that highest magnitude of a CWT coefficient occurred at the

exact location of the crack. The value of the highest magnitude of the CWT is directly correlated to the extent of the damage, and hence it can be considered an indicator of damage. Moreover, the study found that the moving sensor is superior to the fixed sensor, in terms of localization of damage. In another application of wavelet transformations in the localization of damage, Poudel, Fu and Ye [19] and Shahsavari, Bastien, Chouinard and Clément [20] have theoretically localized structural damage in the bridge by employing the wavelet transform with mode shape difference function.

Nguyen and Tran [21] introduced multi-cracks detection in the bridge structure based on wavelet transform, using theoretical VBI model. A moving vehicle will observe small distortions in the vibration responses at the crack locations. The authors used the wavelet transform to effectively find these small distortions so as to identify the crack location. McGetrick and Kim [22] employed the wavelet transforms to identify and localize the bridge damage, by harnessing a passing vehicle responses. The approach has been explored using theoretical VBI model and utilizing scaled laboratory test. The effect of bridge span length, vehicle mass, vehicle velocity, damage size or level to road surface roughness on the accuracy of results were investigated.

In this study, wavelet transform is applied to vehicle responses to detect the drop in the bridge natural frequency due to structural damage. The drop of the natural frequency will be used as an index to reflect the extent of the bridge damage. The study will be carried out using an implicit VBI algorithm to simulate the passage of the instrumented vehicle over the bridge. The vehicle acceleration are recorded and analyzed to quantify the drop in the bridge frequency due to damage, if exist. In addition, the study will investigate the use of a subtracted signal from a two consecutive axles to extract the bridge frequency in order

to substantially remove the effect of the road roughness from the recorded accleration history.

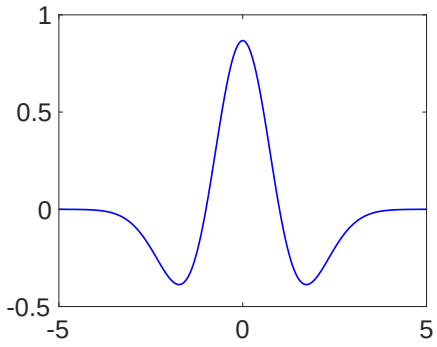

Fig. 1 Mexican hat wavelet functions

2. Wavelet Theory

In 1982, Jean Morlet coined the idea of the wavelet transform [23]. Mathematically, the idea behind wavelet analysis is to express or to approximate a signal or function by a family of functions constructed from dilatations and translations of a single function called the base wavelet [24, 25]. Hence, wavelet transform is similar to the Fourier transform (FT) that uses a series of cosine functions to approximate the objective signal. When applying FT to a signal, it defines the different frequencies contained by the signal with no clue about the time domain properties of the signal. In other words, FT only works as a signal-converting tool from time domain to frequency domain. On the other hand, wavelet method transforms the signal into time-frequency domain. This means that, performing wavelet transforms, a signal is shown in the frequency domain while retaining the time domain

characteristics of the signal. Thus, the approach has a strong potential to identify localized change in bridge properties from a short data recorded from a passing vehicle.

2.1 Continuous Wavelet Transform

The continuous wavelet transform is defined as follows:

$$WT(a,b) = \int_{-\infty}^{+\infty} f(t) \frac{1}{\sqrt{a}} \Psi\left(\frac{t-a}{a}\right) dt \;\; a\epsilon R^{+}, b\epsilon R \qquad (1)$$

Where *WT(a,b)* is the complex wavelet coefficients or wavelet transform; a and b are real scale and translation-parameters. $\Psi_{a,b}(t)$ denotes the conjugate of the complex mother wavelet function which satisfies the properties of $\int_{-\infty}^{+\infty} \Psi(t)dt = 0$and $\int_{-\infty}^{+\infty} |\Psi(t)dt| < \infty$. For example, Mexican hat ('Mexh') wavelet as shown in Fig. 1 is one of the most popular mother wavelet functions and its mathematical expression is:

$$\Psi(t) = (1-t^2)e^{\frac{-t^2}{2}} \qquad (2)$$

When continuous wavelet transform is applied to the objective signal, it returns a series of wavelet coefficient at each scale in the time domain. The scales are correlated to the signal frequencies. A high value for the scale implies having a stretched wavelet, and hence a low-frequency content. In contrast, a low value for the scale implies having a high-frequency content. The mathematical relationship between scale and frequency is defined as follows:

$$F_S = \frac{F_C}{a\Delta} \qquad (3)$$

Where F_S is a pseudo-frequency that correspond to scale a in Hz, F_C is the central frequency of the wavelet in Hz (central frequency refers to the frequency of a periodic

signal that most closely resembles the wavelet), a is the scale of the wavelet, and Δ is the sampling period of the signal. For the Mexican hat wavelet, F_C=0.25 Hz.

2.2 Wavelet energy coefficient

The energy content of the signal is a unique measure for the signal. Similarly, the energy content of a signal can be calculated from its wavelet coefficients and its mathematical expression is:

$$E_{energy} = \sum_a \sum_b |WT(a,b)|^2 \quad (4)$$

Eq.4 indicates that the energy associated with each particular scaling parameter a is expressed as:

$$E_{energy} = \sum_b^N |WT(a,b)|^2 \quad (5)$$

Where N is the number of wavelet coefficients and $WT(a,b)$ represents the wavelet coefficients at scale a.

Table 1 Vehicle and bridge properties

Vehicle properties		Bridge properties	
m_s	14000 kg	Span	15m
k_s	200 kN/m	Density	4800kg/m^3
c_s	10 kN s/m	Width	4 m
m_a	1000 kg	Depth	0.8m
k_a	2750 kN/m	Modulus	2.75×10^{10} N/m^2

For the objective signal, if a major frequency component corresponding to a particular scale '*s*' exists, then its wavelet energy coefficients at that scale will have

relatively high magnitudes at the time when this major frequency component occurs [26]. As a result, the energy plot will point out to the dominating frequencies in the signal. This is why the wavelet analysis could be used to extract the bridge frequency from the dynamic response of a passing vehicle, where the frequency components at the bridge frequencies are expected to show a high energy magnitude in the scale plot.

3. Extracting Bridge Frequency from Numerical VBI Model

3.1 Vehicle Bridge Interaction (VBI) Modeling

This section describes the VBI model employed to simulate the response of the bridge structure under the moving vehicle. The road surface profile is not considered in this simulation. At first, the vehicle is modeled as a quarter-car model crossing a 20-m approach distance followed by a 15-m simply supported finite element (FE) bridge (Fig. 2). The quarter-car travels with constant speed. The vehicle masses are represented by a sprung mass, m_s, and un-sprung mass, m_a represents the vehicle axle mass and body mass respectively. The Degrees of Freedoms (DOFs) that correspond to the bouncing of the sprung and the axle masses are, u_s, and u_a, respectively. The properties of the quarter-car and the bridge are listed in Table 1 and based upon the work of Cebon [27] and Harris, OBrien and González [28]. The dynamic interaction between the vehicle and the bridge is implemented in MATLAB [29, 30]. Unless otherwise mentioned, the used scanning frequency is 1000 Hz. The first natural frequency of bridge, f_b is 3.86Hz. The vehicle frequencies are 0.58Hz and 8.65Hz respectively.

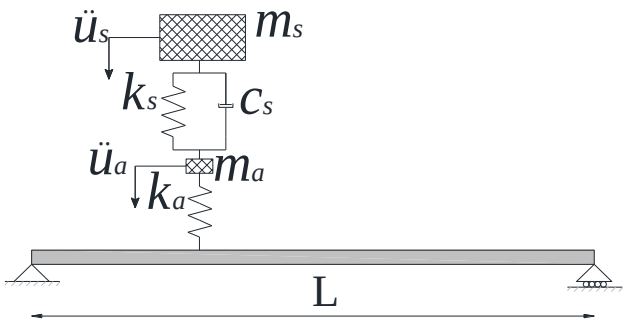

Fig. 2 The quarter car and bridge model

3.2 Identifying Bridge Frequency using the vehicle responses

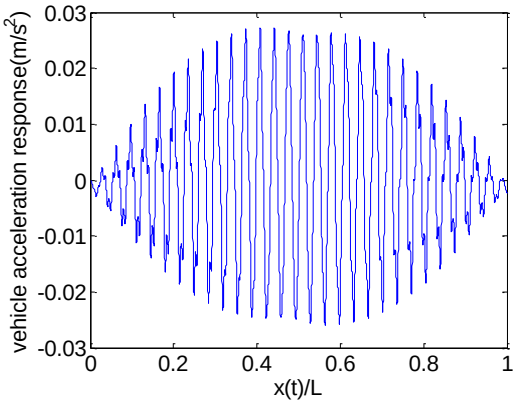

Fig. 3 The vehicle acceleration response

Fig. 3 illustrates the vehicle axle acceleration response for the VBI model mentioned above, where the vehicle velocity is 2m/s. The x-axis shows the normalized position of the vehicle axle on the bridge with respect to the bridge length (L) (0 and 1 when the axle is at the start and at the end of the bridge, respectively). Yang et. al [5, 6] have proved that the acceleration history of a crossing vehicle over a bridge contains the bridge frequency components, therefore the bridge frequency could be extracted after

applying FFT to the signal. Fig. 4 (b) illustrates the spectrum of the recorded acceleration showing a distinctive peak associated with the fundamental frequency of the bridge (3.87 Hz). In addition, the spectrum of Fig. 4 (a) shows the driving frequency extracted as 0.13Hz (the theoretical driving frequency=v/L=0.13Hz).

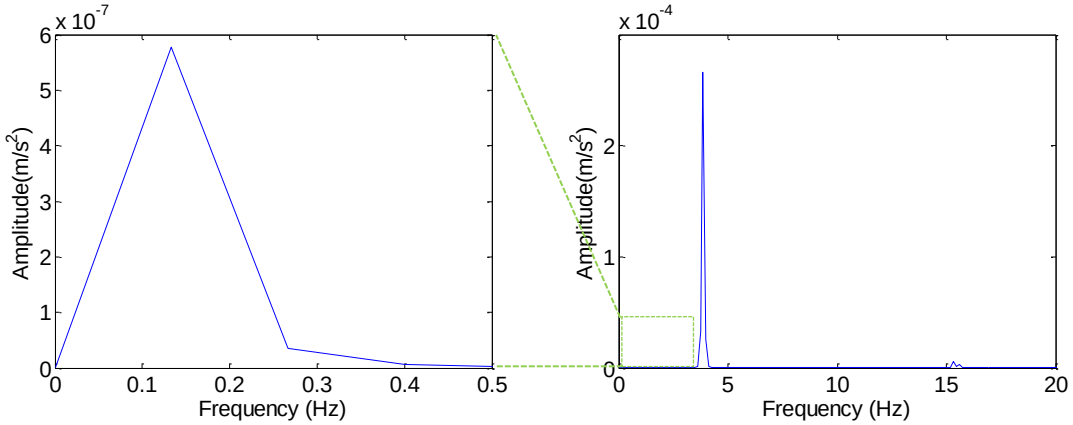

(a) (b)

Fig. 4 Acceleration spectrum of vehicle acceleration history, (a) frequency from 0 to 0.5Hz, (b) frequency from 0 to 20Hz

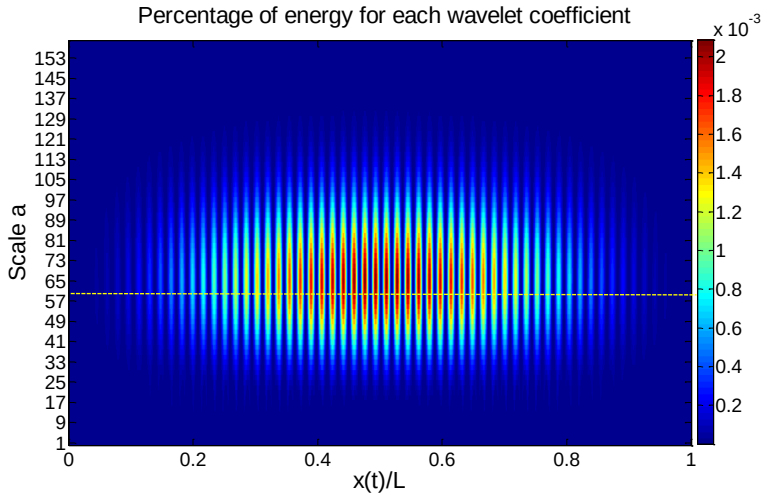

Fig. 5 Percentage of energy for each wavelet coefficient

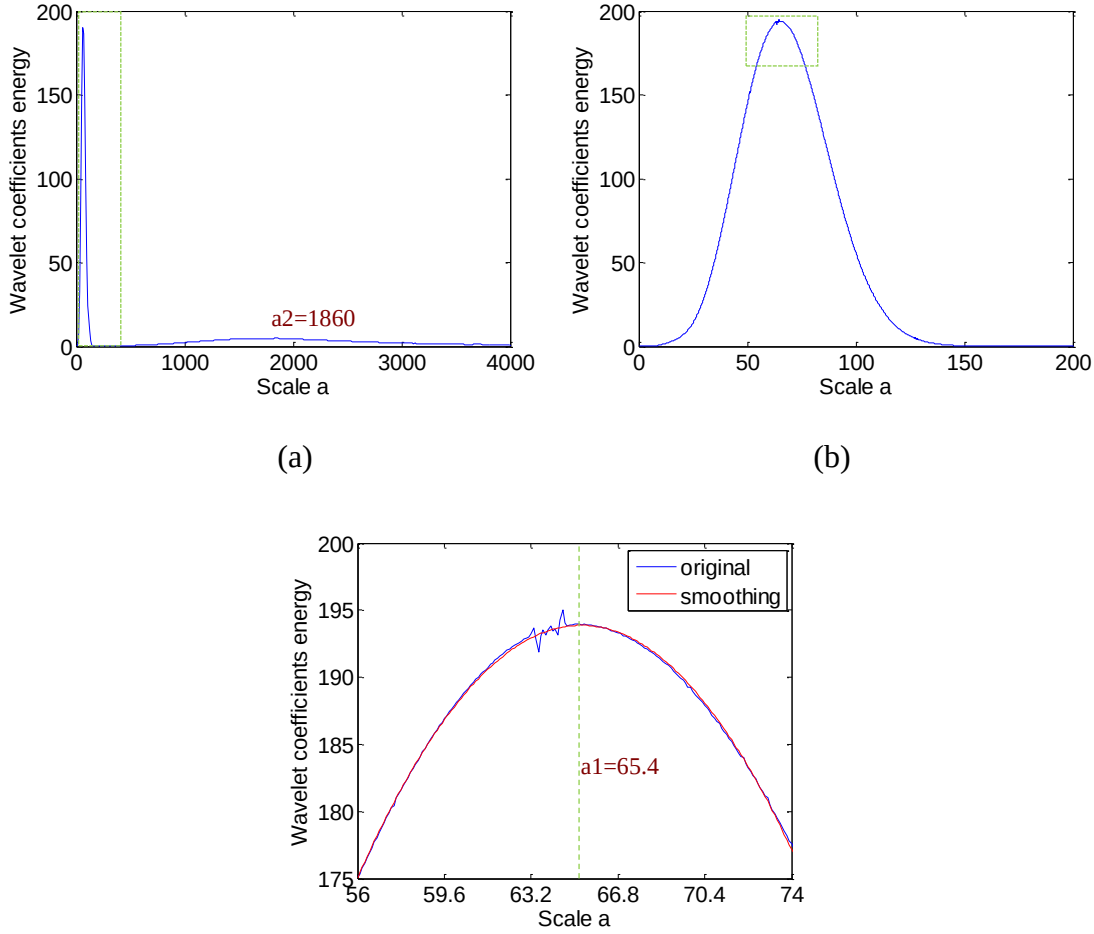

Fig. 6 Wavelet energy coefficient distribution, (a) scale from 1 to 4000; (b) scale from 1 to 200; (c) scale from 56 to 73

The 'Mexican hat' mother wavelet function is used to employ wavelet transform to the vehicle signal, then the 'scaleogram' is plotted as shown in Fig. 5. This 'scaleogram' is a visual representation displays the result from wavelet transforms, which is equivalent to the spectrogram for wavelets. There are three axes: two mutually perpendicular axes with relative distance in horizontal axis and wavelet coefficient *'a'* on the vertical axis, and

'*z'* represents the values of the relative energy '*E*', which is expressed in the plot using colors. Fig. 5, shows a local increase in the absolute value of the wavelet coefficients between *a* =30 and *a* =110, with a dominating peak at approximately *a* =65.

Table 2. Frequency identification at different velocity at span L=15m

Velocity (m/s)	Span (L=15m)	Frequency is calculated by wavelet transform (Hz)
	Theoretical frequency (Hz)	
2	3.86	3.82 (-0.97%)
4		3.84 (-0.51%)
6		3.86 (0.00%)
8		3.89 (0.88%)
10		3.91 (1.36%)

Note: () present the error between identified frequency and theoretical frequency

Equation 5 is used to compute the energy of every scale '*a*'. The wavelet energy coefficient distribution at each scale, varying from 1 to 4000 with 0.1 increments is shown in Fig. 6 (a). This figure shows a sharp and a gentle peak in wavelet coefficient. Fig. 6 (b) shows this sharp increase between *a* =30 and *a* =110 as previously noted in Fig. 5. The peak after smoothing is found at *a*=65.4 (Fig. 6 (c)). The pseudo-frequency corresponding to a=65.4 is calculated using Equation 3 and found to be 3.82 Hz, which is close to the bridge frequency (3.86 Hz). Similarly, the peak of the gentle increase is found at *a*=1860 corresponding to frequency of 0.13Hz, which is represented by the driving frequency.

There are a large number of commonly used mother wavelet functions. When applying different mother functions on the same objective signal, the results may changes.

In this paper, it has been found that not all of these base mother wavelet functions could be used to accurately identify the natural frequency of the bridge. Only can Mexican hat and 'bior2.2' etc. provide the highest accuracy in extracting the bridge frequency from the vehicle responses. In this study, the Mexican hat wavelet will be used in the analysis of the acceleration signal, unless otherwise mentioned.

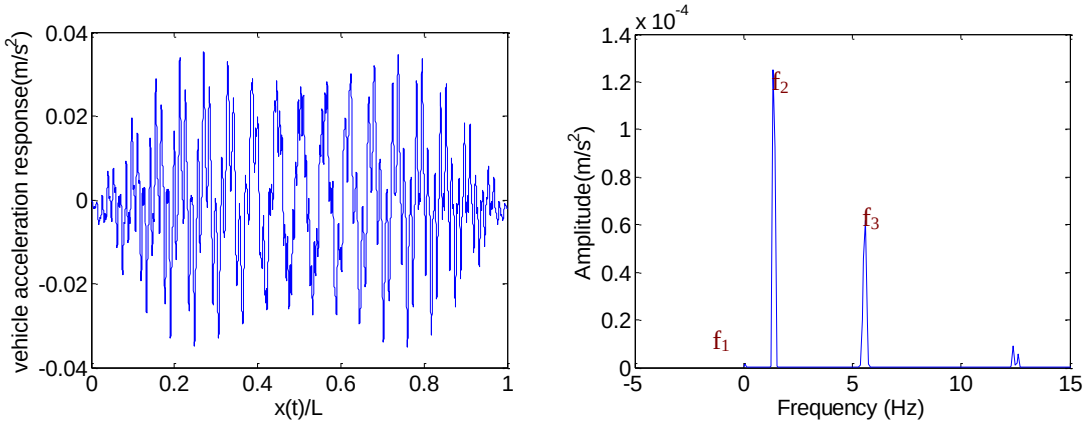

(a) (b)

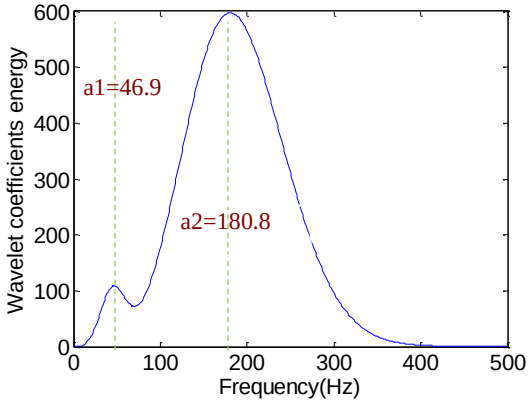

(c)

Fig. 7 Case study on span of 25m (a) the vehicle acceleration response at span=25m. (b) Acceleration spectrum. (c) Wavelet coefficient energy distribution at each scale.

Herein, the study will investigate the efficacy of the Wavelet Transform in extracting the bridge frequency for different speeds. In this part, different velocities (4m/s, 6m/s, 8m/s and 10m/s) are investigated. All other VBI model parameters are kept the same. Utilizing the techniques discussed above, the bridge frequency are extracted for every speed using Wavelet Transform. The results are listed in Table 2. The identified bridge frequency based on wavelet transforms corresponds to a particular scale that has the highest energy.

From Table 2, it is obvious that wavelet transform can give precise results (error less than 1.36%). The increase of vehicle velocity leads to the driving frequency increases. As a result, the peak of gentle increase indicating the driving frequency in wavelet energy coefficient distribution plot will shift to left. However, this shift movement has a slight influence on the peak of sharp increase indicating the bridge frequency in wavelet energy coefficient distribution. Study found that this sharp peak will shift to left slightly. Therefore, as it is shown in Table 2, the identified frequency of bridge increases with the increment of velocity.

The approach has been applied for a 25-m span bridge, all other problem parameters are kept the same. The first and second theoretical natural frequency of the bridge (L=25m) are 1.39 Hz and 5.56 Hz respectively. Fig. 7 shows the original crossing vehicle acceleration history at velocity 2m/s and the corresponding frequencies extracted using both wavelet-based approach and FFT approach.

Fig. 7 (b) demonstrates frequencies extracted using FFT where the spectrum is dominated by first three main frequencies. Based on the work of Yang, Lin and Yau [5], [13, 31], f_1 (=0.08 Hz) corresponds to the driving frequency of the vehicle, f_2 (=1.36 Hz)

presents the 1st natural frequency for the bridge, f_3 (=5.60 Hz) are the second fundamental bridge frequency.

Table 3. Frequency identification at different velocity at span L=25m

Velocity (m/s)	Span (L=25m) Theoretical frequency (Hz)	Frequencies are calculated by wavelet transform (Hz)	
		1st	2rd
2	1st =1.39 2rd =5.56	1.38(-0.52%)	5.33(-4.13%)
4		1.39(0.00%)	5.34(-3.92%)
6		1.41(1.10%)	5.35(-3.72%)
8		1.42(2.16%)	5.41(-2.68%)
10		1.43(2.95%)	5.45(-2.04%)

Note: () presents the error between identified frequency and theoretical frequency.

Similarly, Fig. 7 (c) shows extracted frequencies using the presented wavelet approach. It illustrates two peaks at scale a1 (=46.9) and a2 (=180.8) respectively, which refer to 5.33 Hz and 1.38 Hz. These frequencies shows a proper agreement with the bridge frequencies. The process has been repeated for different speeds, and the results are listed in Table 3.

4. Bridge Damage Identification Using Measurements from a Passing Vehicle

In this section, the change in the bridge frequency is used as a damage index to quantify the damage in the bridge. Damage is modeled using Sinha, Friswell and Edwards

[32] damage model, where the damage is assumed to be extended over a region of three times the beam depth. In this affected area, the element stiffness varies from the minimum values at the crack location to full stiffness at the end of the damaged area. The level of damage is defined as ratio of the depth of the crack to the depth of the intact bridge. For example, if the damage level is 0.6 (or 60%), it means that the crack depth is 0.48 meters for a 0.8-meter deep bridge.

The FFT method is due to the low frequency resolution associated with higher vehicle speeds. Therefore, and for the same reason, FFT cannot be used to monitor the bridge frequency drop due to structural damage. That the frequency step will not pick up the minor changes happened to the bridge frequency due to structural damage. Therefore, the next section will focus on using the Wavelet Transform to track the change in the bridge frequency due the existence of structural damage.

Fig. 8 shows the identified frequencies using wavelet analysis approach for different velocities. The damage located at the middle of the bridge. The bridge is modeled four times, one as an intact bridge, and other three cases of different damage levels (e.g. 20%, 40% and 60%). As it is shown, with the increment of damage level, the theoretical frequencies of bridge decrease ($f_{TI} > f_{TD1} > f_{TD2} > f_{TD3}$). At the same time, the identified frequencies of damaged bridge decrease as well ($f_{II} > f_{ID1} > f_{ID2} > f_{ID3}$). In this figure, the identified results and their theoretical ones matched very well (errors less than1.36%). It is worth to notice that the identified results at the different damage levels are parallel to that at with intact bridge. In other words, the driving frequency will have the same effect on intact bridge or damaged bridge. That means that the identified drop frequency of bridge

is very close to the theoretical one. These identified drop frequency indicates the damage exist and can be used to quantify the structural integrity of the bridge.

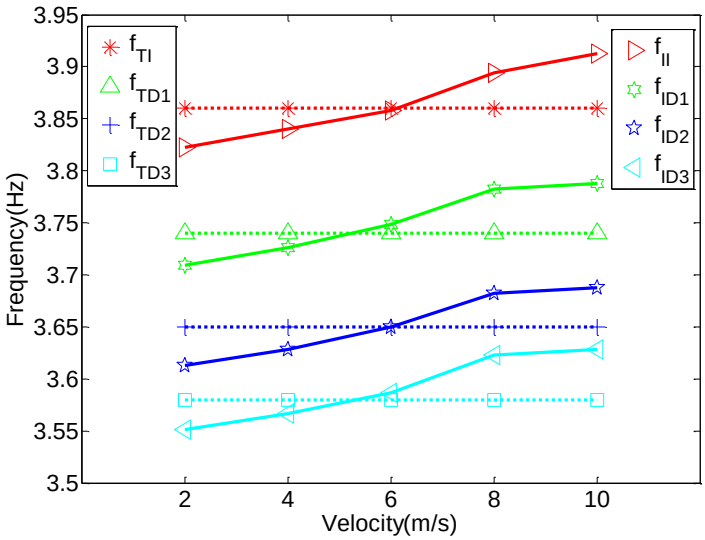

Fig. 8 Frequency identification of bridge at different velocities with wavelet analysis (Note: f_{TI} presents the 1st theoretical frequency of the intact bridge; f_{TD1} presents the 1st theoretical frequency of the damaged bridge at level 0.2; f_{TD2} presents the 1st theoretical frequency of the damaged bridge at level 0.4; f_{TD3} presents the 1st theoretical frequency of the damaged bridge at level 0.6; f_{II} presents the 1st identified frequency of the intact bridge; f_{ID1} presents the 1st identified frequency of the damaged bridge at level 0.2; f_{ID2} presents the 1st identified frequency of the damaged bridge at level 0.4; f_{ID3} presents the 1st identified frequency of the damaged bridge at level 0.6.)

The same process has been repeated for the 25-m bridge. The damage is set at 0.4L with damage level 0.2 and 0.5 respectively. The first two natural frequency of bridge is extracted for different vehicle speeds, and the results are illustrated in Fig. 9 and Fig. 10

respectively. As it is shown, the 1st frequency drop due to the structural damage is very slight (f_{TI}-f_{TD1}=0.02Hz; f_{TD1}-f_{TD2}=0.02Hz). Compared to the 1st frequency, the 2nd frequency showed to be more sensitive to bridge damage.

From the Fig. 9 and Fig. 10, it is obvious that the identified frequencies of the 2nd mode is worse than the 1st mode. The errors between identified result and theoretical one are less than 4.33% in Fig. 9, while errors in Fig. 10 are less than 7.73%. Similarly, the driving frequency will influence the identified results. However, as it is shown, it also shows the same effect on the intact and damaged bridge.

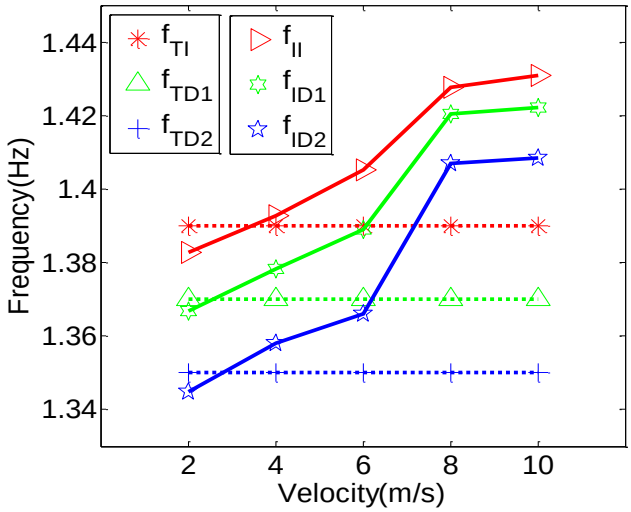

Fig. 9 1st natural frequency of bridge identification with wavelet analysis (Note: f_{TI} presents the 1st theoretical frequency of intact bridge; f_{TD1} presents the 1st theoretical frequency of damaged bridge at level 0.2; f_{TD2} presents the 1st theoretical frequency of damaged bridge at level 0.5; f_{II} presents the 1st identified frequency of intact bridge; f_{ID1} presents the 1st identified frequency of damaged bridge at level 0.2; f_{ID2} presents the 1st identified frequency of damaged bridge at level 0.5)

In summary, the identified frequency of bridge shows a drop in its magnitude due to structural damage. Even though there might be a great error between the extracted and the exact frequencies. Therefore, the proposed approach can be used to quantify the existence of damage 'Level I SHM' using indirect measurements from an inspection truck.

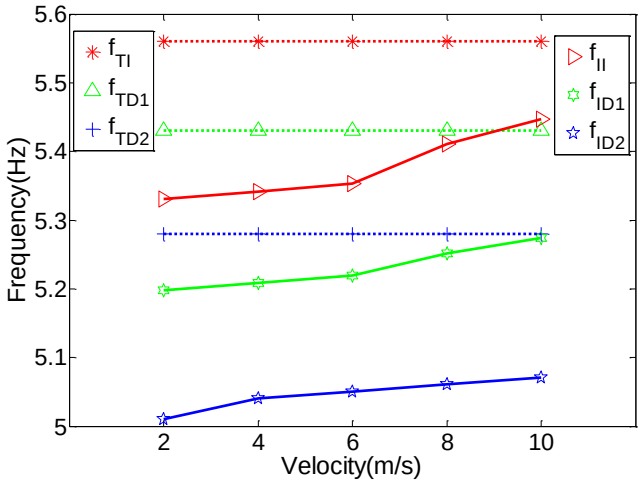

Fig. 10 2nd natural frequency of bridge identification with wavelet analysis (Note: f_{TI} presents the 2nd theoretical frequency of intact bridge; f_{TD1} presents the 2nd theoretical frequency of damaged bridge at level 0.2; f_{TD2} presents the 2nd theoretical frequency of damaged bridge at level 0.5; f_{II} presents the 2nd identified frequency of intact bridge; f_{ID1} presents the 2nd identified frequency of damaged bridge at level 0.2; f_{ID2} presents the 2nd identified frequency of damaged bridge at level 0.5)

5. Extracting Bridge Frequency Using a Half-Car Model

In this part, a theoretical half-car model is adopted to represent the behavior of the inspection vehicle as shown in Fig. 11. This model has four degrees of freedom correspond to the vehicle body bouncing , u_s, the body pitch rotation, θ, and two axle mass bouncing ,

u_{aR}, u_{aF}. The vehicle body mass is represented by the sprung mass, m_s and its moment of inertia is represented as, I_s. The vehicle body is connected to axles through a combination of linear springs have stiffness of k_R or k_F and viscous dampers with damping coefficient, C_R or C_F. The vehicle axles have m_{aR} and m_{aF} masses, the axle masses are connected to the ground with a springs have k_T stiffness. D1 and D2 represent the distance of each axle to the center of gravity of the vehicle. The vehicle properties are listed in Table 4. The first two vibration frequencies of the vehicle are 0.61Hz, 1.02Hz, 8.80Hz, and 8,84Hz.

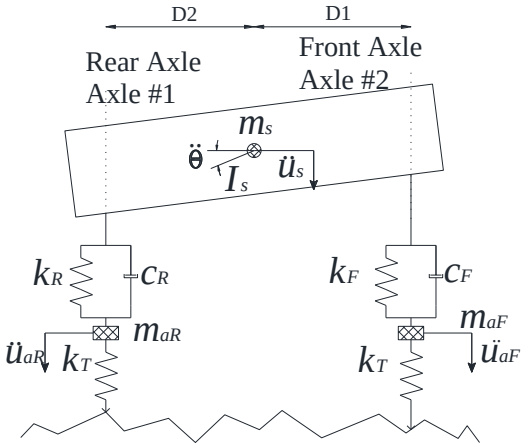

Fig. 11 Half-car model

In this part, the road has a roughness class ‘A’ defined using ISO-8608 [33]. Due to the presence of the road roughness in the problem, the profile excites the vehicle more than the bridge do and hence the vehicle frequencies domain the frequency spectrum. Neither wavelet nor FFT could obtain accuracy result for the bridge frequency. To reduce the road roughness effect, the concept of subtracting the axle acceleration signal is adopted [34]. Herein the acceleration of the rear axle is subtracted from the acceleration of the front axle after shifting the rear axle signal with an interval equal to the time spent by the rear

axle to reach the front axle position. Before processing the concept of subtracting, each collected axle acceleration response is added noisy signal. The subtracted signal is then processed using the wavelet approach presented in this paper. When the velocity is 2 m/s, the front and rear axle signals added with 90*db* noisy signal are presented in Fig. 12 while the subtracted signal is shown in Fig. 13 (a). The introduced wavelet procedure is applied to the subtracted signal, the wavelet energy coefficient is illustrated in Fig. 13 (b).

Table 4. Parameters of half vehicle model

Vehicle properties			
m_s	16600 kg	I_s	95765 kg m^2
k_R	400 kN/m	k_F	400 kN/m
c_R	8 kN s/m	c_F	8 kN s/m
m_{aR}	700 kg	m_{aF}	700 kg
k_T	1750 kN/m	k_F	1750 kN/m
D2	1.05m	D1	1.95m

Similar to the quarter-car model, a clear sharp peak is observed at scale of a1 = 65.5 and the corresponding frequency is 3.82 Hz. Another gentle peak is observed at scale a2=405.0 corresponding to frequency of 0.62Hz, which is represented by the first frequency of vehicle. Noisy signal effect on this subtracting concept has been investigated and the result are listed on Table 5. As it is shown, until intensity of noisy signal to be 20db, the difference response with wavelet transform shows a precise identified frequency of bridge.

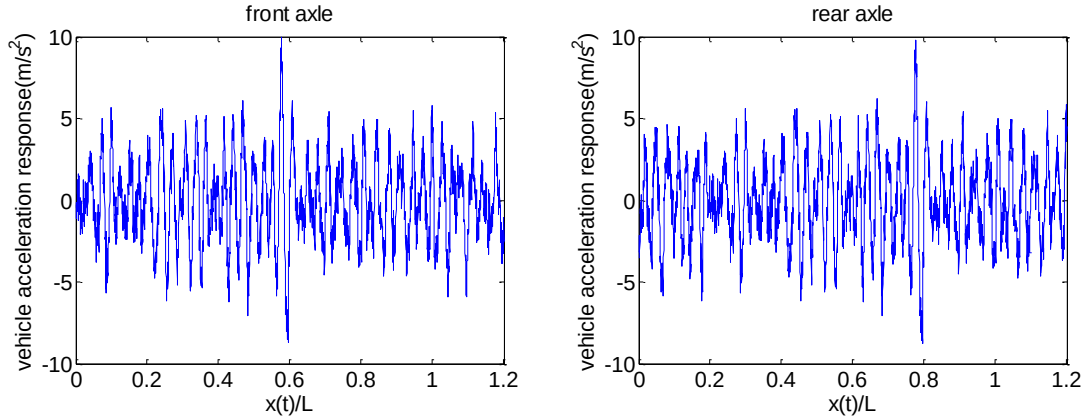

(a) (b)

Fig. 12 Acceleration responses (a) front axle acceleration response. (b) Rear axle acceleration response

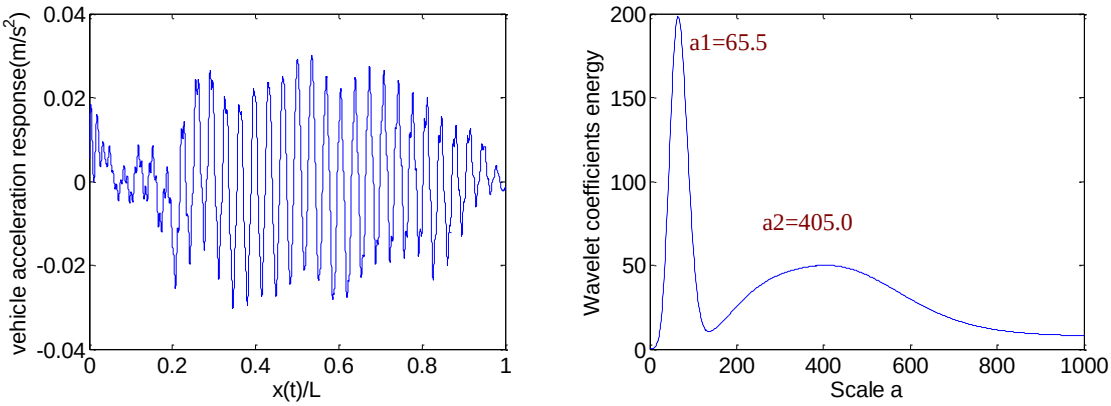

(a) (b)

Fig. 13 Case study result (a) difference response from two axles; (b) its wavelet coefficient energy distribution of each scale

Table 5. Frequency identification at different intensity of noisy signal

Intensity of noisy signal	Span (L=15m) Theoretical frequency (Hz)	Frequency is calculated by Wavelet transform (Hz)
db80	3.86	3.82(-1.03%)
db70		3.82(-1.03%)
db60		3.82(-1.03%)
db50		3.82(-1.03%)
db40		3.82(-1.03%)
db30		3.82(-1.03%)
db20		3.31(-14.19%)

Although road roughness is one of main challenges in “drive-by” monitoring system, the concept of subtracting signals from identical axles is an effective way to decrease its effect or even remove it. Here Fig. 14 shows the identified frequencies of the bridge for different damage levels for a velocity of 2m/s considering the intensity of noisy signal at 40*db*, comparing to their corresponding theoretical frequencies. In this case, the damage is simulated at mid-span. As it is shown, the identified frequencies of bridge are very close to their theoretical frequencies (errors less than -1.53%). In addition, with the increment of damage level, both of identified frequency and theoretical frequencies decrease.

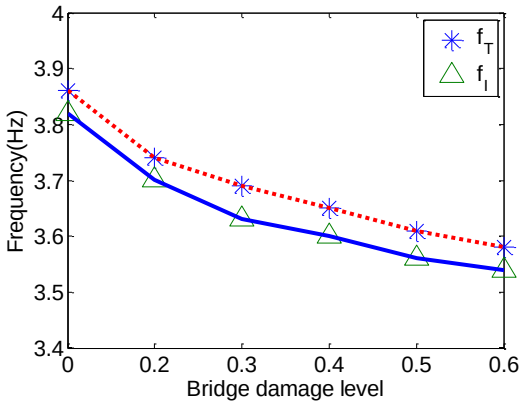

Fig. 14 Bridge frequency identification at different damage level with velocity of 2m/s (Note: f_T presents the theoretical frequency of intact bridge or damaged bridge; f_I presents the identified frequency of intact bridge or damaged bridge; damage level 0 means intact bridge)

CONCLUSIONS

This paper introduces a new method to extract the natural frequency of bridge from indirect measurements of a passing vehicle, based on wavelet analysis. In compare with FFT, the proposed approach is not restricted to the frequency resolution. The approach has been extended to point out to the frequency drop due to the structural damage. The extracted bridge frequencies using the proposed wavelet approach show a drop in its magnitude as the damage extent increases. However, the value of the extracted frequency did not show a good agreement with the theoretical bridge frequency. In contrast, FFT did not show any evidence for damage in the acceleration spectrum. The same results have been found for higher modes of vibrations (2^{nd} mode). The paper examined the sensitivity of the proposed approach to road roughness profile. In this regard, a Half-Car model with

two axles has been utilized, and the signal of the axles have been subtracted with time lag to damp out the road roughness effect on the recorded signal. The subtracted acceleration has been processed using the proposed method and the results shows good agreement between the extracted and theoretical bridge frequencies. The approach has strong potential to provide a quick estimation for the bridge health condition.

ACKNOWLEDGMENT

This research is sponsored by National Science of Foundation (NSF-CNS-1645863). Any opinions, findings, and conclusions or recommendations expressed in this publication are those of the authors and do not necessarily reflect the view of the sponsors.

REFERENCES

[1] Malekjafarian, A., McGetrick, P. J. and Obrien, E. J. A Review of Indirect Bridge Monitoring Using Passing Vehicles. *Shock and Vibration*, 2015 (2015), 1-16.

[2] Chupanit, P. and Phromsorn, C. The importance of bridge health monitoring. *International Science Index*, 6 (2012), 135-138.

[3] Rytter, A. Vibrational based inspection of civil engineering structures (1993).

[4] Carden, E. P. and Fanning, P. Vibration based condition monitoring: a review. *Structural health monitoring*, 3, 4 (2004), 355-377.

[5] Yang, Y. B., Lin, C. W. and Yau, J. D. Extracting bridge frequencies from the dynamic response of a passing vehicle. *Journal of Sound and Vibration*, 272, 3-5 (2004), 471-493.

[6] Yang, Y. B. and Lin, C. W. Vehicle–bridge interaction dynamics and potential applications. *Journal of sound and vibration*, 284, 1 (2005), 205-226.

[7] Yang, Y. B. and Chang, K. C. Extraction of bridge frequencies from the dynamic response of a passing vehicle enhanced by the EMD technique. *Journal of Sound and Vibration*, 322, 4-5 (2009), 718-739.

[8] Lin, C. W. and Yang, Y. B. Use of a passing vehicle to scan the fundamental bridge frequencies: An experimental verification. *Engineering Structures*, 27, 13 (2005), 1865-1878.

[9] Yang, Y. B., Li, Y. C. and Chang, K. C. Constructing the mode shapes of a bridge from a passing vehicle: a theoretical study. *Smart Structures and Systems*, 13, 5 (2014), 797-819.

[10] González, A., O'Brien, E. J. and McGetrick, P. *Detection of bridge dynamic parameters using an instrumented vehicle*. World Conference on Structural Control and Monitoring, City, 2010.

[11] Yang, Y. B. and Chang, K. C. Extracting the bridge frequencies indirectly from a passing vehicle: Parametric study. *Engineering Structures*, 31, 10 (2009), 2448-2459.

[12] Siringoringo, D. M. and Fujino, Y. Estimating bridge fundamental frequency from vibration response of instrumented passing vehicle: Analytical and experimental study. *Advances in Structural Engineering*, 15, 3 (2012), 417-433.

[13] Yang, Y. B., Chang, K. C. and Li, Y. C. Filtering techniques for extracting bridge frequencies from a test vehicle moving over the bridge. *Engineering Structures*, 48 (2013), 353-362.

[14] McGetrick, P., Hester, D. and Taylor, S. Implementation of a drive-by monitoring system for transport infrastructure utilising smartphone technology and GNSS. *Journal of*

Civil Structural Health Monitoring, 7, 2 (2017), 175-189.

[15] OBrien, E. J., Martinez, D., Malekjafarian, A. and Sevillano, E. Damage detection using curvatures obtained from vehicle measurements. *Journal of Civil Structural Health Monitoring*, 7, 3 (2017), 333-341.

[16] González, A., OBrien, E. J. and McGetrick, P. J. *Detection of bridge dynamic parameters using an instrumented vehicle*. World Conference on Structural Control and Monitoring, City, 2010.

[17] Fujino, Y., Kitagawa, K., Furukawa, T. and Ishii, H. *Development of vehicle intelligent monitoring system (VIMS)*. International Society for Optics and Photonics, City, 2005.

[18] Khorram, A., Bakhtiari-Nejad, F. and Rezaeian, M. Comparison studies between two wavelet based crack detection methods of a beam subjected to a moving load. *International Journal of Engineering Science*, 51 (2012), 204-215.

[19] Poudel, U. P., Fu, G. and Ye, J. Wavelet transformation of mode shape difference function for structural damage location identification. *Earthquake Engineering & Structural Dynamics*, 36, 8 (2007), 1089-1107.

[20] Shahsavari, V., Bastien, J., Chouinard, L. and Clément, A. Likelihood-based testing of wavelet coefficients for damage detection in beam structures. *Journal of Civil Structural Health Monitoring*, 7, 1 (2017), 79-98.

[21] Nguyen, K. V. and Tran, H. T. Multi-cracks detection of a beam-like structure based on the on-vehicle vibration signal and wavelet analysis. *Journal of Sound and Vibration*, 329, 21 (2010), 4455-4465.

[22] McGetrick, P. J. and Kim, C. W. A Parametric Study of a Drive by Bridge Inspection System Based on the Morlet Wavelet. *Key Engineering Materials*, 569-570 (2013), 262-

269.

[23] Khorrami, H. and Moavenian, M. A comparative study of DWT, CWT and DCT transformations in ECG arrhythmias classification. *Expert systems with Applications*, 37, 8 (2010), 5751-5757.

[24] Morley, J., Arens, G., Fourgeau, I. and Giard, D. Wave propagation and sampling theory: Part I. *Geophysics*, 47 (1982), 203-221.

[25] Morlet, J. *Sampling theory and wave propagation*. Springer, City, 1983.

[26] Gao, R. X. and Yan, R. *Selection of Base Wavelet*. Springer, City, 2011.

[27] Cebon, D. *Handbook of vehicle-road interaction*. ALWAYS 1999.

[28] Harris, N. K., OBrien, E. J. and González, A. Reduction of bridge dynamic amplification through adjustment of vehicle suspension damping. *Journal of Sound and Vibration*, 302, 3 (2007), 471-485.

[29] Elhattab, A., Uddin, N. and OBrien, E. Drive-by bridge damage monitoring using Bridge Displacement Profile Difference. *Journal of Civil Structural Health Monitoring*, 6, 5 (2016), 839-850.

[30] Elhattab, A., Uddin, N. and Obrien, E. DRIVE-BY BRIDGE DAMAGE DETECTION USING APPARENT PROFILE. *First International Conference on Advances in Civil Infrastructure and Construction Materials (CISM)* (2015), 33-45.

[31] González, A., Covián, E. and Madera, J. Determination of Bridge Natural Frequencies Using a Moving Vehicle Instrumented with Accelerometers and a Geographical Positioning System, 88 (2008).

[32] Sinha, J. K., Friswell, M. I. and Edwards, S. Simplified Models for the Location of Cracks in Beam Structures Using Measured Vibration Data. *Journal of Sound and*

Vibration, 251, 1 (2002), 13-38.

[33] ISO-8608 *Mechanical vibration-Road surface profiles-Reporting of measured data*. International Organization for Standardization (ISO) Geneva, City, 1995.

[34] Keenahan, J., OBrien, E. J., McGetrick, P. J. and González, A. The use of a dynamic truck-trailer drive-by system to monitor bridge damping. *Structural Health Monitoring* (2013), 1475921713513974.

HILBERT TRANSFORM BASED APPROACH TO IMPROVE EXTRACTION OF "DRIVE-BY" BRIDGE FREQUENCY

by

CHENGJUN TAN
NASIM UDDIN

Smart Structures and Systems, an International Journal, (Accepted)

Format adapted [and errata corrected] for dissertation

HILBERT TRANSFORM BASED APPROACH TO IMPROVE EXTRACTION OF "DRIVE-BY" BRIDGE FREQUENCY

Abstract

Recently, the concept of "drive-by" bridge monitoring system using indirect measurements from a passing vehicle to extract key parameters of a bridge has been rapidly developed. As one of the most key parameters of a bridge, the natural frequency has been successfully extracted theoretically and in practice using indirect measurements. The frequency of bridge is generally calculated applying Fast Fourier Transform (FFT) directly. However, it has been demonstrated that with the increase in vehicle velocity, the estimated frequency resolution of FFT will be very low causing a great extracted error. Moreover, because of the low frequency resolution, it is hard to detect the frequency drop caused by any damages or degradation of the bridge structural integrity. This paper will introduce a new technique of bridge frequency extraction based on Hilbert Transform (HT) that is not restricted to frequency resolution and can, therefore, improve identification accuracy. In this paper, deriving from the vehicle response, the closed-form solution associated with bridge frequency removing the effect of vehicle velocity is discussed in the analytical study. Then a numerical Vehicle-Bridge Interaction (VBI) model with a quarter car model is adopted to demonstrate the proposed approach. Finally, factors that affect the proposed approach are studied, including vehicle velocity, signal noise, and road roughness profile.

Keywords: Hilbert Transform, bridge frequency, drive-by bridge inspection, bridge health monitoring, non-destructive evaluation;

1. INTRODUCTION

Bridge structures are the intrinsic components of transportation infrastructure network. Nowadays these structures are increasingly subject to degradation due to aging, environment and overload. Periodic monitoring of bridge is, therefore essential to maintain strategy since it can provide early warning if the inspected bridge becomes unsafe. Traditionally, bridge maintenance has mostly relied to visual inspection approaches which are highly dependent on staff member experience and subjective determine. These approaches can only detect bridge damage when it is visible. A number of bridges collapsed catastrophically such as I-35W Mississippi River bridge, whereas, they had been visually inspected just before the disaster. Thus, Chupanit and Phromsorn (2012) suggested that the visual inspection alone may not be sufficient to assess the bridge health condition.

The last decades, the bridge structural health monitoring (SHM) has developed dramatically which rely on the automatic detection of anomalous structural behavior. One of the most popular SHM approaches assess bridge condition via extracting dynamic properties of the bridge such as natural frequency, damping ratio, and mode shapes from dynamic response of structures for non-destructive damage assessment (Carden 2004, Malekjafarian, McGetrick et al. 2015). In these SHM systems using vibration data from the structure are referred to as the direct approach, which requires a larger number of sensors installed on bridge structures (Carden 2004). These SHM techniques have following drawbacks: expensive, time-consuming and even dangerous (Malekjafarian, McGetrick et al. 2015). From another perspective, the implementation of SHM for short and medium span bridges is not widespread, which represent a large portion of the bridge

inventory of the road network (Malekjafarian, McGetrick et al. 2015). Therefore, there is a necessity to find a less expensive SHM method that can be applied to a wide range of bridges.

Recently, the indirect approach or what has been known as ‘drive-by bridge inspection’ is becoming an intriguing topic in the application of bridge SHM technique. This indirect approach extracts bridge dynamic properties from dynamic response of a passing vehicle over the bridge, which is first proposed by Yang and Lin (2005), Yang and Chang (2009). The authors derived a closed-form solution of vehicle response, where a vehicle is modeled as a sprung mass and a bridge as a simple support beam. It has shown that the vehicle response contains the vibration components dominated by the natural frequency of bridge, and that has been demonstrated by the numerical simulation with VBI model (Wang, Deng et al. 2016). The feasibility of extracting natural frequency of bridge from a passing vehicle in practice has been experimentally verified by Lin and Yang (2005), Yang and Chang (2009).

Following the idea of the indirect approach, González, Obrien et al. (2012), Keenahan, Obrien et al. (2013) theoretically investigated the method of extracting related bridge damping from vehicle history. González, Obrien et al. (2012) pointed out that the damping value of bridge can be calculated by the minimum road profile estimation error from two axles with a half car model. Keenahan, Obrien et al. (2013) presented that the damping change in the bridge can be detected when the axle accelerations of the trailer are subtracted from one another. They pointed out that this method is more effective for monitoring damping in short bridges.

On the other hand, a number of methods for constructing mode shape of the bridge based on such indirect approach were proposed (Zhang, Wang et al. 2012, Malekjafarian and Obrien 2014, Oshima, Yamamoto et al. 2014, Yang, Li et al. 2014, Obrien and Malekjafarian 2016, Malekjafarian and Obrien 2017, Tan, Uddin et al. 2019). Yang, Li et al. (2014) theoretically constructed bridge modal shape from a passing vehicle over the bridge through applying HT combined with band-pass filter technique. They pointed out that such indirect measurements from the instrumented vehicle can provide a better screening for the bridge degrees of freedom (DOF) than the direct measurements from a sensor mounted on the bridge structure. Zhang, Wang et al. (2012) developed a simple approach to approximately extract bridge mode shape squares from the passing vehicle response and proposed a new damage index based on this extraction of mode shape, which is more sensitive to structural damage. The validity of this proposed method has been demonstrated by numerical simulations and simple experiments in the lab.

Furthermore, signal processing tool such as wavelet transform and HT are increasingly applied on the "drive by" bridge SHM (Cunha, Caetano et al. , Yang and Chang 2009, Nguyen and Tran 2010, Hester and González 2012, Khorram, Bakhtiari-Nejad et al. 2012, McGetrick and Kim 2013, Mahato, Teja et al. 2017, Obrien, Malekjafarian et al. 2017, Tan, Elhattab et al. 2017, Tan, Elhattab et al. 2017). On account of their high sensitivity for discontinuity of signal, they are mostly used to localize the structural damage location. In addition, HT can assist to extract higher mode frequency or modal shape of the bridge from the vehicle response.

The natural frequency of bridges as one of the most basic vibration parameters reflecting bridges dynamic characteristic, it was constantly referred as a damage index to

estimate bridge condition (Deng and Cai 2009). In the application of tradition bridge SHM, a published review paper (Carden 2004) presented that there were 65 publications working on the detection of structural damage through frequency drops. However, rarely studies were focused on this point in the application of "drive-by" bridge SHM. One of the main reasons is that the higher vehicle velocity leads to short data of vehicle responses, resulting in low frequency resolution when applied with FFT. Consequently, the identification accuracy of bridge frequency is poor. Tan, Elhattab et al. (2017) developed a wavelet-based approach to identify bridge frequency without restricting to frequency resolution and can be used to detect the frequency drop caused by structural damage. However, it has shown that with the increase in vehicle velocity, the identification accuracy will decrease either. Studies have pointed out that the higher vehicle velocity has a strong negative influence on the recognition of bridge frequency in "drive-by" bridge SHM.

This paper will introduce a new bridge frequency extracting approach from a passing vehicle based on HT combined with band-pass filter technique. At first, in order to highlight the dynamic VBI response, a closed-form solution of vehicle response is adopted in the analytical study. In this regard, the bridge is modeled as a simply supported beam and vehicle as a sprung mass. Deriving this closed-form solution with HT combined with the band-pass filter, formulation representing the bridge frequency is divided. In addition, the vehicle velocity parameter is investigated and it can be removed from this formulation to improve identification accuracy. Then, a numerical VBI model with a quarter car model is adopted to demonstrate the proposed approach. Finally, to further investigate the fidelity of the proposed approach, cases studies are investigated, including vehicle velocity, signal noise, and road roughness profile.

2 Hilbert Transform

In this section, a brief introduction of HT is presented. Mathematically, given a real-valued mono-component function of *s(t)*, the Hilbert transform of *s(t)* is defined as (Huang 2014):

$$\hat{s}(t) = H\big(s(t)\big) = \frac{1}{\pi} PV \int_{-\infty}^{+\infty} \frac{s(\tau)}{t-\tau} d\tau \tag{1}$$

where *PV* denotes the Cauchy principal value. Practically, it defines the HT as the convolution of *s(t)* with the kernel function *1/πt*. Therefore, $\hat{s}(t)$ is referred as the orthogonal projection of *s(t).* Using these two orthogonal component, the analytic signal *z(t)* can be constructed in the form

$$z(t) = s(t) + i\hat{s}(t) = A(t)e^{i\theta(t)} \tag{2}$$

where

$$A(t) = \sqrt{s^2(t) + \hat{s}^2(t)}, \; , \theta(t) = arctan\left(\frac{\hat{s}(t)}{s(t)}\right) \tag{3, 4}$$

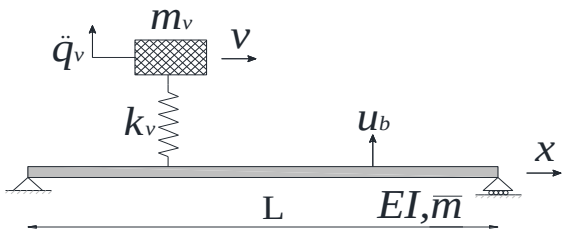

Fig. 1 Numerical model of VBI

In above equation, the time-dependent functions of *A(t)* and *θ(t)* are the instantaneous amplitude function and instantaneous phase function, respectively, of the

original function *s(t)*. Using vector representations in complex plane, *A(t)* and *θ(t)* can be obtained easily.

3. Formulation of the Analytical Theory

In order to highlight the major dynamic characteristics of the coupled VBI system, a simplified numerical model will be adopted, as given in Fig. 1. The vehicle is simply simulated as a lumped mass m_v, supported by a spring of stiffness k_v and passing with constant speed v across a simply supported beam of length L. This beam is assumed to be of the Bernoulli–Euler type with constant cross section and ideal smooth pavement. Through neglecting the damping effects of both bridge and vehicle, the equations of motion for the bridge and vehicle can be written as follows:

$$\bar{m}\ddot{u} + EIu'''' = f_c(t)\delta(x - vt) \tag{5}$$

$$m_v\ddot{u} + k_v(q_v - u|_{x=vt}) = 0 \tag{6}$$

where $\bar{m}$ denotes the bridge mass per unit length, E young elastic modulus, I moment of inertia, $u(x,t)$ vertical displacement of beam, and $q_v(t)$ vertical displacement of the vehicle, measured from the static equilibrium position, and a dot and a prime represent the derivative with relative to time t and longitudinal coordinate x of the beam, respectively. The contact force between beam and vehicle $f_c(t)$ can be expressed as

$$f_c(t) = -m_v g + k_v(q_v - u|_{x=vt}) \tag{7}$$

where g represents the gravitational acceleration.

Using the modal superposition method, the solution of the bridge displacement response $u(x,t)$ in equation (5) can be expressed in term of modal shapes $\sin(n\pi x/L)$ and generalized coordinates $q_{b,n}(t)$,

$$u(x,t) = \sum_{n=1}^{\infty} sin\frac{n\pi x}{L} q_{b,n}(t) \tag{8}$$

Accordingly, one can obtain the solution of the displacement of the test vehicle in equation (6) as following (Yang and Lin 2005, Yang and Chang 2009, Yang, Li et al. 2014)

$$\begin{aligned} q_v(t) = \sum_{n=1}^{\infty} \Bigg\{ & A_{1,n} \cos\left(\frac{(n-1)\pi v}{L}\right) t + A_{2,n} \cos\left(\frac{(n+1)\pi v}{L}\right) t \\ & + A_{3,n} \cos(\omega_v t) + A_{4,n} \cos\left(\omega_{b,n} - \frac{n\pi v}{L}\right) t \\ & + A_{5,n} \cos\left(\omega_{b,n} + \frac{n\pi v}{L}\right) t) \Bigg\} \end{aligned} \tag{9}$$

where the coefficient of $A_{4,n}$ and $A_{5,n}$ are

$$\begin{aligned} A_{4,n} &= \frac{-S_n \Delta_{st,n} \omega_v^2}{2(1-S_n^2)\left(\omega_v - \omega_{b,n} + \frac{n\pi v}{L}\right)\left(\omega_v + \omega_{b,n} - \frac{n\pi v}{L}\right)} \\ A_{5,n} &= \frac{S_n \Delta_{st,n} \omega_v^2}{2(1-S_n^2)(\omega_v + \omega_{b,n} + \frac{n\pi v}{L})(\omega_v - \omega_{b,n} - \frac{n\pi v}{L})} \end{aligned} \tag{10,11}$$

and the bridge frequency $\omega_{b,n}$, vehicle frequency ω_v, velocity parameter S_n, and vehicle-induced static deflection $\Delta_{st,n}$ of the beam, of the n-th mode are defined as

$$\begin{aligned} \omega_{b,n} &= (\frac{\pi v}{L})^2 \sqrt{\frac{EI}{\bar{m}}} \\ \omega_v &= \sqrt{\frac{k_v}{m_v}} \\ S_n &= \frac{n\pi v}{L\omega_{b,n}} \end{aligned} \tag{12,13,14,15}$$

$$\Delta_{st,n}=\frac{-2\omega_v g L^3}{n^4\pi^4 EI}$$

Similar to the coefficient of $A_{4,n}$ and $A_{5,n}$ in equation (10, 11), $A_{1,n}$ $A_{2,n}$ and $A_{3,n}$ are time irrelevant coefficients determined by parameters of ω_v, $\omega_{b,n}$, $\Delta_{st,n}$ and S_n. However, it won't be presented herein since it is not of concern in this study.

Therefore, taking twice derivative of the vehicle displacement response, one can obtain the vehicle acceleration response

$$\begin{aligned}\ddot{q}_v(t)=\sum_{n=1}^{\infty}\Bigg\{&\bar{\bar{A}}_{1,n}\cos\left(\frac{(n-1)\pi v}{L}\right)t+\bar{\bar{A}}_{2,n}\cos\left(\frac{(n+1)\pi v}{L}\right)t\\&+\bar{\bar{A}}_{3,n}\cos(\omega_v t)+\bar{\bar{A}}_{4,n}\cos\left(\omega_{b,n}-\frac{n\pi v}{L}\right)t\\&+\bar{\bar{A}}_{5,n}\cos\left(\omega_{b,n}+\frac{n\pi v}{L}\right)t)\Bigg\}\end{aligned}\tag{16}$$

with the coefficients of $\bar{\bar{A}}_{4,n}$ and $\bar{\bar{A}}_{5,n}$ as

$$\begin{aligned}\bar{\bar{A}}_{4,n}&=\frac{S_n\Delta_{st,n}\omega_v^2}{2(1-S_n^2)(\omega_v-\omega_{b,n}+\frac{n\pi v}{L})(\omega_v+\omega_{b,n}-\frac{n\pi v}{L})}(\omega_{b,n}-\frac{n\pi v}{L})^2\\\bar{\bar{A}}_{5,n}&=\frac{-S_n\Delta_{st,n}\omega_v^2}{2(1-S_n^2)(\omega_v+\omega_{b,n}+\frac{n\pi v}{L})(\omega_v-\omega_{b,n}-\frac{n\pi v}{L})}(\omega_{b,n}+\frac{n\pi v}{L})^2\end{aligned}\tag{17,18}$$

Apparently, the vehicle acceleration response of equation (16) is dominated by five frequencies, i.e., two shifted driving frequencies $(n-1)\pi v/L$ and $(n+1)\pi v/L$, vehicle frequency ω_v, and two shifted bridge frequencies $\omega_{b,n}-n\pi v/L$ and $\omega_{b,n}+n\pi v/L$.

To extract the frequency of bridge from the vehicle acceleration response with this proposed HT approach, the component response corresponding to the bridge frequency of n-th mode should be singled out via an appropriate filtering technique. According to equation (16), the extracted component response R_b associated with single frequency of bridge (n-th mode) is (Yang, Li et al. 2014)

$$R_b(t) = \bar{\bar{A}}_{4,n} \cos\left(\omega_{b,n} - \frac{n\pi v}{L}\right) t + \bar{\bar{A}}_{5,n} \cos\left(\omega_{b,n} + \frac{n\pi v}{L}\right) t \tag{19}$$

The filtering signal of R_b is a narrow-band time series and thus can be applied with HT to produce its transform pair,

$$\hat{R}_b(t) = H[(R_b(t))] = \bar{\bar{A}}_{4,n} \sin\left(\omega_{b,n} - \frac{n\pi v}{L}\right) t + \bar{\bar{A}}_{5,n} \sin\left(\omega_{b,n} + \frac{n\pi v}{L}\right) t \tag{20}$$

In general, the bridge frequency $\omega_{b,n}$ is much greater than the driving frequency nπv/L, especially at lower vehicle velocity. Accordingly, the coefficients $\bar{\bar{A}}_{4,n}$and $\bar{\bar{A}}_{5,n}$ can reduce to

$$\bar{\bar{A}}_{4,n} = (\omega_{b,n})^2 \frac{S_n \Delta_{st,n} \omega_v^2}{2(1 - S_n^2)(\omega_v - \omega_{b,n})(\omega_v + \omega_{b,n})}$$

$$\bar{\bar{A}}_{5,n} = -(\omega_{b,n})^2 \frac{S_n \Delta_{st,n} \omega_v^2}{2(1 - S_n^2)(\omega_v - \omega_{b,n})(\omega_v + \omega_{b,n})} \tag{21,22}$$

As equation (21) and (22) shown, the two coefficients $\bar{\bar{A}}_{4,n}$ and $\bar{\bar{A}}_{5,n}$ are equal in magnitude, but opposite in sign, i.e., $\bar{\bar{A}}_{4,n}$ +$\bar{\bar{A}}_{5,n}$=0. Accordingly, the bridge component response $R_b(t)$ and its Hilbert transform $\hat{R}_b(\mathrm{t})$ can be expressed as

$$R_b(t) = -2\bar{\bar{A}}_{4,n} \sin(\omega_{b,n} t) \sin\left(\frac{n\pi v}{L} t\right)$$

$$\hat{R}_b(t) = 2\bar{\bar{A}}_{4,n} \cos(\omega_{b,n} t) \sin\left(\frac{n\pi v}{L} t\right) \tag{23,24}$$

From the introduce of Hilbert transform aforementioned, the instantaneous amplitude history of $A(t)$ can be obtained as

$$A(t) = \sqrt{R_b^2(t) + \hat{R}_b^2(t)} = \left|2\bar{\bar{A}}_{4,n} \cdot \sin\left(\frac{n\pi v}{L} t\right)\right| = 2\left|\bar{\bar{A}}_{4,n}\right| \cdot \left|\sin\left(\frac{n\pi v}{L} t\right)\right| \tag{25}$$

Replacing x with vt in equation (25) yields

$$A\left(\frac{x}{v}\right) = 2\left|\bar{\bar{A}}_{4,n}\right| \cdot \left|\sin\left(\frac{n\pi x}{L}\right)\right| \tag{26}$$

This equation shows that the instantaneous amplitude history of $A\left(\frac{x}{v}\right)$ of the extracted component response is represented by the mode shape function $\sin\left(\frac{n\pi x}{L}\right)$ of the bridge (in absolute value) multiplied by a constant and time-irreverent coefficient $2\left|\bar{\bar{A}}_{4,n}\right|$, which is a function of the bridge frequency $\omega_{b,n}$, vehicle frequency ω_v, velocity parameter S_n, and vehicle-induced static deflection $\Delta_{st,n}$ of the beam. It reveals that once the component response corresponding to the certain mode shape of the bridge can be extracted from the response of a passing vehicle when it passed over the bridge, its instantaneous amplitude history is representative of the corresponding mode of the bridge (Yang, Li et al. 2014).

On the other hand, the instantaneous phase $\theta(t)$can be derived as

$$\theta(t) = \arctan\left(\frac{\hat{R}_b(t)}{R_b(t)}\right) = \arctan\left(-cot\omega_{b,n}t\right) = \omega_{b,n}t - \frac{\pi}{2} \tag{27}$$

Herein, it is demonstrated that the bridge frequency can be represented by the slope of instantaneous phase. However, this result has relied on the assumption of that the driving frequency $n\pi v/L$ is much smaller than the bridge frequency. In fact, with the increase of vehicle velocity, the driving frequency cannot be neglected in comparison to the bridge frequency. Therefore, the following section will focus on presenting formula derivation considering this driving frequency.

Set a ratio α of $\bar{\bar{A}}_{5,n}$ to $\bar{\bar{A}}_{4,n}$ from equations (17) and (18) and it can be expressed as

$$\alpha = \frac{\bar{\bar{A}}_{5,n}}{\bar{\bar{A}}_{4,n}} = -\frac{(1+S_n)^2}{(1-S_n)^2} \cdot \frac{(1-{\mu_n}^2(1-S_n)^2)}{(1-{\mu_n}^2(1+S_n)^2)} \tag{28}$$

where μ_n is defined as the ratio of the n-th mode natural frequency of bridge $\omega_{b,n}$ to the vehicle frequency ω_v,

$$\mu_n = \frac{\omega_{b,n}}{\omega_v} \tag{29}$$

Then, the component response of R_b and its Hilbert transform $\hat{R}_b$ can be expressed as

$$\begin{aligned} R_b &= \bar{\bar{A}}_{4,n} \cdot \left[(1+\alpha)\cos\left(\omega_{b,n}t\right)\cos\left(S_n\omega_{b,n}t\right) + (1 \right. \\ &\quad \left. - \alpha)\sin\left(\omega_{b,n}t\right)\sin\left(S_n\omega_{b,n}t\right)\right] \\ \hat{R}_b &= \bar{\bar{A}}_{4,n} \cdot \left[(1+\alpha)\sin\left(\omega_{b,n}t\right)\cos\left(S_n\omega_{b,n}t\right) - (1 \right. \\ &\quad \left. - \alpha)\cos\left(\omega_{b,n}t\right)\sin\left(S_n\omega_{b,n}t\right)\right] \end{aligned} \tag{30,31}$$

In this way, the instantaneous phase $\theta(t)$ can be derived as

$$\theta(t) = \arctan\left(\frac{\hat{R}_b(t)}{R_b(t)}\right) = \arctan\left(\frac{\tan\left(\omega_{b,n}t\right) - \frac{1-\alpha}{1+\alpha}\tan(S_n\omega_{b,n}t)}{1 + \frac{1-\alpha}{1+\alpha}\tan(S_n\omega_{b,n}t)\tan\left(\omega_{b,n}t\right)}\right) \tag{32}$$

Here assumes a time varying coefficient $\beta(t)$ and make it content

$$\tan(\beta(t)) = \frac{1-\alpha}{1+\alpha}\tan\left(S_n\omega_{b,n}t\right) \tag{33}$$

Therefore, the instantaneous phase $\theta(t)$ of equation (30) can be expressed as follows

$$\theta(t) = \omega_{b,n}t - \beta(t) \tag{34}$$

Obviously, the equation (34) shows that the slope of the sum of instantaneous phase $\theta(t)$ and $\beta(t)$ represents the bridge frequency. Comparing to the equation (27), it needs to calculate the term of $\beta(t)$, which is related to the vehicle velocity parameter S_n.

Although the proposed HT based approach indicates that the slope of sum $\theta(t) + \beta(t)$ is potential to extract the bridge nature frequencies from a passing vehicle removing vehicle speed effect, it is subject to two main challenges. One is imposed by the requirement of extracted component response R_b associated with single frequency of

bridge (n-th mode) from the passing vehicle acceleration history. For this point, it can carry out by feasible signal processing tools, such as singular spectrum and band-pass filters technique, and so on. In this regard, the bridge frequency actually has already been known in signal processing. But this is not contradictory to the present approach for improving extracting bridge frequency. Because this already known bridge frequency can obtain from applying FFT directly, wavelet analysis approach (Tan, Elhattab et al. 2017) or other ways, which does not remove the effect of the driving frequency and therefore, is considered as a poor identification (marked as $\bar{\omega}_b$ here). This present approach aims to obtain highly accurate identification of a bridge frequency. Although poor identification of bridge frequency can be easily obtained, how to extract R_b from the passing vehicle acceleration is still challengeable. Equation (26) shows that the perfect extracted R_b can obtain results of corresponding the mode shape of the bridge, which can instruct us to extract apposite R_b from the axle responses.

Another challenge is imposed by the calculation of $\beta(t)$, since it is related to the bridge frequencies as shown equation (33). The poor estimated frequency of a bridge $\bar{\omega}_b$ can be used instead. This section will investigate that how much the $\bar{\omega}_b$ influences on $\beta(t)$ as well as the final accuracy of the bridge frequency identification. According to equation (28), assume $\omega_b = 3.86Hz$, $\omega_v = 10.33Hz$ and S_n=0.1; a signal is created by $s(t) = \cos(\omega_b - S_n\omega_b)\,t + \alpha\cos(\omega_b + S_n\omega_b)\,t$, where α is calculated based on equation (28). In this case, the total effect time is 1.296s with time steps as 0.002s. Then the HT based approach is applied to extract ω_b from signal $s(t)$. In this processing, $\beta(t)$ is calculated using the given frequency $\bar{\omega}_b$, whose errors varies from -40% to 40% with 10% increment.

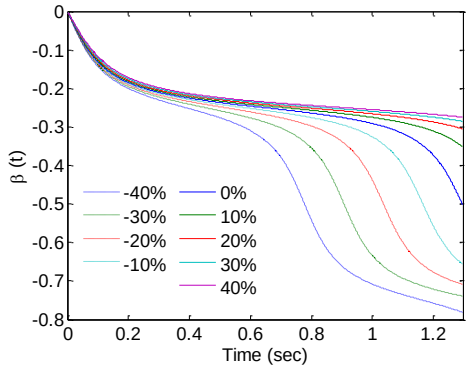

Fig. 2. $\beta(t)$ plot calculations at different $\bar{\omega}_b$

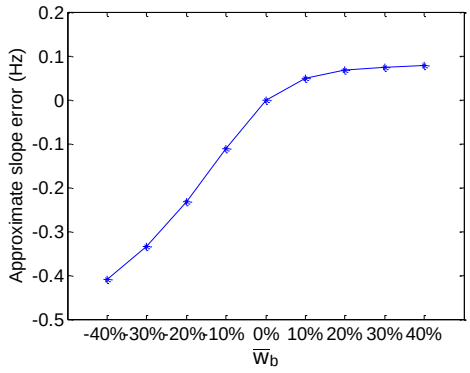

Fig. 3. The error of approximate slope of $\beta(t)$

Fig. 2 shows the $\beta(t)$ plots computed at different given frequency $\bar{\omega}_b$ with S_n=0.1. Fig. 3 illustrates the error of approximate slope of these $\beta(t)$ plots comparing to the theoretical one. As it has shown, the lower the given frequency $\bar{\omega}_b$, the greater the error result, as well as to the greater $\bar{\omega}_b$, although their errors are obviously lower than the lower given frequency $\bar{\omega}_b$. It is no doubts that these errors of $\beta(t)$ will result in the error to final ω_b identification as well. Fig. 4 shows the error of ω_b identification after applied the proposed HT approach. As expected, the HT based approach apparently and effectively

improve the ω_b estimation. To further explain the feasibility of the proposed approach, the results of more cases analysis when $S_n = 0.01, 0.05, 0.15$ and 0.20 are illustrated in Fig. 4 as well. It is worth to notice that the total effect time of signal will be changed corresponding to S_n. For instance, when $S_n = 0.2$, the length of total effect time is changed to 0.648s. From the Fig. 4, the higher S_n will magnify this estimated error, although all of the estimated frequencies have been dramatically improved after applied with the HT based approach in comparison to the given frequency $\bar{\omega}_b$. Practically, the improved estimated frequency can be utilized as a newly given frequency $\bar{\omega}_b$ to recalculate $\beta(t)$ and estimated frequency again and one can repeat these steps until the convergence of ω_b. Fig. 5 shows the cycle calculation results in the condition of the first given $\bar{\omega}_b = -40\%\ \omega_b$ with S_n=0.1. As it has shown, after enough cycles, the estimated frequency will be convergence and extremely close to theoretical one. Fig. 6 shows all case studies result after five loops' calculation. All of the errors are lower than 0.5%.

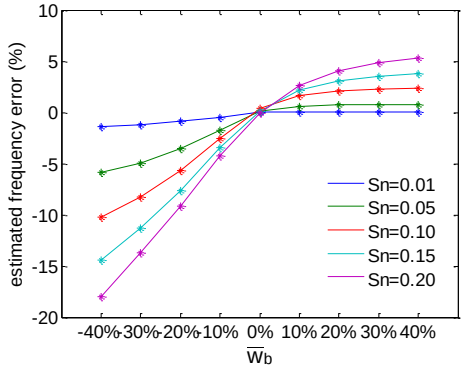

Fig. 4. Final estimated frequency error

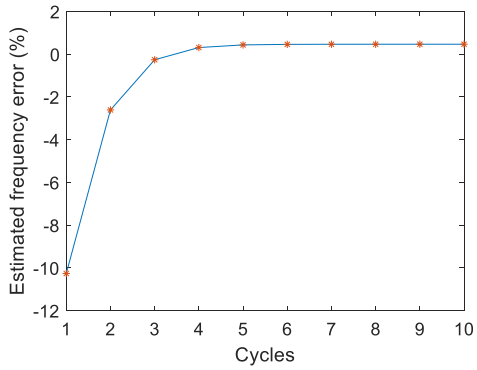

Fig. 5. Cycle calculation results

It reaches the conclusion that the calculation of precise β(t) is not a challenge anymore conducted by the repeat computation. Once the single component response R_b can be extracted precisely, the bridge frequency can be identified with high accuracy. Therefore, the proposed HT based approach to improve bridge frequency identification of a passing vehicle is summarized as follows:

(1) Acquisition of the vehicle acceleration responses.

(2) Obtaining the poor bridge frequencies $\bar{\omega}_b$ applying FFT directly, or wavelet analysis (Tan, Elhattab et al. 2017), etc.

(3) Extracting a series of single component response R_b at a series of band-pass filters with $\bar{\omega}_b$.

(4) Calculating instantaneous amplitude history $A(t)$ of HT at each R_b; simultaneously calculating the MAC (modal assurance criteria) between $A(t)$ and theoretical mode shape of the bridge.

(5) Choosing the optimum R_b who provides the maximum MAC.

(6) Calculating the instantaneous phase $\theta(t)$ of HT at the obtained optimum R_b and calculating the time-varying coefficient $\beta(t)$.

(7) Computing an improved bridge frequency with $\beta(t)$ and $\theta(t)$ and using the improved bridge frequency to calculate the time-varying coefficient $\beta(t)$ again.

(8) Repeating step (7) until the improved identified frequency convergence (convergence is the final bridge frequency identification).

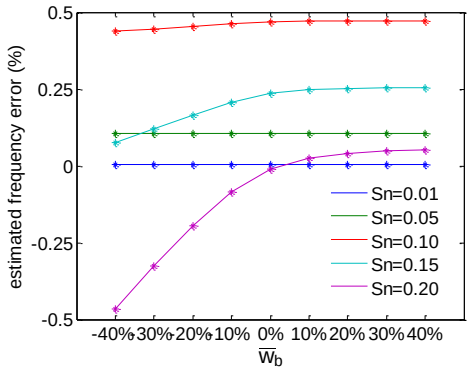

Fig. 6. The estimated frequency error after 5 loops calculation

4 Case studies

To verify the feasibility of the proposed approach on improving bridge frequency from a passing vehicle, a quarter-car of VBI model was adopted as shown in Fig. 7. The quarter-car travels with constant speed over the bridge. The vehicle is modeled as a quarter-car model crossing a 50-m approach distance followed by a 20-m simply supported finite element (FE) bridge. The vehicle masses are represented by a sprung mass, m_s, and un-sprung mass, m_a represents the vehicle axle mass and body mass respectively. The Degrees of Freedoms (DOFs) that correspond to the bouncing of the sprung and the axle masses are, u_s, and u_a, respectively. All properties of VBI model is listed in *Table 1* and based upon the work of Cebon (1999). The dynamic interaction between the vehicle and the bridge is

implemented in MATLAB (Tan, Elhattab et al. 2017). The road surface profile is not considered in this simulation. Unless otherwise mentioned, the used scanning frequency is 500 Hz. The first two natural frequencies of bridge, f_b is 2.171Hz and 8.683Hz respectively. The vehicle frequencies are 0.581Hz and 10.333Hz respectively.

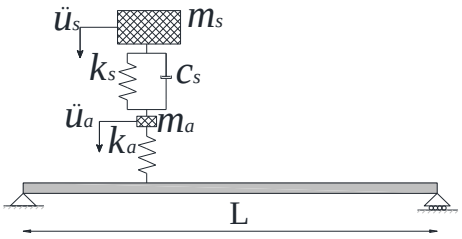

Fig. 7. The quarter car and bridge model

Table 1. Vehicle and bridge properties

Vehicle properties		Bridge properties	
m_s	14000 kg	Span	20m
k_s	200 kN/m	Density	4800kg/m^3
c_s	10 kN s/m	Width	4 m
m_a	700 kg	Depth	0.8m
k_a	2750 kN/m	Modulus	2.75×10^{10} N/m^2

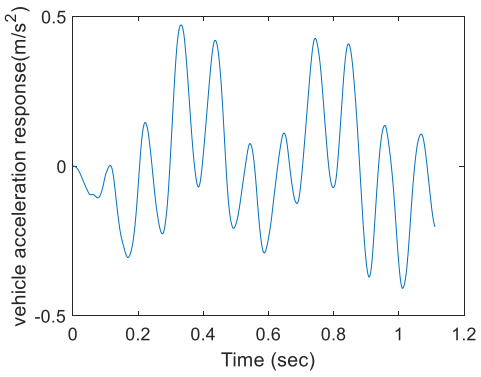

Fig. 8. The vehicle acceleration response

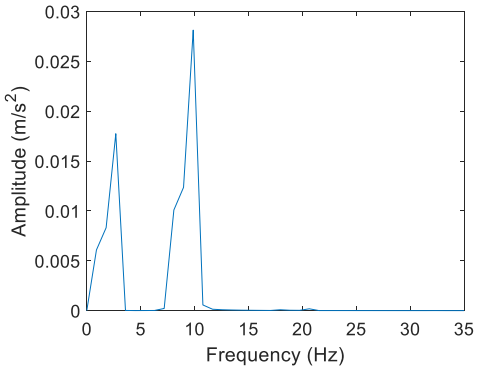

Fig. 9. Acceleration spectrum of vehicle acceleration history

Fig. 8 illustrates the vehicle axle acceleration response for the VBI model mentioned above, where the vehicle velocity is 18m/s. As aforementioned in the analytical theory, this passing vehicle history contains the bridge frequency components. Therefore, the natural frequency of bridge can be extracted after FFT applying to the signal of Fig. 8. Fig. 9 illustrates the spectrum of the recorded response showing two distinctive peaks according to the frequency of 2.693Hz and 9.874Hz respectively, which represents the first two bridge natural frequencies of the bridge, respectively. Since the frequency resolution of FFT is low with short data at the condition of higher vehicle velocity. The spectrum of

the test vehicle with FFT cannot point out the precious frequencies of bridges. With the increase in vehicle velocity, the frequency resolution of FFT will be worse. Thus, FFT can only provide a poor frequency identification for short data of the passing vehicle acceleration response. In addition, FFT cannot be used to detect the bridge frequency drop caused by bridge structure damages so as to assess bridge condition. The following section will utilize the proposed HT based approach to improve the extraction of the bridge frequencies.

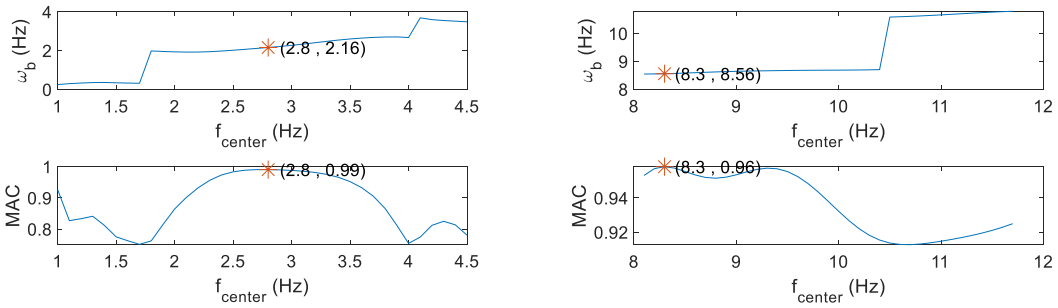

(a) 1st bridge frequency (b) 2nd bridge frequency

Fig. 10. Bridge frequencies identification at a series of band-pass filters

Generally, the maximum error applying FFT directly will be not greater than 2 times of the theoretical driving frequency (in this case: $f_d = \frac{v}{L} = 0.9Hz$) because both of the shift frequency and frequency resolution are equal to f_d. For example, in this case, the real first natural bridge frequency should be in the range of $f_{r1} = 2.693 - 2 \times 0.9 = 0.893$; $f_{r2} = 2.693 + 2 \times 0.9 = 4.493$. Then a zero-phase digital 'Butterworth' band-pass filter with a lower order as 6 is applied to the recorded acceleration response to extract the single modal component response. For this band-pass filter, the center

frequency f_{center} varies from f_{r1} to f_{r2}, and the two-cut-off frequencies are $f_{c1} = f_{center} - 2 \times f_d$ and $f_{c2} = f_{center} + 2 \times f_d$, respectively.

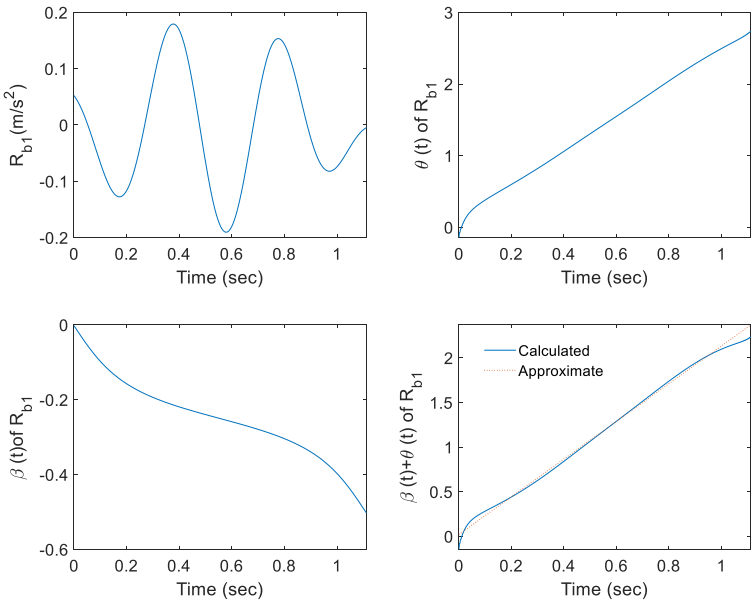

Fig. 11. The improved 1st bridge frequency identification details; top left: single component R_{b1} after band-pass filter; top right: the instantaneous phase θ(t); bottom left: the time varying coefficient β(t); bottom right: θ(t)+β(t)

Therefore, these band-pass filters are applied to extract the first two single component responses R_{b1} and R_{b2} of the bridge, and then these series of extracted R_{b1} and R_{b2} are used to improve the bridge frequency ω_b identification based on the aforementioned procedures. For this case, the results are illustrated in Fig. 10. As it has shown, when the $f_{center} = 2.8Hz$, the corresponding R_{b1} has the maximum MAC and obtains the final $\omega_b = 2.16Hz$, which is extremely close to the theoretical one with regard to the first bridge frequency. Similarly, the 2nd bridge frequency has been improved apparently after applying the proposed approach.

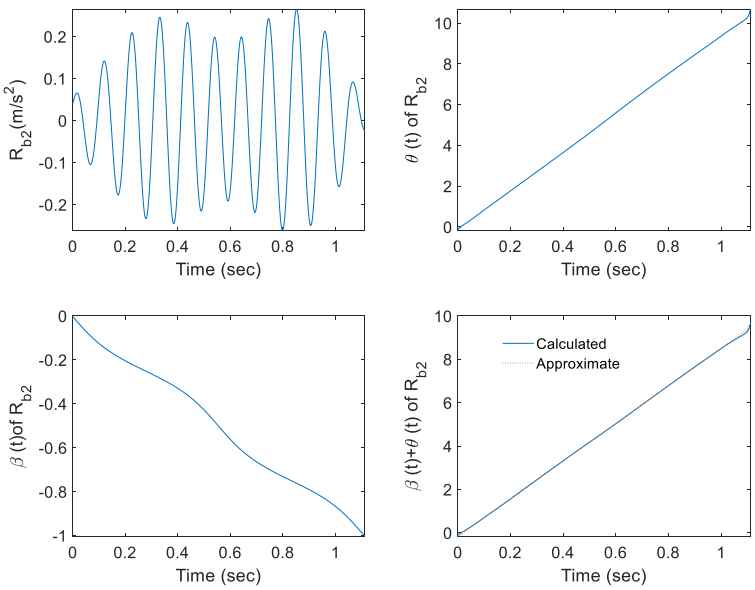

Fig. 12. The improved 2nd bridge frequency identification details; top left: single component R_{b2} after band-pass filter; top right: the instantaneous phase θ(t); bottom left: the time varying coefficient β(t); bottom right :θ(t)+β(t)

Fig. 11 and Fig. 12 show the details for improving the bridge frequency ω_b identification based on HT approach. As shown, these $\theta(t)$ plots are represented by a nearly straight line and their approximate slopes are calculated as 2.39 and 9.55 respectively. These calculated slopes can be considered as bridge frequencies as equation (27) considering the vehicle velocity parameter effect. However, the errors are great comparing to the theoretical one. Actually, the $\beta(t)$ plots are represented by this vehicle speed effect and clearly, they cannot be ignored directly. From the equation (34), the slopes of plots of $\theta(t) + \beta(t)$ represent the high accuracy identification of bridge frequency removing the effect of vehicle velocity effect and their approximate slopes are calculated as 2.16 and 8.56 respectively.

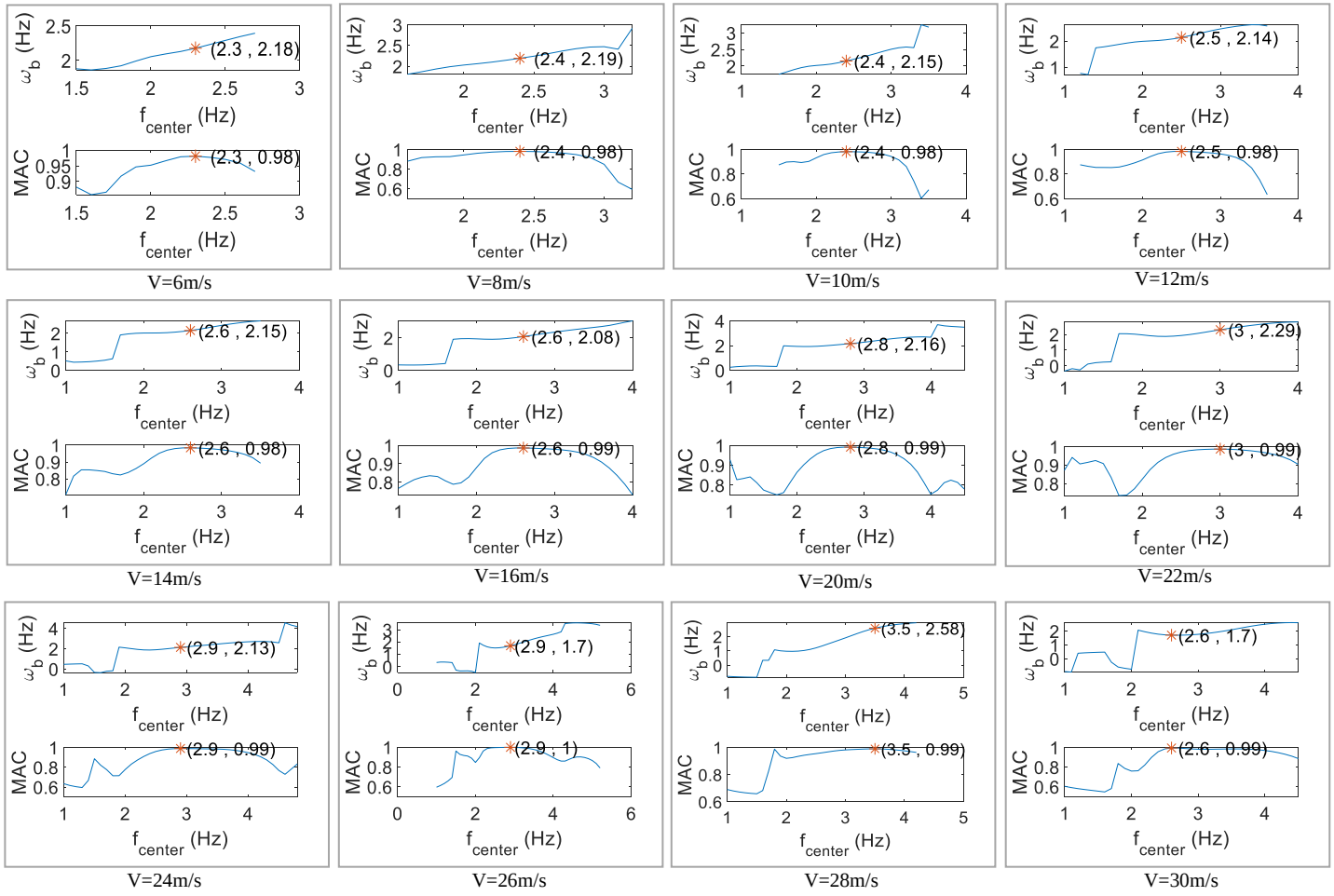

Fig. 13. The improved 1st bridge frequency identification at different vehicle speeds.

4.1 Effect of Vehicle Speed

In this case, the effect of the vehicle speed on improving the bridge frequency identification is studied for a series of vehicle speeds: v from 6 to 30 m/s with incensement of 2 m/s. Other parameters of VBI remain identical to that studied previously. By following the same procedure, the improved first two bridge frequencies can be extracted from a passing vehicle for each vehicle speed, as shown in Fig. 13 and Fig. 14. Table 2 lists the final bridge frequencies identification values of ω_b and results from HHT directly comparing to theoretical ones.

In the above processing analysis, all of the poor bridge frequencies identification $\bar{\omega}_b$ are obtained from the FFT spectrum. As it has shown, the $\bar{\omega}_b$ have a greater error at higher vehicle speed. In Table 2, the maximum identification error of FFT is -35.84% for 1st bridge frequency and 20.68% for 2nd bridge frequency. Obviously, the proposed approach has improved the bridge frequencies from a passing vehicle in most the cases. The identification error is less than 1.97% for 2nd bridge frequency. It is observed that when the vehicle speed is not greater than 26 m/s, the results of the improved 1st bridge frequencies are precious and error is less than 5.68%. In contrast, when the vehicle speed is equal to or greater than 26 m/s, the proposed HT based approach is not able to improve the bridge natural frequencies from the poor identification results with FFT.

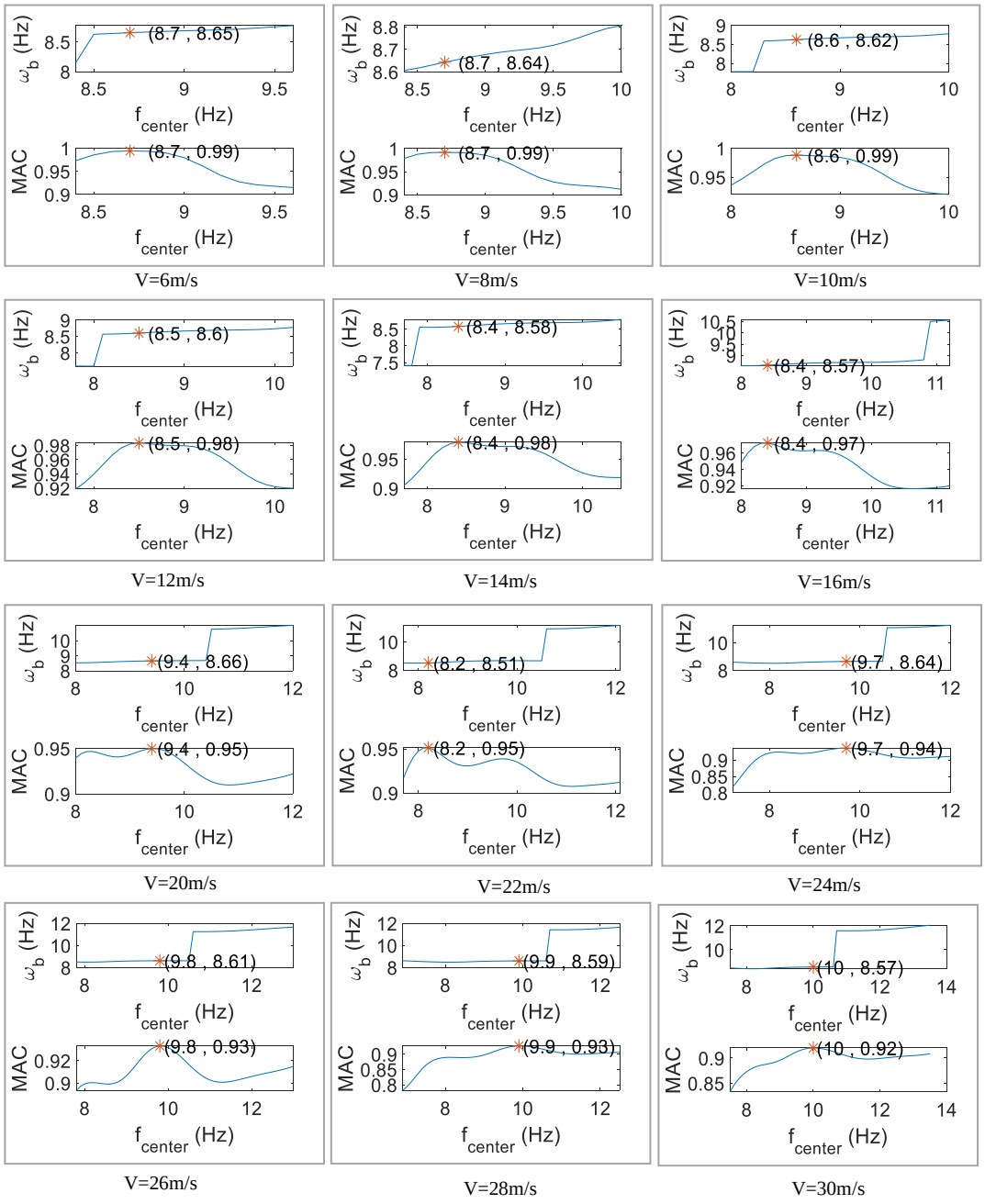

Fig. 14. The improved 2nd bridge frequency identification at different vehicle speeds.

Table 2. The improved bridge frequencies identification results at different vehicle speeds

Velocities (m/s)		6	8	10	12	14	16	18	20	22	24	26	28	30
1st	HT (Hz)	2.18	2.19	2.15	2.14	2.15	2.08	2.16	2.29	2.14	2.13	1.70	2.58	1.70
	Error (%)	0.23	1.02	-0.78	-1.48	-0.75	-4.06	-0.48	5.68	-1.40	-1.71	-21.81	18.94	-21.46
	FFT (Hz)	2.10	2.40	2.50	2.40	2.09	2.40	2.69	2.00	2.20	2.39	2.59	1.39	1.50
	Error (%)	-3.33	10.48	15.06	10.48	-3.49	10.39	24.06	-8.05	1.25	10.21	19.35	-35.84	-31.04
2nd	HT (Hz)	8.65	8.64	8.62	8.60	8.58	8.57	8.56	8.66	8.51	8.64	8.61	8.59	8.57
	Error (%)	-0.34	-0.46	-0.69	-0.91	-1.16	-1.29	-1.45	-0.30	-1.97	-0.49	-0.83	-1.05	-1.30
	FFT (Hz)	8.99	9.19	8.99	8.99	9.08	9.58	9.87	9.98	9.89	9.57	10.36	9.75	10.48
	Error (%)	3.57	5.87	3.55	3.57	4.55	10.38	13.72	14.94	13.90	10.21	19.34	12.28	20.68

4.2 Effect of noise

To further investigate the feasibility of this proposed method, the effect of noise are investigated. In order to simulate the polluted measurements, white noise is added to the simulated responses of the vehicle. The noise response is calculated as following formula:

$$\ddot{u}_{noise} = \ddot{u}_{calculated} + E_p N_{oise} \sigma(\ddot{u}_{calculated}) \quad (35)$$

where $\ddot{u}_{noise}$ is the polluted acceleration; E_p is the noise level and N_{oise} is a standard normal distribution vector with zero mean value and unit standard deviation. $\ddot{u}_{calculated}$ is the calculated acceleration, and $\sigma(\ddot{u}_{calculated})$ is their standard deviations.

Table 3. The errors of improved bridge frequencies results at different levels of noise

Noise level \ Velocity (m/s)		6	8	10	12	14	16	18	20	22	24	26	28	30
1st	0.05	0.22	0.97	-0.73	-1.42	-0.85	-4.02	-1.96	2.67	-1.30	0.00	-24.86	17.31	-21.39
	0.1	0.06	1.01	-0.45	-2.06	-0.81	-3.88	-2.31	5.78	0.93	0.34	-24.60	17.45	-22.44
	0.15	5.28	0.88	-0.71	-3.61	-0.62	4.68	-0.75	5.89	3.54	0.52	-20.97	16.94	-24.04
	0.2	-1.72	0.74	-2.58	-1.55	-2.72	-6.37	-0.53	5.31	-1.22	-4.69	-26.78	-63.09	-18.72
	0.25	2.75	1.22	-0.64	-3.52	8.87	-6.42	-2.14	5.85	-4.46	-4.35	-25.42	-55.91	-16.54
2nd	0.05	-0.34	-0.46	-0.69	-0.93	-1.16	-1.28	-1.46	-0.29	-1.97	-0.48	-0.85	-0.94	-1.38
	0.1	-0.33	-0.47	-0.69	-0.87	-1.16	-1.32	-1.46	-0.29	-2.00	-0.54	-0.78	-1.17	-1.52
	0.15	-0.35	-0.45	-0.67	-0.92	-1.17	-1.34	-0.14	-0.24	-2.09	-0.41	-0.89	-1.37	38.81
	0.2	-0.34	-0.48	-0.71	-0.94	-1.09	-1.23	-0.21	0.10	-2.21	-0.42	-0.58	-1.08	38.71
	0.25	-0.31	-0.48	-0.69	-0.95	-1.15	-1.29	-1.45	-0.56	-2.28	-0.32	-0.94	-1.38	38.78

Note: the errors are represented by percentage (%) comparing to theoretical ones.

The different levels of noise: $E_p = 0.05$, 0.1, 0.15, 0.20 and 0.25 are investigated in this study. By following the same procedure, all the results of the improved bridge frequencies are listed in Table 3. As it has shown, the proposed approach is not sensitive to noise, possibly because the procedure of band-pass filtering almost removes the effect of noise, as long as the FFT can get the generally accurate bridge frequencies $\bar{\omega}_b$. The result of the 2nd bridge frequency is better than that of 1st. The maximum identification error is 8.87% for 1st bridge frequency (except for 26, 28 and 30 m/s) and 2.28% for 2nd bridge frequency (except for 30 m/s).

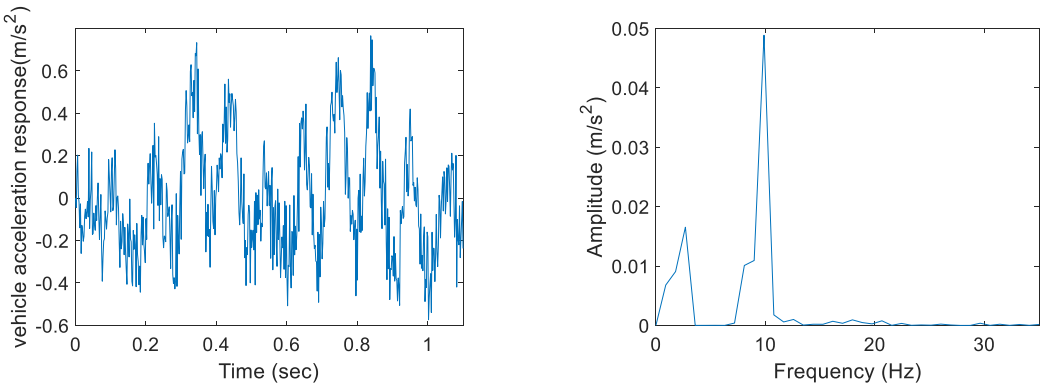

(a) The vehicle acceleration response (b) Acceleration spectrum

Fig. 15. The vehicle acceleration response and spectrum

4.3 Effect of Surface Roughness

In this case, the effect of road surface roughness is investigated by letting the instrumented vehicle pass over the bridge with rough road profile. The road roughness profile is generated according to the PSD (power spectrum density) curve of "class A" (ISO 1995).

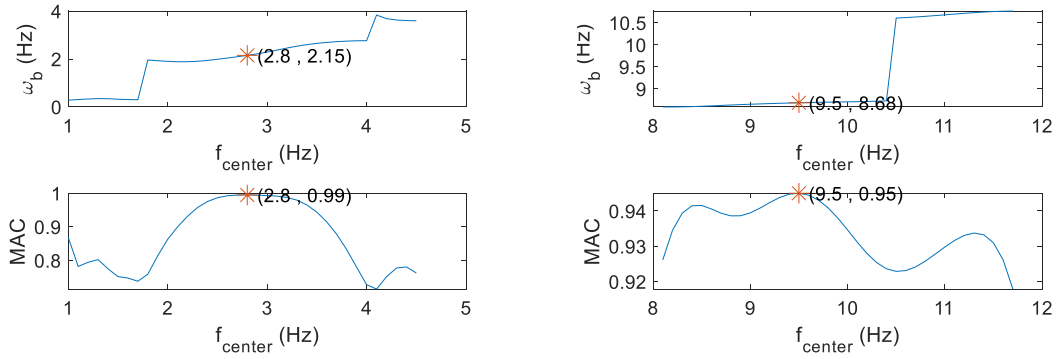

(a) 1st bridge frequency (b) 2nd bridge frequency

Fig. 16. Bridge frequencies identification considering the road surface profile

Fig. 15 shows the original crossing vehicle acceleration history at velocity 18 m/s with road roughness and the corresponding frequencies extracted using FFT. As it has shown, at the "class A" road roughness profile, the FFT can still extract the bridge frequency and the first two bridge frequencies are recognized as 2.693Hz and 9.874Hz respectively. Similar to the effect of noise, the following band-pass filtering process can partially remove the component of response generated by the uneven road surface from the vehicle response. Therefore, the proposed approach can still improve the bridge frequency. The results are shown in Fig. 16. As expected, it provides the highly precious identification. When the road roughness condition is worse, the FFT may not extract the bridge frequency directly from a passing vehicle acceleration. The concept of subtracting signals from identical axles is a promising way to overcome it (González, Obrien et al. 2012, Yang, Li et al. 2012).

5. Potential application and challenges

As one of the most important parameters of bridges, frequencies can be used to detect structural damage through frequencies change (Carden 2004). In this study, bridge damage is simulated using the method proposed by Sinha, Friswell et al. (2002), where the damage is assumed to be extended over a region of three times the beam depth. The element stiffness in this damage region varies from a minimum value at the exact crack location to full stiffness at the edge of the damaged area. The damage level is defined as a ratio of the depth of the crack to the depth of the intact bridge. For example, if the damage level is 0.2 or 20%, it means that the crack depth is 0.16 meters for a 0.8 meters deep bridge.

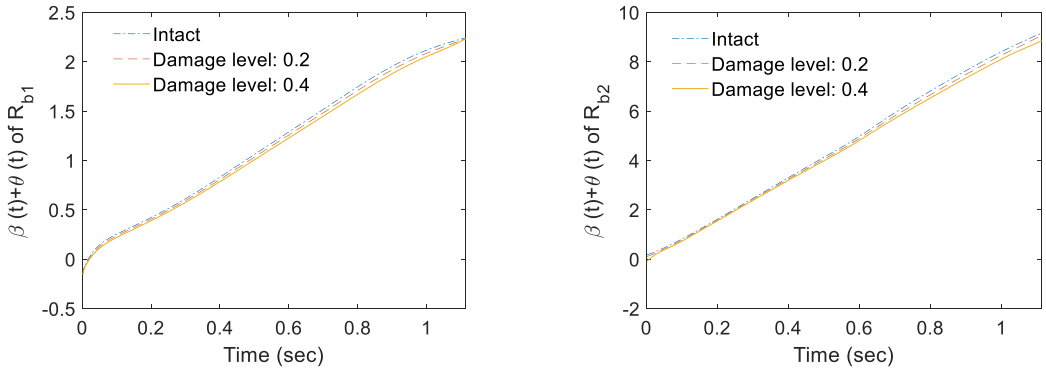

(a) R_{b1} (b) R_{b2}

Fig. 17. β(t)+θ(t) plots at different damage levels

The FFT method, as mentioned previously, could not be used to accurately identify the bridge frequency at higher speeds. This is due to the low frequency resolution associated with higher vehicle speeds. Therefore, and for the same reason, FFT cannot be used to monitor the shift in the bridge frequency due to structural damages. The frequency step of FFT will not pick up the minor changes happened to the bridge frequency due to structural

damages. Therefore, the next section will focus only on using the HT based approach to track the change in the bridge frequency due to the existence of structural damages.

In this case, the damage located at the 0.7L (L=span length) of the bridge. The bridge is modeled three times, one as an intact bridge, and other two cases of different damage levels (e.g. 20% and 40%). By following the procedures mentioned above using the same band-pass filter, Fig. 17 illustrates results of $\beta(t) + \theta(t)$ plots representing the final bridge identification. Herein, all parameters of the VBI model are kept same with the above and the vehicle velocity is 18m/s. As it has shown, there is clear difference of slope in $\beta(t) + \theta(t)$ plots in these three cases. With the increase of damage level, the slope in $\beta(t) + \theta(t)$plots representing bridge frequency decreases, which can point out the drop of bridge natural frequency due to the structural damage.

Similarly, different velocities (6m/s, 8m/s, 10m/s, 12m/s and 14m/s) are studied, and the results are illustrated in Fig. 18 and Fig. 19. In this study, other parameters of VBI remain identical to that studied previously.

As they are shown, with the increment of damage level, the theoretical frequencies of bridge decrease ($f_{TI} > f_{TD1} > f_{TD2}$). Similarly, the identified frequencies of damaged bridge decrease as well ($f_{II} > f_{ID1} > f_{ID2}$). Although the improved bridge frequencies applying HT based approach are not exact to the theoretical ones, the drop of frequencies is clearly found. The error is less than 2.77% for the 1st bridge frequency and 1.16% for the 2nd bridge frequency. It has concluded that the proposed approach is not restricted to frequency resolution, which is able to point out the frequencies drop due to the structural damage. This may indicate a promising way to estimate bridge conditions. However, it is observed that the frequency changes are small/less than 0.1 Hz and 0.3 Hz, for 1st and 2nd mode shape

respectively. The result is consistent with Chen, Spyrakos et al. (1995) presented that the lower frequencies are not sensitive to structural damage, usually less than 5%. The higher modes have demonstrated to achieve improved identification results, but they are usually unavailable in the field (Salawu 1997). In practical, it is difficult to detect this kind of small change, because of the effect of environment, e.g. noise and temperature. Chen, Spyrakos et al. (1995) showed that the environment can have a significant effect on the results, and can be as high as 5-10%.

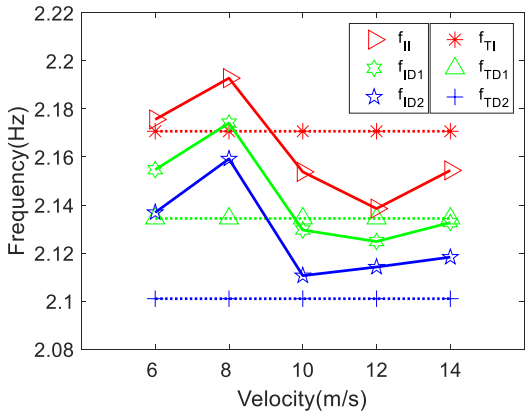

Fig. 18. The 1st bridge frequency estimation at different bridge conditions (*Note: f_{TI} presents the 1st theoretical frequency of the intact bridge, f_{TD1} presents the 1st theoretical frequency of the damaged bridge at level 0.2, f_{TD2} presents the 1st theoretical frequency of the damaged bridge at level 0.4, f_{II} presents the 1st identified frequency of the intact bridge, f_{ID1} presents the 1st identified frequency of the damaged bridge at level 0.2, fID2 presents the 1st identified frequency of the damaged bridge at level 0.4)

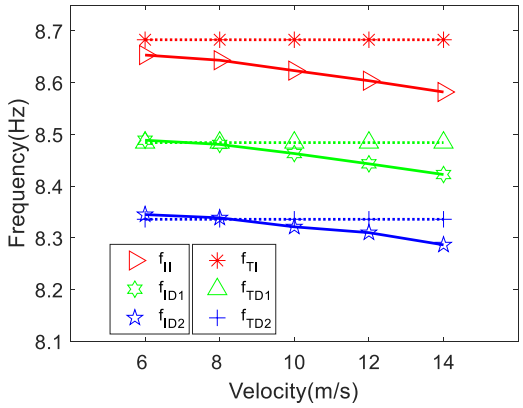

Fig. 19. The 2nd bridge frequency estimation at different bridge conditions (* Note: f_{TI} presents the 2nd theoretical frequency of the intact bridge, f_{TD1} presents the 2nd theoretical frequency of the damaged bridge at level 0.2, f_{TD2} presents the 2nd theoretical frequency of the damaged bridge at level 0.4, f_{II} presents the 2nd identified frequency of the intact bridge, f_{ID1} presents the 2nd identified frequency of the damaged bridge at level 0.2, fID2 presents the 2nd identified frequency of the damaged bridge at level 0.4)

CONCLUSIONS

This paper introduces a new approach combined with HT and band-pass filter technique to improve the bridge natural frequency identification from a passing vehicle. The proposed approach improves the identified frequency iteratively, where the initial value can be achieved by applying FFT directly. In contrast to FFT, the proposed approach is not restricted to the frequency resolution. Hence, this paper preliminarily found that the proposed approach is able to detect the frequencies drop due to the bridge structural damage. In this regard, it is a promising way to estimate bridge conditions. However, the observed drop is very small in addition to the environment effect, which may limit the

effectiveness of the proposed approach to structural damage detection. Nevertheless, it has shown improved identification of bridge frequencies over than FFT, without limitation to resolution. In addition, the proposed approach is not sensitive to vehicle velocity and signal noise.

ACKNOWLEDGMENT

This research is sponsored by National Science of Foundation (NSF-CNS-1645863). Any opinions, findings, and conclusions or recommendations expressed in this publication are those of the authors and do not necessarily reflect the view of the sponsors.

REFERENCES

Carden, E. P. (2004). "Vibration Based Condition Monitoring: A Review." Structural Health Monitoring 3(4): 355-377.

Cebon, D. (1999). Handbook of vehicle-road interaction.

Chen, H., et al. (1995). "Evaluating structural deterioration by dynamic response." Journal of Structural Engineering 121(8): 1197-1204.

Chupanit, P. and C. Phromsorn (2012). "The importance of bridge health monitoring." International Science Index 6: 135-138.

Cunha, A., et al. "An indirect bridge inspection method incorporating a wavelet-based damage indicator and pattern recognition."

Deng, L. and C. Cai (2009). "Bridge model updating using response surface method and

genetic algorithm." Journal of Bridge Engineering 15(5): 553-564.

González, A., et al. (2012). "Identification of damping in a bridge using a moving instrumented vehicle." Journal of Sound and Vibration 331(18): 4115-4131.

Hester, D. and A. González (2012). "A wavelet-based damage detection algorithm based on bridge acceleration response to a vehicle." Mechanical Systems and Signal Processing 28: 145-166.

Huang, N. E. (2014). "Hilbert–Huang Transform and Its Applications." 16.

ISO, I. (1995). Mechanical vibration-Road surface profiles-Reporting of measured data, International Organization for Standardization (ISO) Geneva.

Keenahan, J., et al. (2013). "The use of a dynamic truck-trailer drive-by system to monitor bridge damping." Structural Health Monitoring 13(2): 143-157.

Khorram, A., et al. (2012). "Comparison studies between two wavelet based crack detection methods of a beam subjected to a moving load." International Journal of Engineering Science 51: 204-215.

Lin, C. W. and Y. B. Yang (2005). "Use of a passing vehicle to scan the fundamental bridge frequencies: An experimental verification." Engineering Structures 27(13): 1865-1878.

Mahato, S., et al. (2017). "Combined wavelet–Hilbert transform-based modal identification of road bridge using vehicular excitation." Journal of Civil Structural Health Monitoring 7(1): 29-44.

Malekjafarian, A., et al. (2015). "A Review of Indirect Bridge Monitoring Using Passing Vehicles." Shock and Vibration 2015: 1-16.

Malekjafarian, A. and E. J. Obrien (2014). "Identification of bridge mode shapes using

Short Time Frequency Domain Decomposition of the responses measured in a passing vehicle." Engineering Structures 81: 386-397.

Malekjafarian, A. and E. J. Obrien (2017). "On the use of a passing vehicle for the estimation of bridge mode shapes." Journal of Sound and Vibration 397: 77-91.

McGetrick, P. J. and C. W. Kim (2013). "A Parametric Study of a Drive by Bridge Inspection System Based on the Morlet Wavelet." Key Engineering Materials 569-570: 262-269.

Nguyen, K. V. and H. T. Tran (2010). "Multi-cracks detection of a beam-like structure based on the on-vehicle vibration signal and wavelet analysis." Journal of Sound and Vibration 329(21): 4455-4465.

Obrien, E. J. and A. Malekjafarian (2016). "A mode shape-based damage detection approach using laser measurement from a vehicle crossing a simply supported bridge." Structural Control and Health Monitoring 23(10): 1273-1286.

Obrien, E. J., et al. (2017). "Application of empirical mode decomposition to drive-by bridge damage detection." European Journal of Mechanics - A/Solids 61: 151-163.

Oshima, Y., et al. (2014). "Damage assessment of a bridge based on mode shapes estimated by responses of passing vehicles." Smart Structures and Systems 13(5): 731-753.

Salawu, O. (1997). "Detection of structural damage through changes in frequency: a review." Engineering Structures 19(9): 718-723.

Sinha, J. K., et al. (2002). "Simplified Models for the Location of Cracks in Beam Structures Using Measured Vibration Data." Journal of Sound and Vibration 251(1): 13-38.

Tan, C., et al. (2017). "“Drive-by” bridge frequency-based monitoring utilizing wavelet

transform." Journal of Civil Structural Health Monitoring 7(5): 615-625.

Tan, C., et al. (2017). Wavelet Based Damage Assessment and Localization for Bridge Structures. 26th ASNT Research Symposium.

Tan, C., et al. (2019). "Extraction of Bridge Modal Parameters Using Passing Vehicle Response." Journal of Bridge Engineering 24(9): 04019087.

Wang, W., et al. (2016). "Number of stress cycles for fatigue design of simply-supported steel I-girder bridges considering the dynamic effect of vehicle loading." Engineering Structures 110: 70-78.

Yang, Y. B. and K. C. Chang (2009). "Extracting the bridge frequencies indirectly from a passing vehicle: Parametric study." Engineering Structures 31(10): 2448-2459.

Yang, Y. B. and K. C. Chang (2009). "Extraction of bridge frequencies from the dynamic response of a passing vehicle enhanced by the EMD technique." Journal of Sound and Vibration 322(4-5): 718-739.

Yang, Y. B., et al. (2012). "Using two connected vehicles to measure the frequencies of bridges with rough surface: a theoretical study." Acta Mechanica 223(8): 1851-1861.

Yang, Y. B., et al. (2014). "Constructing the mode shapes of a bridge from a passing vehicle: a theoretical study." Smart Structures and Systems 13(5): 797-819.

Yang, Y. B. and C. W. Lin (2005). "Vehicle–bridge interaction dynamics and potential applications."

Zhang, Y., et al. (2012). "Damage detection by mode shape squares extracted from a passing vehicle." Journal of Sound and Vibration 331(2): 291-307.

EXTRACTION OF BRIDGE MODAL PARAMETERS USING PASSING VEHICLE RESPONSE

by

CHENGJUN TAN
NASIM UDDIN
EUGENE J. OBRIEN
PATRICK J MCGETRICK
CHUL-WOO KIM

Journal of Bridge Engineering, Volume 24, Issue 9

Format adapted [and errata corrected] for dissertation

EXTRACTION OF BRIDGE MODAL PARAMETERS USING PASSING VEHICLE RESPONSE

Abstract

Bridge modal parameters play an important role in bridge engineering; they can serve as useful indices for many applications such as numerical mode calibration and updating, and bridge structural health monitoring. Recently, the indirect monitoring of bridges is increasingly investigated and developed as it avoids the need for instrumentation on all bridges of a network. The natural frequencies of bridge have been extracted from the dynamic response of a vehicle numerically and in the field. This paper proposes an algorithm to extract the bridge mode shapes using indirect measurement enhanced by the Hilbert Transform as well as the damping ratio of the bridge. The theoretical closed-form equations are derived for a vehicle-bridge interaction model where the vehicle is represented as a moving sprung mass passing over a simply supported beam at a constant low speed. Then a numerical simulation with a quarter-car model is adopted to verify the proposed algorithm, including case studies on the influence of the vehicle speed and road roughness. In addition, a laboratory test is conducted to further investigate the feasibility of the proposed algorithm.

Keyword: Structural health monitoring; Bridge; Modal parameters; Drive-by; Hilbert Transform; Vehicle-bridge interaction.

Introduction

Bridge structures are an intrinsic part of any transportation network. Assessing the condition of these structures is essential to ensure the required level of safety and effective operation of transport facilities. In order to maintain the bridge structural integrity, it is necessary to estimate the extent and location of structural damage through periodic monitoring. Over the past two decades, as an alternative to manual inspection, there is increasing interest in electronic monitoring of bridges, referred to as Structural Health Monitoring (SHM), often by obtaining modal parameters of the bridge from dynamic vibration (Carden 2004; Chang et al. 2003; Chrysostomou and Stassis 2008; Doebling et al. 1998; Magalhães et al. 2012). Generally, to identify the bridge modal parameters, quite a number of sensors need to be installed directly on the bridge deck to record dynamic responses through vibration experiments. Many related research projects, both numerical and experimental, have been carried out (Deng and Cai 2009; Grande and Imbimbo 2016; Magalhães et al. 2012).

Recently, the idea of indirect measurement for bridge monitoring has gained popularity as a field of research, which is first proposed by Yang et al. (2004). This refers to use of the response measured indirectly in a passing vehicle to extract dynamic properties of bridges (Lin and Yang 2005; Yang and Lin 2005). Via vehicle/bridge dynamic interaction, the vehicle suspension system is excited by the bridge displacement as well as by the surface roughness (Malekjafarian and Obrien 2017; Wang et al. 2016). Therefore, it is possible to identify the bridge modal parameters from the indirect measurement, if there is enough measurement time and a sufficiently smooth road surface profile. In comparison with the traditional approaches, where a limited number of sensors

are mounted on the bridge, the indirect approach offers much more spatial information, as well as higher resolution in mode shapes, because the instrumented vehicle can receive the vibration characteristics of each point as it passes over the entire bridge (Deng and Cai 2009; Yang et al. 2014). In principal, only one sensor needs to be deployed on the vehicle.

Through this concept of indirect measurement, the natural frequencies of bridges have been extracted from the dynamic responses of vehicles, both numerically and in practice (Deng et al. 2019; McGetrick et al. 2009; Tan et al. 2017; Tan et al. 2018; Yang and Lin 2005; Yang and Chang 2009). A small number of studies estimate the bridge damping ratio using an instrumented vehicle (González et al. 2012; Keenahan et al. 2013; McGetrick et al. 2009). McGetrick et al. (2009) showed that in the spectra of vehicle accelerations, the intensity of Power Spectral Density (PSD) at both bridge and vehicle frequency peaks, decreases with increased bridge damping. As a result, the changes in the magnitude of PSD can be used as an indicator of damage in the bridge (Keenahan et al. 2013). In a theoretical study, González et al. (2012) adopt a half-car Vehicle Bridge Interaction (VBI) model with a road profile, to assess bridge damping by minimizing the sum of squared errors and hence estimate damping.

In an alternative strategy, a number of researchers have studied the feasibility of constructing the bridge mode shapes using indirect measurements (Kong et al. 2016; Kong et al. 2017; Malekjafarian and Obrien 2014; Malekjafarian and Obrien 2017; Marulanda et al. 2017; Obrien and Malekjafarian 2016; Oshima et al. 2014; Yang et al. 2014; Zhang et al. 2012). Zhang et al. (2012) first attempted an indirect approach to the extraction of mode shape-related characteristics of a bridge and verify its feasibility numerically and experimentally. They proposed the installation of a controllable shaker on a vehicle and

the recording of the applied forces. Oshima et al. (2014) proposed a multi-axle truck-trailer convoy system for bridge damage detection and estimated the mode shape using an indirect approach. The vehicles perform two functions, both exciting the bridge and measuring the response to that excitation at three or more moving points simultaneously. For *N* trailers, *N* segments of bridge response are recorded at the same time at different locations on the bridge. By applying Singular Value Decomposition to these signals, a mode shape vector containing *N* components, corresponding to the defined areas, are identified for each mode. This approach finds the mode shapes, but with low resolution.

Malekjafarian and Obrien (2014) proposed a novel algorithm which uses Short Time Frequency Domain Decomposition to estimate bridge mode shapes from the dynamic response of the vehicle, an improvement on the concept proposed in by Malekjafarian and Obrien (2017); (Obrien and Malekjafarian 2016). However it has only been verified in numerical studies so far. Kong et al. (2016) proposed a method using a specialized vehicle consisting of a tractor and two following trailers to extract the bridge modal properties, which can eliminate the effect of road roughness and the driving-related frequencies from the vehicle response, and numerically verified it. Marulanda et al. (2017) developed an approach of mode shapes identification using mobile sensors under harmonic excitation.

Yang et al. (2014) theoretically developed the possibility of constructing the bridge mode shapes directly from a transform of the measured response on a passing vehicle; they used the Hilbert Transform (HT). This algorithm is considered as a single-input-single-output system where the bridge is only excited by one moving point under the wheel and the response is measured at the same point. It neglects bridge damping, which is found to have a non-negligible impact on the extracted mode shapes.

This paper proposes an algorithm to extract the damping ratios and mode shapes of bridges from indirect measurements considering the bridge damping, enhanced by HT. First the theoretical closed-form solution is derived based on a simple VBI model where the vehicle is represented by a moving sprung mass and is passing over a simply supported beam at a constant low speed. Then, through numerical simulation, the feasibility of the new approach is demonstrated and the factors that affect the accuracy of the proposed algorithm are investigated. Finally, a laboratory experiment is carried out to further demonstrate the feasibility of the proposed algorithm.

Hilbert Transform

The Hilbert transform (HT) of a function, $s(t)$, is defined by:

$$\hat{s}(t) = H\big(s(t)\big) = \frac{1}{\pi} P.V. \int_{-\infty}^{+\infty} \frac{s(\tau)}{t-\tau} d\tau \quad (1)$$

in which *P.V.* denotes the Cauchy principal value. In practice, HT is defined as the convolution of $s(t)$ with a unit impulse function of $P.V.1/\pi t$. The HT has a particularly simple representation in the frequency domain: it imparts a phase shift of 90° to every Fourier component of a function, i.e. $H(\cos(\omega t)) = \cos(\omega t - \pi/2)$, where $\omega > 0$. Using the signal of $s(t)$and $\hat{s}(t)$, one can obtain an analytical signal, $z(t)$, represented by the sum of real and imaginary parts, as follows:

$$z(t) = s(t) + i\hat{s}(t) = A(t)e^{i\theta(t)} \quad (2)$$

where

$$A(t) = \sqrt{s^2(t) + \hat{s}^2(t)};\ \theta(t) = tan^{-1}\left(\frac{\hat{s}(t)}{s(t)}\right) \quad (3)$$

The time-dependent functions, $A(t)$ and $\theta(t)$, represent the instantaneous amplitude and instantaneous phase of the analytical signal, respectively. It is well known that the instantaneous amplitude function, (t), can be regarded as the envelop function of $s(t)$ (Huang 2014). The HT has the basic property of linearity, i.e., if a_1 and a_2 are arbitrary (complex) scalars, and $g_1(t)$ and $g_2(t)$ are signals, then

$$H\big(a_1\, g_1(t) + a_2\, g_2(t)\big) = a_1\, \hat{g}_1(t) + a_2\, \hat{g}_2(t) \quad (4)$$

Further, the HT behaves well with respect to convolution, since

$$H\big(\, g_1(t) *\, g_2(t)\big) = \hat{g}_1(t) *\, g_2(t) = \, g_1(t) *\, \hat{g}_2(t) \quad (5)$$

Theoretical Formula and Algorithm

Analytical Theory

To highlight the dynamic characteristics of the coupled vehicle and bridge interaction (VBI), a simply-supported beam traversed by a sprung mass vehicle is considered (Figure 1) (Brady et al. 2006; Frýba 2013). The following assumptions are adopted without losing the generality of the problem: (1) the beam is of the Bernoulli–Euler type with constant cross section; (2) only a single moving vehicle is considered passing on the beam at any one time; (3) the vehicle mass is assumed to be small compared with that of the bridge, and the inertial effect of the vehicle is neglected; (4) the vehicle passes over the beam at a constant speed; (5) the damping of the beam is of the Rayleigh

type; (6) road roughness is ignored in the derivation and (7) before the arrival of the vehicle, the bridge is at rest.

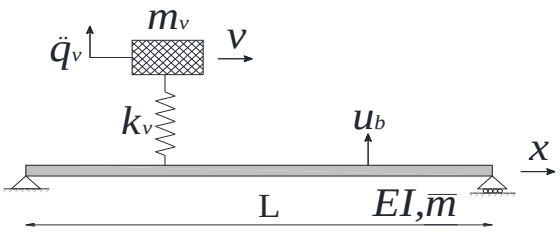

Figure 1. Theoretical model of vehicle and bridge

As shown in Figure 1, the vehicle is simply modeled as a lumped mass m_v, supported by a spring of stiffness k_v and it passes over a simply supported beam of length L. The modeled beam is assumed to be of constant mass density $\bar{m}$ per unit length, have constant bending rigidity EI, external damping coefficient, $c_{b,e}$, and internal damping coefficient $c_{b,i}$. The external damping system represents the resistance in some types of bearing; the internal damping system characterizes the viscoelastic properties of the material. Based on these assumptions, the equations of motion for the bridge and vehicle are:

$$\bar{m}\ddot{u} + c_{b,e}\dot{u} + c_{b,i}I\,\dot{u}'''' + EIu'''' = f_c(t)\delta(x - vt) \qquad (6)$$

$$m_v\ddot{q}_v + k_v(q_v - u|_{x=vt}) = 0 \qquad (7)$$

where $u(x,t)$ denotes the vertical displacement of the modeled beam; $q_v(t)$ denotes the vertical displacement of the vehicle, measured from its static equilibrium position, and a dot and a prime represent the derivative with respect to time t and with respect to longitudinal coordinate x, respectively.

With the assumption that the bridge mass is much greater than the vehicle mass ($m_v/\bar{m}L \ll 1$), the total displacement response of the bridge to the moving vehicle can be expressed as (Yang et al. 2004):

$$u(x,t) = \frac{\Delta_{st,n}}{\sqrt{(1-S_n^2)^2+4S_n^2\varepsilon_{b,n}^2}} \times \left[\sin\left(\frac{n\pi vt}{L} - \alpha\right) sin\frac{n\pi vt}{L} - \frac{S_n}{\sqrt{1-\varepsilon_{b,n}^2}} e^{-\varepsilon_{b,n}\omega_{b,n}t} \sin(\omega_{d,n}t - \beta) sin\frac{n\pi vt}{L} \right] \quad (8)$$

where $\omega_{b,n}$ represents the natural frequency of the bridge for the n^{th} mode, $\varepsilon_{b,n}$ is the corresponding damping ratio; ω_v is the vibration frequency of the vehicle; α and β are the phase angles; $\Delta_{st,n}$ is the static deflection induced by the vehicle for the n^{th} mode; S_n is a non-dimensional speed parameter, and $\omega_{d,n}$ is the damped frequency of vibration of the beam and,

$$\omega_{b,n} = (\frac{n\pi}{L})^2 \sqrt{\frac{EI}{\bar{m}}} \quad (9)$$

$$\varepsilon_{b,n} = 2\bar{m}\omega_{b,n} \quad (10)$$

$$\omega_v = \sqrt{\frac{k_v}{m_v}} \quad (11)$$

$$\alpha = \tan^{-1}(\frac{2S_n\varepsilon_{b,n}}{1-S_n^2}) \quad (12)$$

$$\beta = \tan^{-1}(\frac{2\varepsilon_{b,n}\sqrt{1-\varepsilon_{b,n}^2}}{1-S_n^2-2\varepsilon_{b,n}^2}) \quad (13)$$

$$S_n = \frac{n\pi v}{L\omega_{b,n}} \quad (14)$$

$$\Delta_{st,n} = \frac{-2\omega_v g L^3}{n^4\pi^4 EI} \quad (15)$$

$$\omega_{d,n} = \sqrt{1-\varepsilon_{b,n}^2}\,\omega_{b,n} \quad (16)$$

Substituting the total displacement of the bridge, $u(x,t)$ in Eq. (8), one can obtain the vehicle displacement by Duhamel's integral (Hu and Tang 2005) and differentiating it twice to obtain the vehicle acceleration response as:

$$\ddot{q}_v(t) = \sum_n \frac{\Delta_{st,n}}{2\sqrt{(1-S_n^2)^2+4S_n^2\varepsilon_{b,n}^2}}\left\{\bar{\bar{A}}_{1,n}\cos\left(\frac{2n\pi vt}{L}-\alpha\right)+\bar{\bar{A}}_{2,n}cos(\omega_v t+\alpha)+\right.$$

$$\bar{\bar{A}}_{3,n}\cos(\omega_v t-\alpha)+e^{-\varepsilon_{b,n}\omega_{b,n}t}\left[\bar{\bar{A}}_{4,n}cos(\omega_v t+\beta)+\bar{\bar{A}}_{5.n}sin(\omega_v t+\beta)+\right.$$

$$\bar{\bar{A}}_{6.n}cos\left(\omega_{b,n}t+\frac{n\pi vt}{L}-\beta\right)+\bar{\bar{A}}_{7.n}\cos\left(\omega_{b,n}t-\frac{n\pi vt}{L}-\beta\right)+\bar{\bar{A}}_{8.n}sin\left(\omega_{b,n}t+n\pi vt/\right.$$

$$\left.\left.L-\beta\right)+\bar{\bar{A}}_{9.n}\sin\left(\omega_{b,n}t-n\pi vt/L-\beta\right)\right]\right\}(17)$$

where the coefficients of $\bar{\bar{A}}_{6,n}$, $\bar{\bar{A}}_{7,n}$, $\bar{\bar{A}}_{8,n}$ and $\bar{\bar{A}}_{9,n}$ as follow (others are also constant non-time coefficients and are not presented here, as they are not of concern in this study):

$$\bar{\bar{A}}_{6,n} = \frac{-S_n\omega_{b,n}^2}{2\sqrt{1-\varepsilon_{b,n}^2}}\left\{\frac{\mu_n(1+S_n)^3+\varepsilon_{b,n}^2\mu_n(1+S_n)+(1+S_n)^2-\varepsilon_{b,n}^2}{\left[(\mu_n(1+S_n)+1)^2+\varepsilon_{b,n}^2\mu_n^2\right]}+\right.$$

$$\left.\frac{-\mu_n(1+S_n)^3-\varepsilon_{b,n}^2\mu_n(1+S_n)+(1+S_n)^2-\varepsilon_{b,n}^2}{\left[(\mu_n(1+S_n)-1)^2+\varepsilon_{b,n}^2\mu_n^2\right]}\right\}(18)$$

$$\bar{\bar{A}}_{7,n} = \frac{-S_n\omega_{b,n}^2}{2\sqrt{1-\varepsilon_{b,n}^2}}\left\{\frac{-\mu_n(1-S_n)^3-\varepsilon_{b,n}^2\mu_n(1-S_n)-(1-S_n)^2+\varepsilon_{b,n}^2}{\left[(\mu_n(1-S_n)+1)^2+\varepsilon_{b,n}^2\mu_n^2\right]}+\right.$$

$$\left.\frac{\mu_n(1-S_n)^3+\varepsilon_{b,n}^2\mu_n(1-S_n)-(1-S_n)^2+\varepsilon_{b,n}^2}{\left[(\mu_n(1-S_n)-1)^2+\varepsilon_{b,n}^2\mu_n^2\right]}\right\} \qquad (19)$$

$$\bar{\bar{A}}_{8,n} = \frac{-S_n\omega_{b,n}^2\varepsilon_{b,n}}{2\sqrt{1-\varepsilon_{b,n}^2}}\left\{\frac{-\mu_n(1+S_n)^2-\varepsilon_{b,n}^2\mu_n-2(1+S_n)}{\left[(\mu_n(1+S_n)+1)^2+\varepsilon_{b,n}^2\mu_n^2\right]}+\frac{\mu_n(1+S_n)^2+\varepsilon_{b,n}^2\mu_n-2(1+S_n)}{\left[(\mu_n(1+S_n)-1)^2+\varepsilon_{b,n}^2\mu_n^2\right]}\right\} \qquad (20)$$

$$\bar{\bar{A}}_{9,n} = \frac{-S_n\omega_{b,n}^2\varepsilon_{b,n}}{2\sqrt{1-\varepsilon_{b,n}^2}}\left\{\frac{\mu_n(1-S_n)^2+\varepsilon_{b,n}^2\mu_n+2(1-S_n)}{\left[(\mu_n(1-S_n)+1)^2+\varepsilon_{b,n}^2\mu_n^2\right]}+\frac{-\mu_n(1-S_n)^2-\varepsilon_{b,n}^2\mu_n+2(1-S_n)}{\left[(\mu_n(1-S_n)-1)^2+\varepsilon_{b,n}^2\mu_n^2\right]}\right\} \qquad (21)$$

where $\mu_n = \frac{\omega_{b,n}}{\omega_v}$ (22)

To successfully identify the mode shape of a bridge, the component response corresponding to the frequency of the n^{th} bridge mode should be singled out from the vehicle accelerations, which is feasible by implementing an appropriate signal processing

tool, such as the band-pass filters or singular spectrum analysis (Yang et al. 2014). In this way, the extracted bridge component response associated with the n^{th} mode is

$$R_b = e^{-\varepsilon_{b,n}\omega_{b,n}t}\left[\bar{\bar{A}}_{6.n}cos\left(\omega_{b,n}t+\frac{n\pi vt}{L}-\beta\right)+\bar{\bar{A}}_{7.n}\cos\left(\omega_{b,n}t-\frac{n\pi vt}{L}-\beta\right)+\right.$$

$$\left.\bar{\bar{A}}_{8.n}sin\left(\omega_{b,n}t+n\pi vt/L-\beta\right)+\bar{\bar{A}}_{9.n}\sin\left(\omega_{b,n}t-n\pi vt/L-\beta\right)\right] \quad (23)$$

Then this extracted R_b is processed by the HT to yield its transform pair,

$$\hat{R}_b = e^{-\varepsilon_{b,n}\omega_{b,n}t}\left[\bar{\bar{A}}_{6.n}sin\left(\omega_{b,n}t+\frac{n\pi vt}{L}-\beta\right)+\bar{\bar{A}}_{7.n}\sin\left(\omega_{b,n}t-\frac{n\pi vt}{L}-\beta\right)-\right.$$

$$\left.\bar{\bar{A}}_{8.n}sin\left(\omega_{b,n}t+\frac{n\pi vt}{L}-\beta\right)-\bar{\bar{A}}_{9.n}\sin\left(\omega_{b,n}t-n\pi vt/L-\beta\right)\right] \quad (24)$$

If the vehicle moves slowly enough, the driving frequency $n\pi v/L$ is regarded as much less than the bridge frequency $\omega_{b,n}$, i.e. $S_n \ll 1$. Accordingly, the coefficients of R_b and $\hat{R}_b$ reduce to the following:

$$\bar{\bar{A}}_{6,n} = -\bar{\bar{A}}_{7,n} = \frac{-S_n\omega_{b,n}^2}{2\sqrt{1-\varepsilon_{b,n}^2}}\left\{\frac{\mu_n+\varepsilon_{b,n}^2\mu_n+1-\varepsilon_{b,n}^2}{[(\mu_n+1)^2+\varepsilon_{b,n}^2\mu_n^2]}+\frac{-\mu_n-\varepsilon_{b,n}^2\mu_n+1-\varepsilon_{b,n}^2}{[(\mu_n-1)^2+\varepsilon_{b,n}^2\mu_n^2]}\right\} \quad (25)$$

$$\bar{\bar{A}}_{8,n} = -\bar{\bar{A}}_{9,n} = \frac{-S_n\omega_{b,n}^2\varepsilon_{b,n}}{2\sqrt{1-\varepsilon_{b,n}^2}}\left\{\frac{-\mu_n-\varepsilon_{b,n}^2\mu_n-2}{[(\mu_n+1)^2+\varepsilon_{b,n}^2\mu_n^2]}+\frac{\mu_n+\varepsilon_{b,n}^2\mu_n-2}{[(\mu_n-1)^2+\varepsilon_{b,n}^2\mu_n^2]}\right\} \quad (26)$$

Therefore, from Eq. (3), the instantaneous amplitude of R_b can be obtained as

$$A(t) = \sqrt{R_b^2(t)+\hat{R}_b^2(t)} = 2\sqrt{\bar{\bar{A}}_{6,n}^2+\bar{\bar{A}}_{8,n}^2}e^{-\varepsilon_{b,n}\omega_{b,n}t}\left|sin\frac{n\pi vt}{L}\right| \quad (27)$$

Replacing x with vt in Eq. (27) yields

$$A\left(\frac{x}{v}\right) = \sqrt{R_b^2(t)+\hat{R}_b^2(t)} = 2\sqrt{\bar{\bar{A}}_{6,n}^2+\bar{\bar{A}}_{8,n}^2}e^{-\varepsilon_{b,n}\omega_{b,n}x/v}\left|sin\frac{n\pi x}{L}\right| \quad (28)$$

In comparison with Yang et al. (Yang et al. 2014), Eq. (28) shows that the amplitude history $A(\frac{x}{v})$ of the extracted component response includes the mode shape function $sin\frac{n\pi x}{L}$ of the bridge (in absolute value) multiplied by a constant non-time (or position)-

related coefficient, $2\sqrt{\bar{\bar{A}}_{6,n}^2 + \bar{\bar{A}}_{8,n}^2}$. However, the bridge damping is observed to shift the mode shape in the amplitude history. The following numerical study will provide evidence that the mode shape shift caused by bridge damping is non- negligible. Therefore, the construction of the mode shape from the amplitude of HT needs to be reformulated as $A_{mod,n} = A\left(\frac{x}{v}\right)/e^{-\varepsilon_{b,n}\omega_{b,n}x/v}$ and its normalization, which is feasible when the speed of the test vehicle is constant.

Algorithm

In the analytical theory, there is a significant assumption that the vehicle mass is negligible compared to the bridge mass. In addition, the most important point of the proposed algorithm is to keep the vehicle speed as low-and-constant as possible. Its effect on accuracy will be investigated through numerical simulation in the following. Based on the above derivation, the procedural steps for identifying the bridge modal parameters using a passing vehicle response, are as follows (see Figure 2):

(1) Record the axle acceleration, $R(t)$, during its passage over the bridge.

(2) Identify the bridge natural frequencies $\omega_{b,n}$ from the recorded signal, $R(t)$; this step can be carried out using signal processing techniques such as Fourier Transform (McGetrick et al. 2009; Yang and Lin 2005; Yang et al. 2014) or Wavelet Transform (Tan et al. 2017).

(3) Single out the component response associated with a bridge natural frequency from $R(t)$. Principally, with known frequency, $\omega_{b,n}$, the component response

$R_{b,n}(t)$ associated with $\omega_{b,n}$ can be extracted with standard signal processing tools, such as band-pass filtering or singular spectrum analysis. A band-pass filter is applied in this paper. In practice, selecting a suitable filter and obtaining the optimum $R_{b,n}(t)$, is another challenge. Here, the parameters are varied to overcome it. In a 3 dB bandwidth band-pass filter, the parameters of the central frequency, f_c and the quality factor, Q, determine the filter. The lower and upper cutoff frequencies are represented by $f_l = f_c(\sqrt{1+\frac{1}{4Q^2}} - \frac{1}{2Q})$ and $f_u = f_c(\sqrt{1+\frac{1}{4Q^2}} + \frac{1}{2Q})$, respectively. It is noted that a low Q factor gives a broad (wide) bandwidth, while a high Q factor gives a narrow (small) bandwidth. By changing the values of f_c and Q, the component response, $R_{b,n}(t)$, is found.

(4) From these responses, $R_{b,n}(t)$, the HT is computed to yield $\hat{R}_{b,n}(t)$, and then a series of instantaneous amplitudes, $A_n(t)$, calculated.

(5) Assuming a series of damping ratios, $\varepsilon_{b,n}$ each amplitude function is adjusted as $A\left(\frac{x}{v}\right)/e^{-\varepsilon_{b,n}\omega_{b,n}x/v}$ and normalized to find the mode shapes $A_{mod,n}$.

(6) Calculate the modal assurance criteria (MAC) of the achieved $A_{mod,n}$ values and compare to theoretical mode shapes.

(7) The value of $A_{mod,n}$ with the highest MAC is the bridge mode shape. Hence, for all $R_{b,n}(t)$ and $\varepsilon_{b,n}$, identify the maximum MAC and hence the final $A_{mod,n}$ and bridge damping ratio.

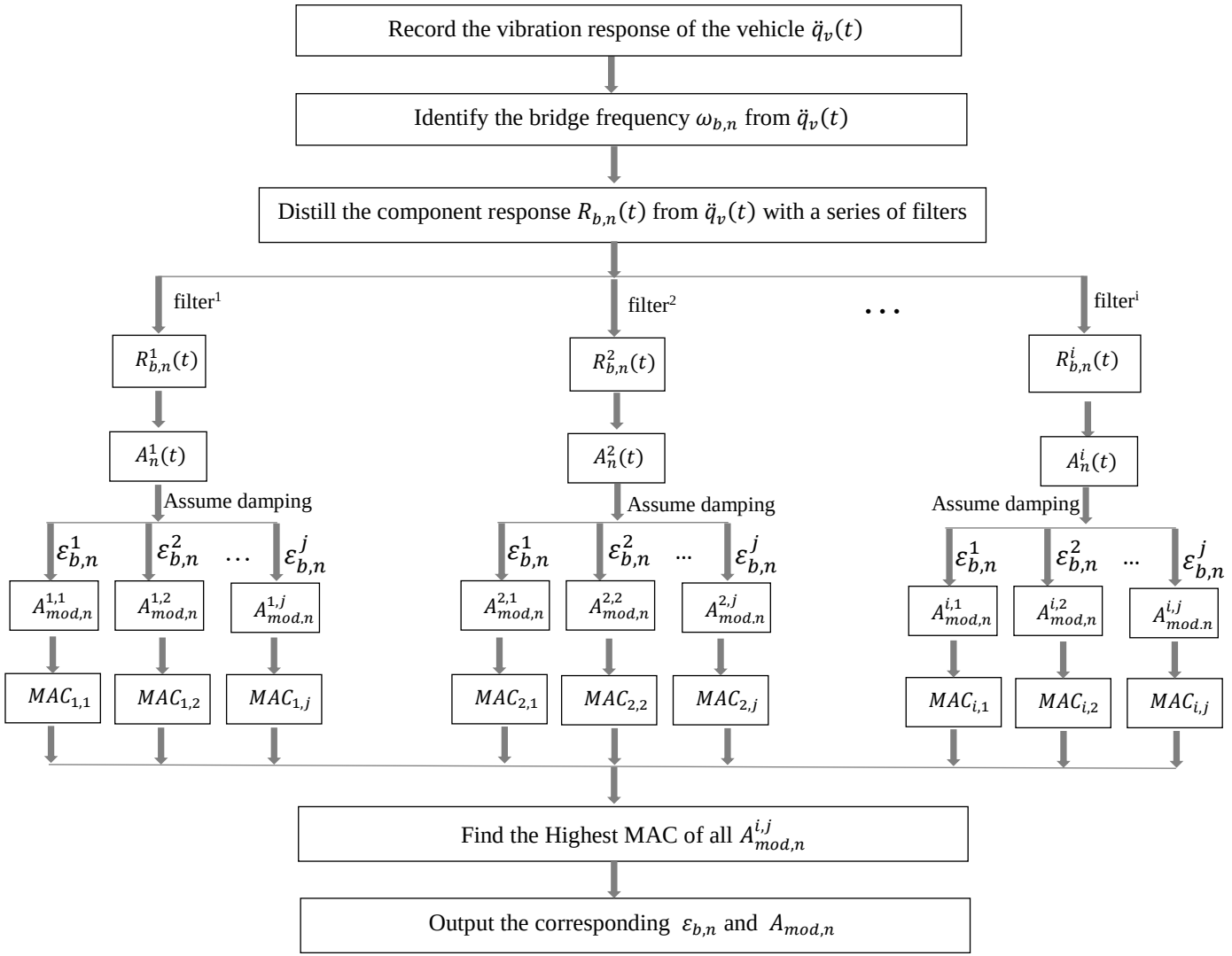

Figure 2. Flow chart

Numerical Simulation

To verify the feasibility of extracting the damping ratio and mode shapes of a bridge from a passing vehicle, a quarter-car VBI model is adopted as shown in *Figure 3*. The road surface profile is not considered at first and the vehicle is assumed to travel at constant speed. The vehicle and bridge properties, listed in Table 1, are based on the recommendations of (Cebon 1999). As shown in the proposed algorithm, it is essential to identify the bridge frequencies from the vehicle response. However, Yang and Lee (2018) pointed out that the higher vehicle damping tends to suppress the vehicle frequencies and make the bridge frequencies invisible of the vehicle's spectra. Besides, they also showed that the vehicle damping improves the identification of the first bridge frequency from vehicle's spectra considering the road surface roughness. Hence, a suitable vehicle damping is adopted here. The dynamic interaction between the vehicle and the bridge is modeled in MATLAB. Except where otherwise mentioned, the scanning frequency used is 200 Hz. The first two natural frequencies of the bridge, f_b, are 1.39 Hz and 5.56 Hz. The vehicle frequencies are 0.58 Hz and 8.65 Hz.

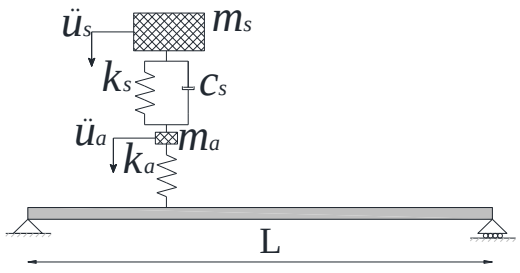

Figure 3. The VBI model used in simulations

Table 1. Vehicle and bridge properties

Vehicle properties		Bridge properties	
m_s	14000 kg	Span	25 m
k_s	200 kN/m	Density	4800 kg/m^3
c_s	10 kN s/m	Width	4 m
m_a	1000 kg	Depth	0.8 m
k_a	2750 kN/m	Modulus	2.75×10^{10} N/m^2

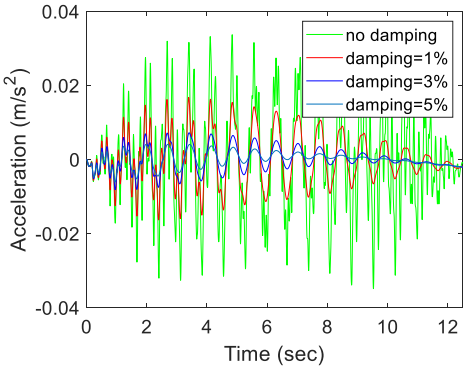

Figure 4. The vehicle acceleration responses

The Effect of Bridge Damping

Figure 4 illustrates the vehicle acceleration responses resulting from bridge damping for four scenarios: no damping, 1% (bridge) damping ratio, 3% damping ratio and 5% damping ratio. Rayleigh damping is applied in each case. To possess enough low speed of the moving vehicle as the assumption of theoretical analysis, 2 m/s is adopt in this case as suggestion of (Yang et al. 2014). These responses are processed by the fast Fourier

transform to yield the frequency spectrum as shown in *Figure 5*. The first identified frequency, at around 1.38 Hz, can be recognized as the first bridge frequency. Using band-pass filters, the component responses corresponding to the first identified bridge frequency are decomposed from the accelerations, as shown in *Figure 6* (a). The HT is applied to these filtered signals to yield the instantaneous amplitudes, $A(t)$, as shown in *Figure 6* (b).

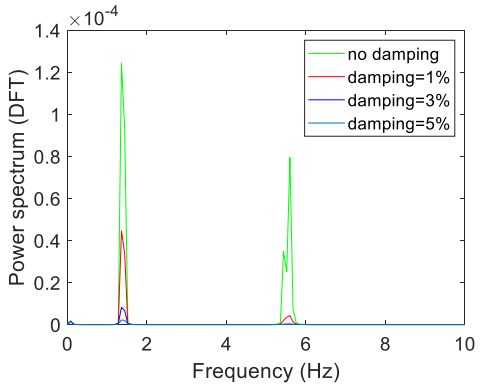

Figure 5. The spectrum of Accelerations

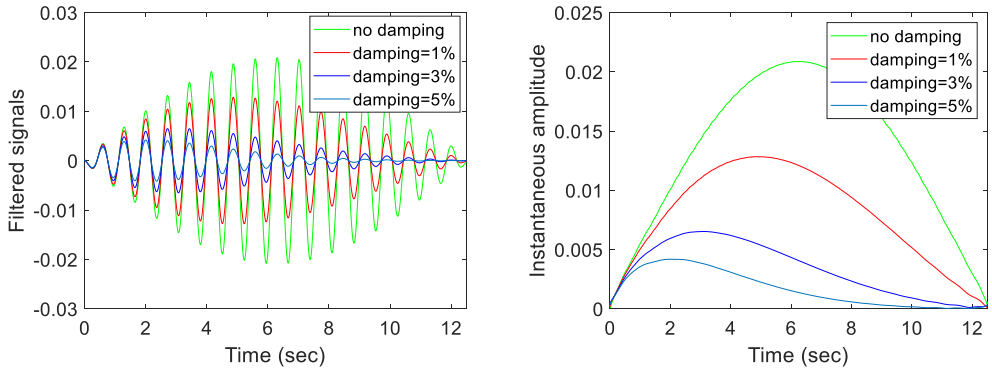

(a) (b)

Figure 6. Filtered results (a) The filtered signals; (b) the instantaneous amplitude

The separated component without damping oscillates with varying amplitudes that are similar to the first mode shape of the bridge. Consequently, its instantaneous amplitude

$A(t)$ is quite close to the theoretical first mode shape of the bridge. However, it is observed that the bridge damping shrinks and shifts the instantaneous amplitude, $A(t)$, in comparison to that without damping. Based on the algorithm presented by Yang et al. (2014), which ignores the bridge damping and utilizes the normalized instantaneous amplitude of HT associated with the filtered signal to represent the bridge mode shape directly, the results are illustrated on *Figure 7*, referred as to non-corrected mode shape in this paper.

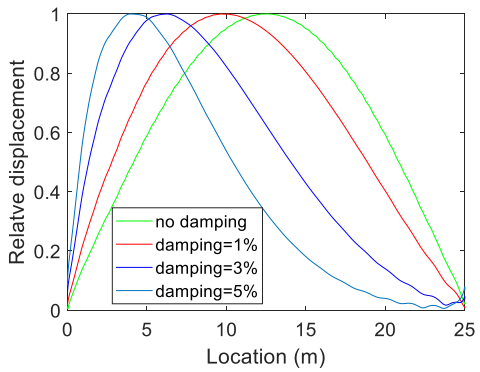

Figure 7. The non-corrected results of extracted mode shape

As it has shown, the bridge damping apparently left-shifts the extracted mode shape, which causes a greater error on the construction of the bridge mode shape with HT, although the value of damping ratio is as small as 1%. The instantaneous amplitude with damping is revised with $A(t)/e^{-\varepsilon_{b,n}\omega_{b,n}t}$ and the results are shown in *Figure 8* (a). These' revised instantaneous amplitudes are extremely close to that without damping and confirm the theoretical analysis, indicating that this process can remove the damping effect on the mode shape extracted with HT. Therefore, the proposed algorithm, referred as to corrected approach, can improve to extract the bridge mode shape from a passing vehicle acceleration

when the bridge damping exists. These revised instantaneous amplitudes are normalized in *Figure 8* (b) and represented to the bridge mode shape.

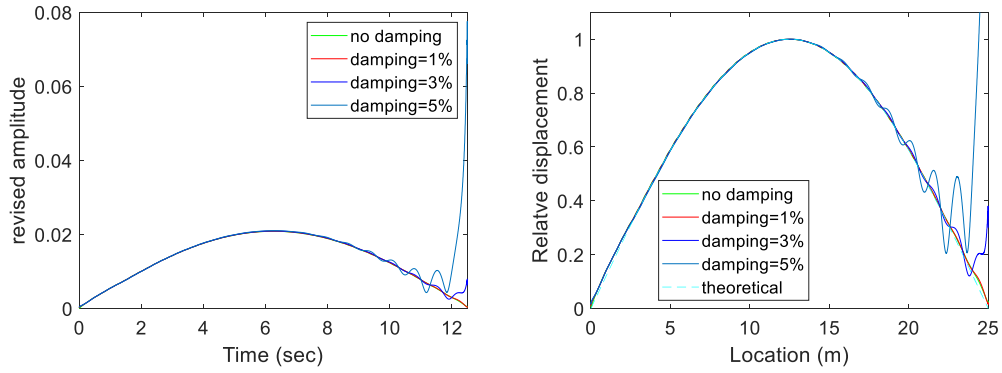

(a) (b)

Figure 8. Revised result (a) Revised instantaneous amplitude, $A(t)$; (b) Normalized A_{mod} of the bridge

However, it is found that the higher bridge damping ratio generates a stronger edge-effect as shown in *Figure 8*, which negatively affects accuracy of the proposed algorithm on the mode shape construction and damping ratio identification. This edge-effect happens, because the end section of instantaneous amplitude, A(t) is not smooth enough when the damping ratio is higher, and the revising process bestially amplifies this section. To overcome it, one can appropriately smooth the instantaneous amplitude, $A(t)$, before revising it. Otherwise, the strong edge-effect section should not be involved in calculating the MAC.

Extracting Damping Ratio and Mode Shapes

This section applies the steps described above to extract the bridge damping ratio and mode shape. The same case with a damping ratio of 1% is considered. A wide range of band-pass filter parameters are considered; central frequency, f_c, ranges from 0.789 Hz to 3.239 Hz in steps of 0.01 Hz, and the factor, Q ranges from 0.15 to 4.9 in steps of 0.25. For each f_c and Q, following Steps (3) and (4) of the proposed algorithm, a series of instantaneous amplitudes, (t), is obtained. The corrected function, $A(t)/e^{-\varepsilon_{b,n}\omega_{b,n}t}$, is applied in all cases, with the assuming damping ratio ranging from zero to 0.03 in steps of 0.0005, to create M_{odal} and then normalize it. For each (Q, f_c) pair, only one record for the maximum MAC results in these assumed damping ratios. The results for all parameter pairs are illustrated in *Figure 9*. As shown, the maximum MAC happens when $f_c = 1.689$ Hz and Q = 0.9, implying lower and upper cutoff frequencies of 0.994 Hz and 2.871 Hz respectively. For this band-pass filter, the component R(t) associated with the first bridge frequency is decomposed as shown in *Figure 10* (a) and the corresponding instantaneous amplitude is as illustrated in *Figure 10* (b).

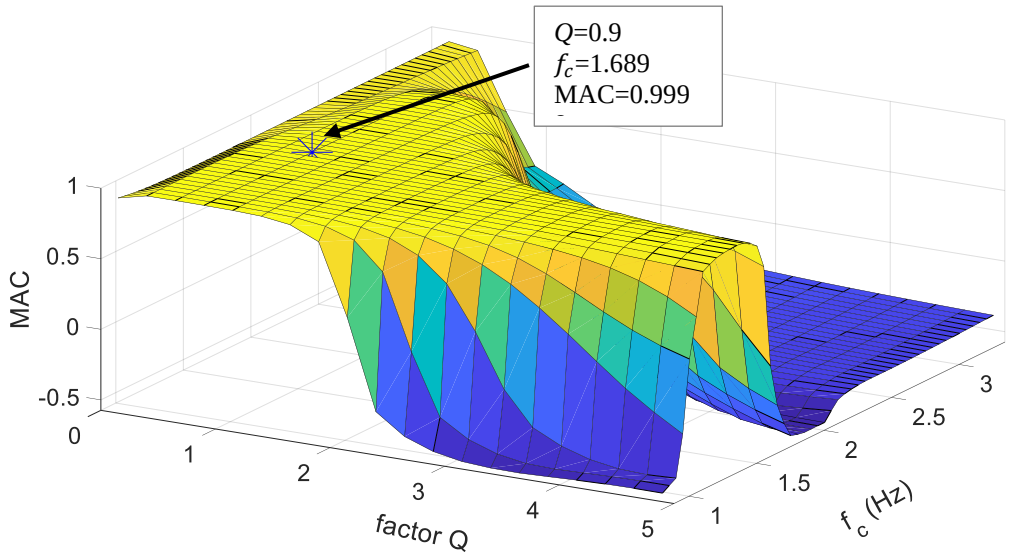

Figure 9. Maximum values of MAC for each assumed parameter pair in the band-pass filter

This instantaneous amplitude is applied to the function, $A(t)/e^{-\varepsilon_{b,n}\omega_{b,n}t}$ to remove the effect of damping and to obtain A_{mod} for each assumed damping ratio. Each value of A_{mod}, for every damping ratio, yields a MAC that is compared to the theoretical one, as shown in *Figure 11*. When damping ratio equals the actual value of 1%, the highest MAC value occurs. The extracted mode shape, with a very high MAC value of 0.9998, is shown *Figure 12* and compares very well to the theoretical one. In addition, *Figure 12* shows a great improvement of the extracted mode shape with the proposed algorithm comparing to that of non-corrected.

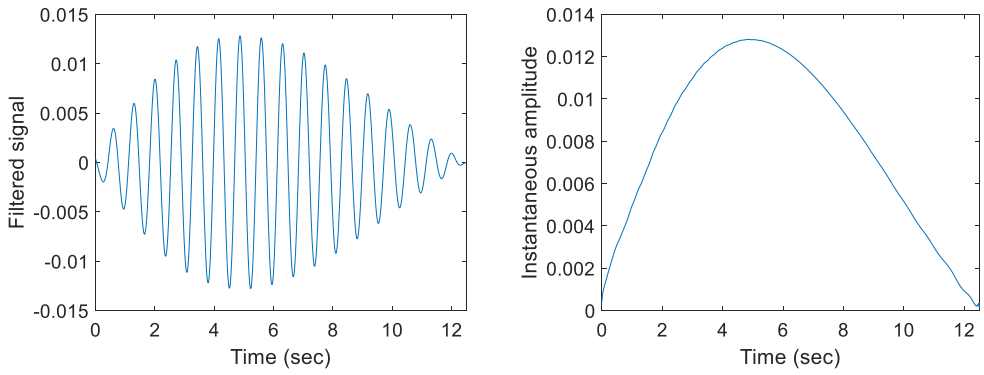

(a) (b)

Figure 10. Case study 1 (a) The filtered signal of vehicle response, (b) The corresponding instantaneous amplitude

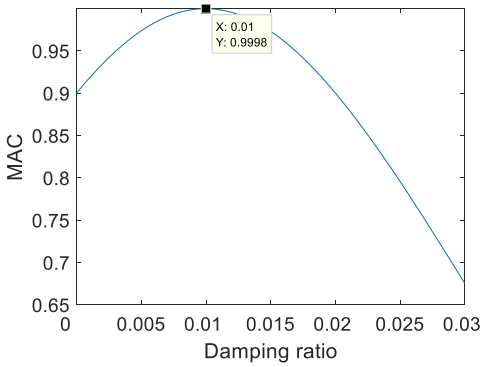

Figure 11. Variation of MAC value with damping ratio (highest MAC corresponds to actual damping)

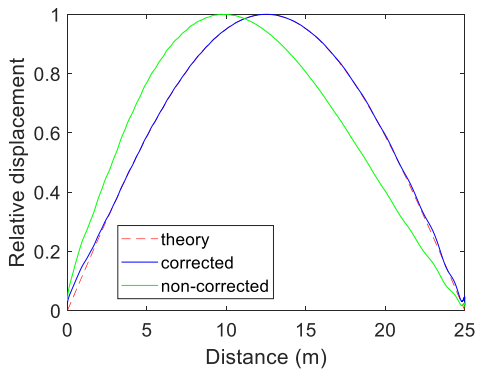

Figure 12. The extracted first mode shape of the bridge

The Effect of Vehicle Speed

The effect of the vehicle speed on the proposed algorithm is studied, considering five different vehicle speeds: v =2, 4, 6, 8 and 10 m/s. The remaining properties of the VBI model are kept the same as above. Following the same procedure, the mode shape and damping ratio are identified for each vehicle speed and presented in *Table 2*. The extracted mode shapes of the bridge are shown in *Figure 13*. The effect of vehicle speed on the identified results can be clearly seen in *Table 2* and *Figure 13*.

When the vehicle speed is slow (2 or 4 m/s), the constructed mode shape and identified damping ratio match very well with the actual ones. As vehicle speed increases, the errors in both damping ratio and mode shape become greater. When the vehicle is 10m/s, the error is as high as 125%. This finding is consistent with the theoretical analysis and studies of (Malekjafarian and Obrien 2014; Yang et al. 2014).

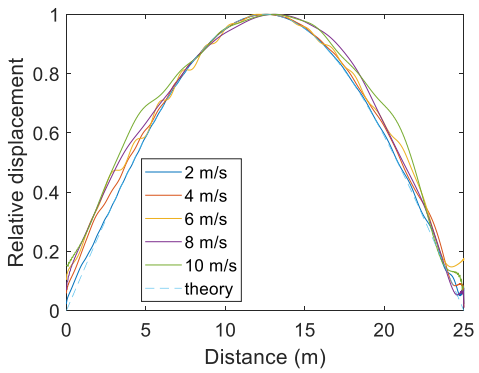

Figure 13. The extracted first mode shape of the bridge for different vehicle speeds

Table 2. Extracted damping for different vehicle speeds

Speed (m/s)	2	4	6	8	10
Damping ratio (Error %)	0.0100 (0%)	0.0100 (0%)	0.0105 (5%)	0.0160 (60%)	0.0225 (125%)
MAC	0.9998	0.9989	0.9968	0.9939	0.9914

Case Study of Higher Mode Shape

This section investigates the extraction of a higher mode shape and associated damping ratio. The vehicle acceleration of *Figure 4*, with a damping ratio of 1%, is considered (vehicle speed = 2 m/s; without road roughness). As before, the optimum band-pass filter is first found and applied to obtain the component response associated with the second frequency of the bridge, shown in Figure 14 (a). The corresponding instantaneous amplitude of the HT can also be obtained and is shown in Figure 14 (b). Clearly, the damping ratio has a greater effect on the higher mode shape amplitude than on the first mode shape. Nevertheless, the proposed algorithm can accurately identify the damping

ratio as 0.01 and the second mode shape of the bridge with high MAC of 0.9986. The extracted results are shown in Figure 14 (c) and (d).

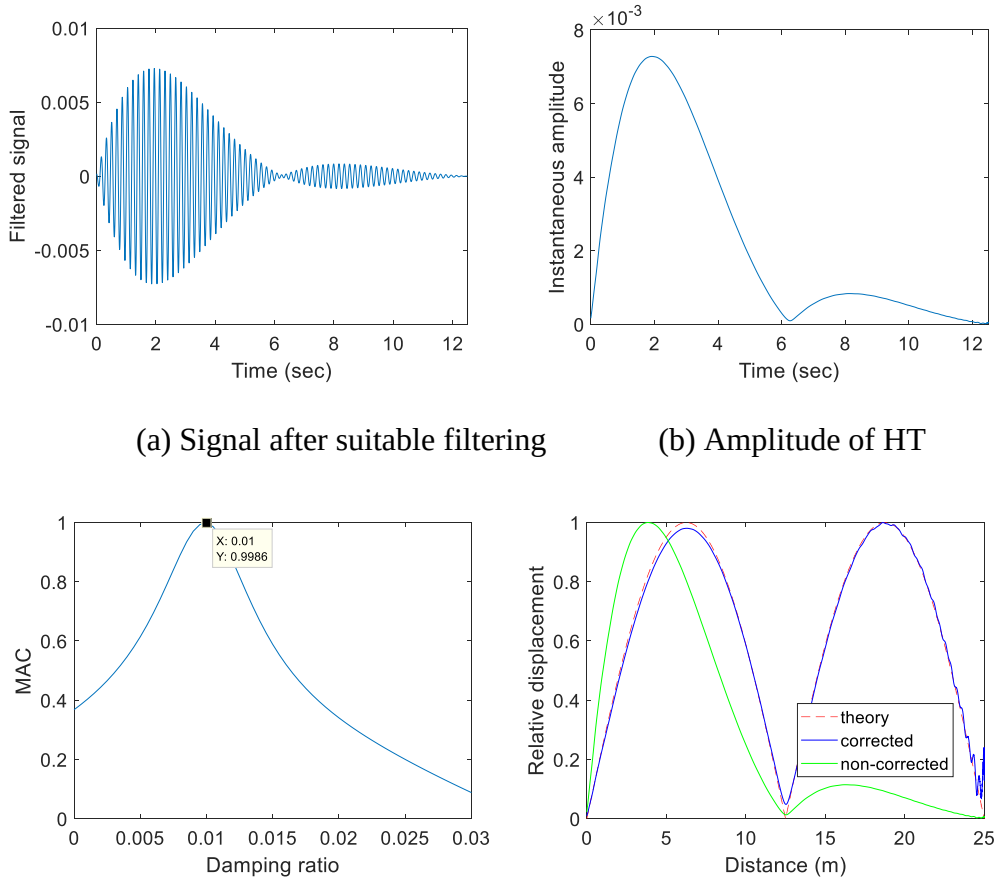

(a) Signal after suitable filtering (b) Amplitude of HT

(c) Damping ratio versus MAC (d) Extracted mode shape

Figure 14. The bridge higher modal parameters identification

The Effect of Road Surface Roughness

The effect of road surface roughness is investigated in this section. The road profile is generated randomly according to the power spectrum density curve of a "class A" profile, as presented by ISO 8608 (ISO 1995). *Figure 15* illustrates the vehicle acceleration

response considering the generated road roughness when the vehicle velocity is 2 m/s. Followed as the above-described process, the mode shapes associated with the first two natural frequency of the bridge are extracted, as shown in *Figure 16* (a) and (b), respectively. In this case, for the 1st mode shape of the bridge, the damping ratio and MAC value are calculated as 0.011 (10% error) and 0.9878, respectively; for the 2nd mode shape, the damping ratio and MAC value is calculated as 0.005 (50% error) and 0.9060, respectively. Although the band-pass filter can partially remove the random vibration caused by the road roughness, the road roughness has negative impact on the proposed algorithm, especially for the higher modes. Since the road roughness emerges a wide range of spatial frequency into the vehicle acceleration, the road roughness effect cannot be removed completely from the extracted mode shapes, using the frequency-domain filtering technique (Yang and Lee 2018; Yang et al. 2014). In addition, the extracted higher modes are easier to mingle with the road roughness, because of their lower amplitudes of higher modes comparing to those of lower modes (Yang et al. 2014).

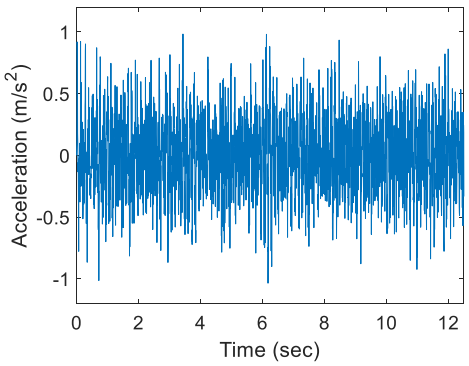

Figure 15. Recorded vehicle response at road roughness

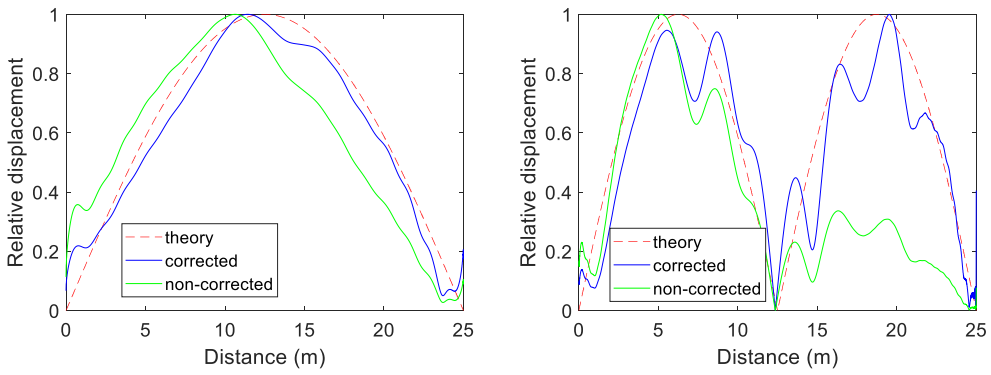

(a) (b)

Figure 16. The extracted mode shapes of the bridge; (a) 1st mode shape; (2) 2nd mode shape

Laboratory Studies

A scaled moving vehicle laboratory experiment is performed to investigate the feasibility of using indirect measurement to monitor bridge health. The scaled bridge model used in the experiment is summarized in *Figure 17*. Two approach spans are used for vehicle acceleration and deceleration. The main span is a 5.4 m simply supported steel beam. The beam properties, obtained from the manufacturer and free vibration tests, are listed in *Table 3*. The road surface roughness is also considered in the experiment as shown in *Figure 17* (e). This road profile was scaled using an electrical tape to pave on both wheel paths of the test vehicle at the interval of 100 mm, based on a real road profile measured on a 40.4 m road bridge in Japan (Kim et al. (2005)), which was categorized as very good (class A) according to the ISO 8608 (ISO 1995). This road profile is intended to be

representative of that expected on a typical highway bridge. However, there are some discrepancies with the measured profile since the scaled road profile as a superposition of steps is formed by a simple construction method using layered tape and plastic strips (McGetrick et al. 2015).

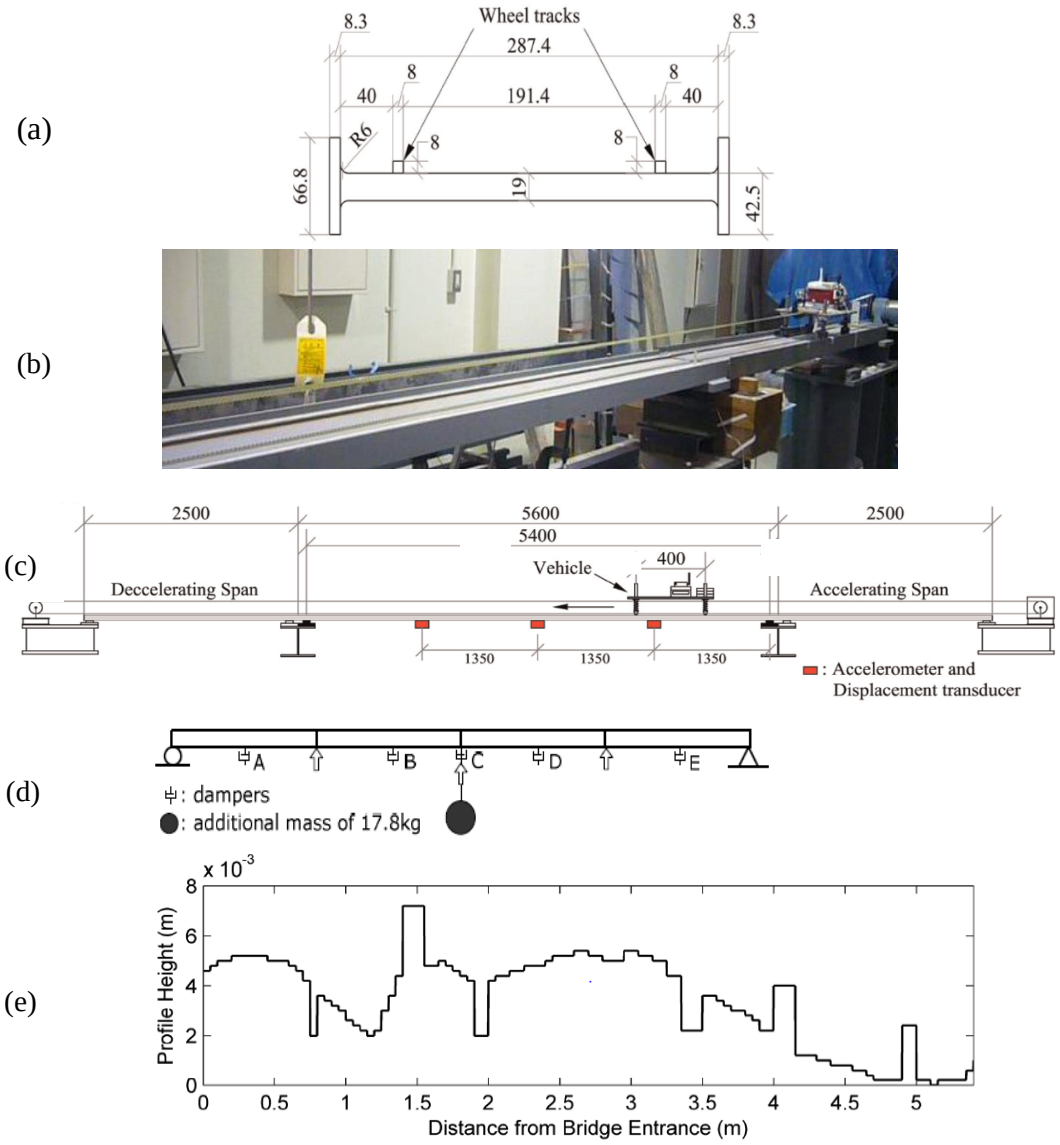

Figure 17. Experimental bridge: (a) beam cross section (unit: mm), (b) elevation of set-up, (c) laboratory set-up (unit: mm), (d) experimental setup for changing damping ratio, (e) experimental road profile.

A scaled moving vehicle laboratory experiment is performed to investigate the feasibility of using indirect measurement to monitor bridge health. The scaled bridge model used in the experiment is summarized in *Figure 17*. Two approach spans are used for vehicle acceleration and deceleration. The main span is a 5.4 m simply supported steel beam. The beam properties, obtained from the manufacturer and free vibration tests, are listed in *Table 3*. The road surface roughness is also considered in the experiment as shown in *Figure 17* (e). This road profile was scaled using an electrical tape to pave on both wheel paths of the test vehicle at the interval of 100 mm, based on a real road profile measured on a 40.4 m road bridge in Japan (Kim et al. (2005)), which was categorized as very good (class A) according to the ISO 8608 (ISO 1995). This road profile is intended to be representative of that expected on a typical highway bridge. However, there are some discrepancies with the measured profile since the scaled road profile as a superposition of steps is formed by a simple construction method using layered tape and plastic strips (McGetrick et al. 2015).

The damping of the test beam was varied in this experiment, and can be categorized in three scenarios: Scenario 1 – no change to the test beam; Scenario 2 – applying old displacement transducer at point C on the bridge; Scenario 3 – applying old displacement transducers at points A, B, C, D and E and a mass of 17.8 kg at mid-span, as shown in *Figure 17* (d). The old transducers are used as they provide frictional resistance to bridge displacements at the chosen locations. The damping constant changes from 1.6% for the initial case to 2.1% and 4.3% due to an additional damper at mid-span and five additional dampers respectively. The additional mass is performed to adjust the bridge frequency as

frequently damage, that causes changes in damping may cause some change in frequency. The additional mass brings about the first natural frequency drop of bridge from 2.69 Hz to 2.50 Hz.

Table 3. Structural properties of model girder

Span length L (m)	Material density (kg/m^3)	Cross sectional area, A (m^2)	1st natural frequency (Hz)	Damping ratio for 1st mode, ε	Second moment of area m^4
5.4	7800	6.7×10^{-3}	2.69	0.0016	5.77×10^{-7}

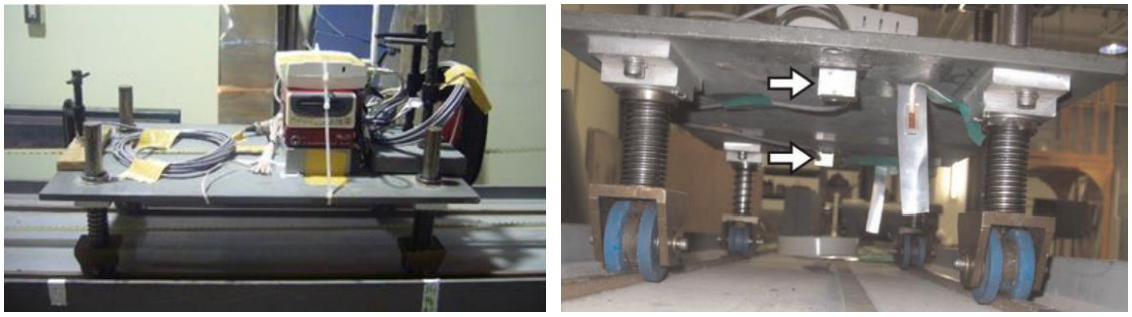

(a) (b)

Figure 18. Experimental vehicle, (a) side view; (b) end view showing sensors.

A scaled two-axle vehicle model is instrumented for the experiments as shown in *Figure 18*. Two accelerometers are mounted on the center of the front and rear axles respectively to monitor the vehicle bounce motion. This instrumented vehicle also includes a wireless router and data logger that allow the axle acceleration data to be recorded

remotely. The vehicle model configurations is given in *Table 4*. The axle spacing and track width are 0.4 and 0.2 m, respectively.

Table 4. Vehicle model properties

	Mass (kg)	Suspension stiffness (N/m)	Suspension damping ($N \cdot s/m$)
Axle 1	7.9	2680	16.006
Axle 2	13.445	4570	27.762

The test vehicle was propelled by a motor and pulley system. Its speed, therefore, was maintained constant by an electronic controller as it passed over the bridge. The entry and exit of the vehicle to the beam were monitored using strain sensors in order to synchronize measurements; entry and exit points appeared as peaks in the strain signals. The instrumented vehicle speed was 0.93 m/s in this experiment. The vehicle repeatedly crossed the bridge, five times for each scenario, at this speed. More details of this experiment are given in references (Kim et al. 2011; Kim et al. 2014; McGetrick et al. 2015).

In this experiment, extracting the frequency of the bridge using the acceleration signal measured on the vehicle was well investigated and is presented by Kim et al. (2011); Kim et al. (2014). This paper focuses on the extraction of the damping ratio and mode shape of the bridge from the vehicle response. The unsprung acceleration was recorded on the rear axle of the vehicle.

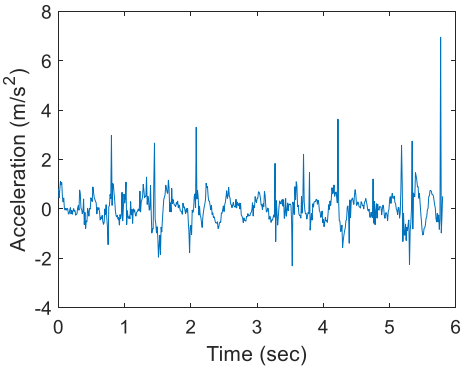

Figure 19. Rear axle acceleration

Figure 19 illustrates one of five recorded vehicle acceleration signals during its passage over the bridge in scenario 1 (time 0 is when it entered the bridge; the end time is when it left the bridge). Followed the described algorithm, a series of parameters for the band-pass filter and damping ratios are assumed. At these assumed values, the highest MAC of the first mode shape is found when $f_c = 2.44$ Hz and $Q = 4.5$, which gives a damping ratio of 0.0165. The values of MAC for each assumed parameter pair of the band-pass filter are plotted in *Figure 20*. The results for this maximum MAC, are shown in *Figure 21*. The bridge damping ratio is identified as 0.0165 (compared to the actual value of 0.016). The extracted mode shape is also good with a high MAC of 0.9933. In addition, the proposed algorithm is demonstrated that is able to greatly improve the extraction of mode shape compared to non-corrected results.

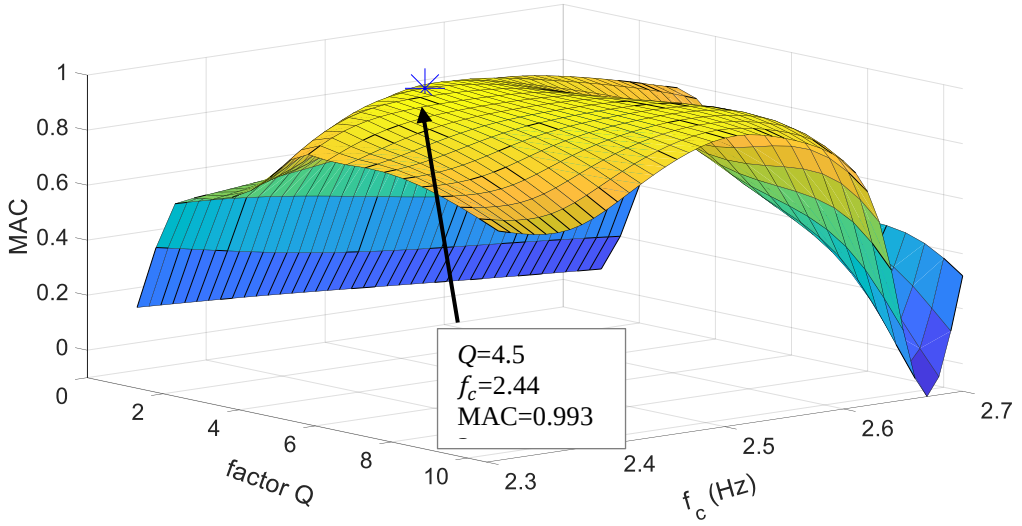

Figure 20. MAC versus parameters of band-pass filter

Similarly, applying the proposed algorithm to all of the recorded accelerations, the extracted damping ratios and MAC values are listed in *Table 5*. As shown, the extracted mode shapes match the theoretical ones quite well, with high MAC values. The mean of the five MAC values for the three scenarios are 0.99, 0.96 and 0.97, respectively. Scenario 2 gives the worst extracted mode shape, perhaps because only one transducer was fitted at mid-span which makes the bridge less homogenous than, for example, when five transducers are distributed evenly.

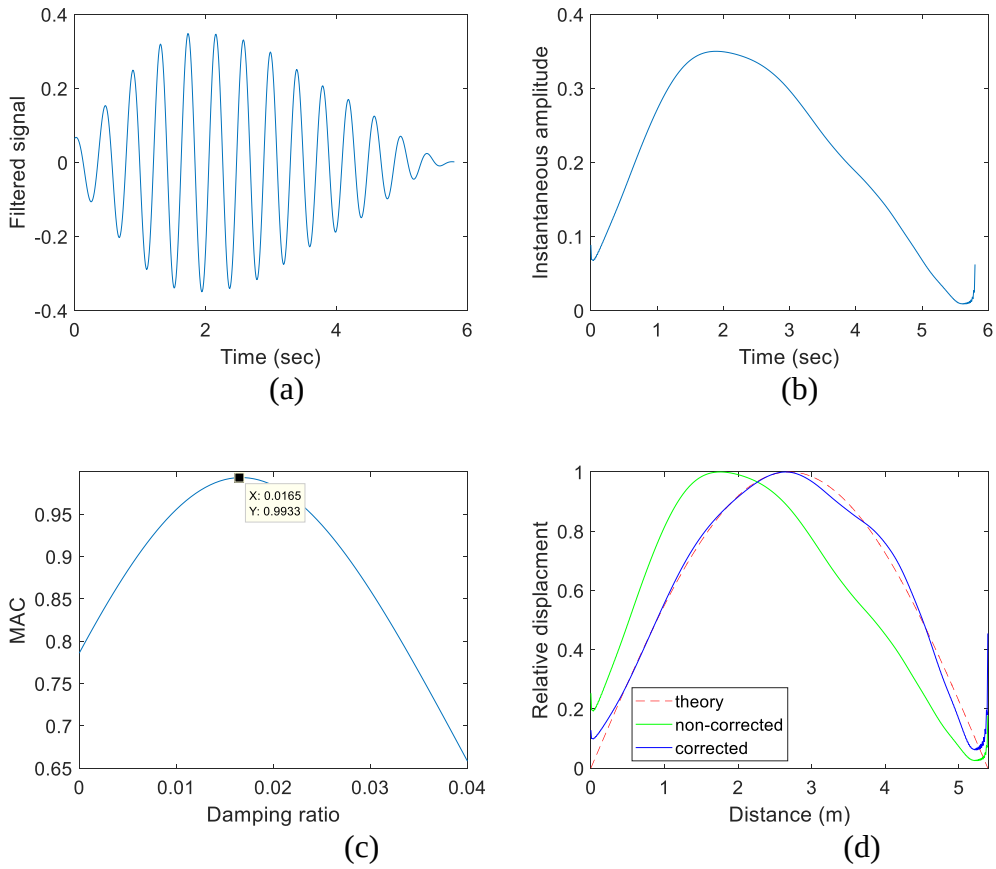

Figure 21. Extraction of mode shape for Test No. 1, Scenario 1; (a) the filtered signal; (b) the corresponding instantaneous amplitude of HT; (c) Damping ratio versus MAC; (d) the extracted mode shape

The identified mean damping ratios for the three scenarios are 0.0155, 0.0201 and 0.0270, respectively; while the corresponding theoretical values are 0.016, 0.021 and 0.043, respectively. The results for scenarios 1 and 2 match the theoretical values very well. While the results for scenarios 3 shows a greater error. It is found that this error is due to the strong edge-effect result in the higher bridge damping ratio, which is consistent with the simulation studies. To overcome it, the algorithm is slightly modified, that is, the MAC calculation does not consider the edge-effect section (here simply ignore the last tenth of

the entire bridge span). Therefore, the modal parameters are extracted again, and the results are listed in *Table 5* as well, referred as scenarios 3*. The mean damping ratio is identified as 0.0421 matching the theoretical one of 0.043 very well. The test No.1 for scenarios 3* is taken as example, shown in *Figure 22*. It is apparently observed that the higher damping ratio has stronger edge-effect compared to that of 1.6%. The non-corrected algorithm does not function at all for scenarios 3*.

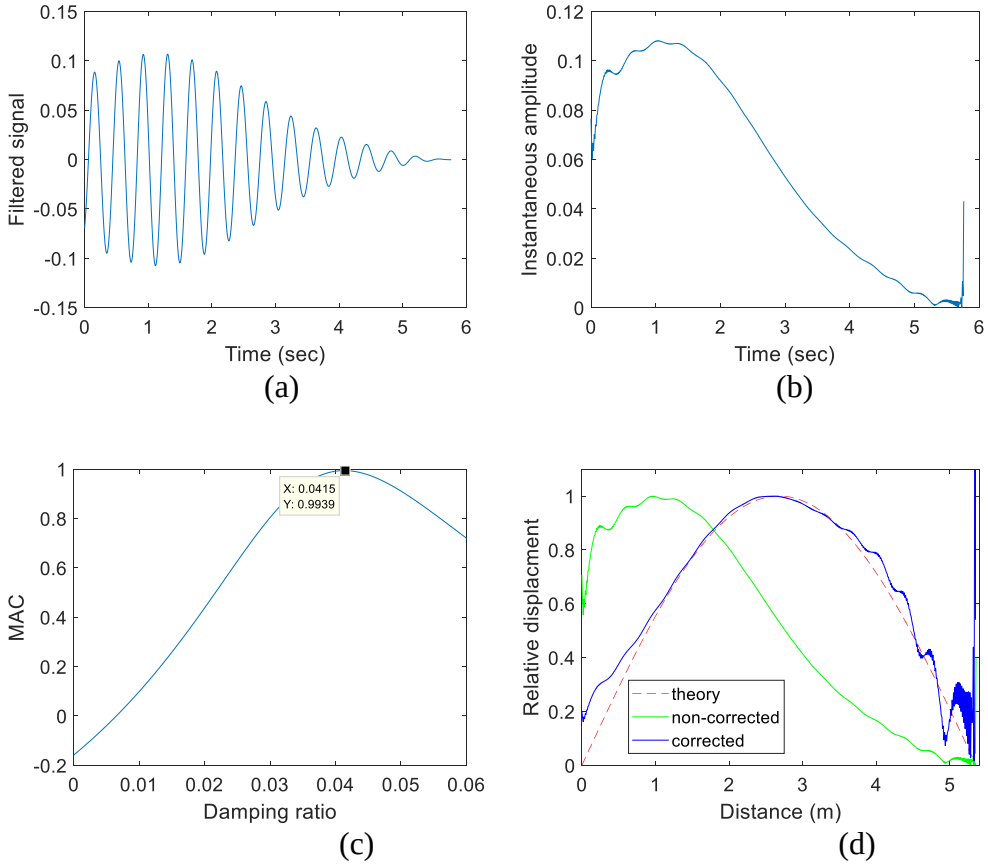

Figure 22. Extraction of mode shape for Test No. 1, Scenario 3*; (a) the filtered signal; (b) the corresponding instantaneous amplitude of HT; (c) Damping ratio versus MAC; (d) the extracted mode shape

Table 5. Extracted results for three scenarios with different damping ratios, ε

Scenario	Extracted result	Test No.					Mean of 5 tests	Standard deviation
		1	2	3	4	5		
Scenario 1 (ε = 0.016)	Damping ratio	0.0165	0.0165	0.0145	0.0135	0.0155	0.0155	0.0014
	MAC	0.9933	0.9903	0.9871	0.9945	0.9899	0.9910	0.0029
Scenario 2 (ε = 0.021)	Damping ratio	0.0200	0.0225	0.0185	0.0180	0.0215	0.0201	0.0019
	MAC	0.9768	0.9310	0.9639	0.9812	0.9454	0.9597	0.0212
Scenario 3 (ε = 0.043)	Damping ratio	0.0285	0.0305	0.015	0.031	0.0315	0.0270	0.0070
	MAC	0.9725	0.9650	0.9937	0.9710	0.9546	0.9711	0.0143
Scenario 3* (ε = 0.043)	Damping ratio	0.0415	0.0420	-	0.0430	0.0420	0.0421	0.0006
	MAC	0.9939	0.9924	-	0.9934	0.9920	0.9929	0.0009

Note: - means no calculation for this test No.

It is of note that both the extracted damping ratio and mode shape are very accurate for Scenario 1, compared to the theoretical values. When the bridge damping ratio is high, there is strong edge-effect of extracted mode shape, leading to a greater error of the damping ratio estimation. By ignoring this edge-effect section of MAC, one can obtain accurate damping ratio, but the extracted mode shape is still contaminated at edge-effect section. One promising approach to avoid that, is to appropriately smooth the instantaneous amplitude of HT before reversing it as aforementioned.

CONCLUSION

This paper proposes an algorithm to extract bridge modal parameters, with a focus on damping ratio and mode shapes, using the dynamic response of a passing vehicle. The Hilbert Transform is applied to the filtered signals. The feasibility of the concept is established through theoretical analysis, numerical simulation and laboratory experiments. It is demonstrated that the proposed algorithm is greatly improves the extracted mode shape over the algorithm presented by Yang et al. (2014). A key limitation of the proposed algorithm at this time is a requirement for the vehicle to have a low and constant speed. Besides, the high bridge damping generates a strong edge-effect of the extracted mode shapes, negatively affecting the accuracy of the proposed algorithm. In the simulations, it is found that an increase in vehicle speed decreases the precision of the extracted results. The proposed algorithm is also shown to be capable of extracting the modal parameters of the second mode shape with relatively good precision. In addition, it is found that although the band-pass filter can partially remove the random vibration caused by the road roughness, the road roughness with Class A, i.e., roughness condition of 'very good' has negative impact on the proposed algorithm, especially for the higher modes.

The laboratory experiments provide further evidence of the potential of the proposed algorithm. It accurately identifies the bridge damping so as to detect the first increase of that, only using one sensor installed on instrumented vehicle. It is concluded that the proposed algorithm is able to detect the change of bridge damping ratio and higher accuracy mode shapes, and has potential for application in the use of indirect measurement to monitor bridge health.

ACKNOWLEDGMENT

The National Science of Foundation of the United States (NSF-CNS- 1645863, and NSF-CSR- 1813949) sponsors this research. Any opinions, findings, conclusions or recommendations expressed in this publication are those of the authors and do not necessarily reflect the view of the sponsors.

REFERENCES

Brady, S. P., O'Brien, E. J., and Žnidarič, A. (2006). "Effect of vehicle velocity on the dynamic amplification of a vehicle crossing a simply supported bridge." *Journal of Bridge Engineering*, 11(2), 241-249.

Carden, E. P. (2004). "Vibration Based Condition Monitoring: A Review." *Structural Health Monitoring*, 3(4), 355-377.

Cebon, D. (1999). *Handbook of vehicle-road interaction*.

Chang, P. C., Flatau, A., and Liu, S. (2003). "Health monitoring of civil infrastructure." *Structural health monitoring*, 2(3), 257-267.

Chrysostomou, C. Z., and Stassis, A. (2008). "Health-monitoring and system-identification of an ancient aqueduct." *Smart Structures and Systems*, 4(2), 183-194.

Deng, L., and Cai, C. (2009). "Bridge model updating using response surface method and genetic algorithm." *Journal of Bridge Engineering*, 15(5), 553-564.

Deng, L., and Cai, C. (2009). "Identification of parameters of vehicles moving on bridges."

Engineering Structures, 31(10), 2474-2485.

Deng, L., Yan, W., and Nie, L. (2019). "A simple corrosion fatigue design method for bridges considering the coupled corrosion-overloading effect." *Engineering Structures*, 178, 309-317.

Doebling, S. W., Farrar, C. R., and Prime, M. B. (1998). "A summary review of vibration-based damage identification methods." *Shock and vibration digest*, 30(2), 91-105.

Frýba, L. (2013). *Vibration of solids and structures under moving loads*, Springer Science & Business Media.

González, A., Obrien, E. J., and McGetrick, P. J. (2012). "Identification of damping in a bridge using a moving instrumented vehicle." *Journal of Sound and Vibration*, 331(18), 4115-4131.

Grande, E., and Imbimbo, M. (2016). "A multi-stage approach for damage detection in structural systems based on flexibility." *Mechanical Systems and Signal Processing*, 76, 455-475.

Hu, H., and Tang, J. (2005). "A convolution integral method for certain strongly nonlinear oscillators." *Journal of sound and vibration*, 285(4-5), 1235-1241.

Huang, N. E. (2014). "Hilbert–Huang Transform and Its Applications." 16.

ISO (1995). "Mechanical vibration—Road surface profiles—Reporting of measured data."

Keenahan, J., Obrien, E. J., McGetrick, P. J., and Gonzalez, A. (2013). "The use of a dynamic truck-trailer drive-by system to monitor bridge damping." *Structural Health Monitoring*, 13(2), 143-157.

Kim, C.-W., Isemoto, R., Toshinami, T., Kawatani, M., McGetrick, P., and O'Brien, E. J. "Experimental investigation of drive-by bridge inspection." *Proc., 5th International*

Conference on Structural Health Monitoring of Intelligent Infrastructure (SHMII-5), Cancun, Mexico, 11-15 December, 2011, Instituto de Ingeniería, UNAM.

Kim, C. W., Isemoto, R., McGetrick, P. J., Kawatani, M., and Obrien, E. J. (2014). "Drive-by bridge inspection from three different approaches." *Smart Structures and Systems*, 13(5), 775-796.

Kim, C. W., Kawatani, M., and Kim, K. B. (2005). "Three-dimensional dynamic analysis for bridge–vehicle interaction with roadway roughness." *Computers & structures*, 83(19-20), 1627-1645.

Kong, X., Cai, C., and Kong, B. (2016). "Numerically extracting bridge modal properties from dynamic responses of moving vehicles." *Journal of Engineering Mechanics*, 142(6), 04016025.

Kong, X., Cai, C. S., Deng, L., and Zhang, W. (2017). "Using Dynamic Responses of Moving Vehicles to Extract Bridge Modal Properties of a Field Bridge." *Journal of Bridge Engineering*, 22(6), 04017018.

Lin, C. W., and Yang, Y. B. (2005). "Use of a passing vehicle to scan the fundamental bridge frequencies: An experimental verification." *Engineering Structures*, 27(13), 1865-1878.

Magalhães, F., Cunha, A., and Caetano, E. (2012). "Vibration based structural health monitoring of an arch bridge: from automated OMA to damage detection." *Mechanical Systems and Signal Processing*, 28, 212-228.

Malekjafarian, A., and Obrien, E. J. (2014). "Identification of bridge mode shapes using Short Time Frequency Domain Decomposition of the responses measured in a passing vehicle." *Engineering Structures*, 81, 386-397.

Malekjafarian, A., and Obrien, E. J. (2017). "On the use of a passing vehicle for the estimation of bridge mode shapes." *Journal of Sound and Vibration*, 397, 77-91.

Marulanda, J., Caicedo, J. M., and Thomson, P. (2017). "Mode shapes identification under harmonic excitation using mobile sensors." *Ingeniería y Competitividad*, 19(1), 140-145.

McGetrick, P. J., González, A., and Obrien, E. J. (2009). "Theoretical investigation of the use of a moving vehicle to identify bridge dynamic parameters." *Insight - Non-Destructive Testing and Condition Monitoring*, 51(8), 433-438.

McGetrick, P. J., Kim, C.-W., González, A., and Brien, E. J. O. (2015). "Experimental validation of a drive-by stiffness identification method for bridge monitoring." *Structural Health Monitoring: An International Journal*, 14(4), 317-331.

Obrien, E. J., and Malekjafarian, A. (2016). "A mode shape-based damage detection approach using laser measurement from a vehicle crossing a simply supported bridge." *Structural Control and Health Monitoring*, 23(10), 1273-1286.

Oshima, Y., Yamamoto, K., and Sugiura, K. (2014). "Damage assessment of a bridge based on mode shapes estimated by responses of passing vehicles." *Smart Structures and Systems*, 13(5), 731-753.

Tan, C., Elhattab, A., and Uddin, N. (2017). "“Drive-by’’ bridge frequency-based monitoring utilizing wavelet transform." *Journal of Civil Structural Health Monitoring*, 7(5), 615-625.

Tan, C., Uddin, N., and Elhattab, A. (2018). "Utilizing Hilbert Transform to Assess the Bridge Health Condition." *ICVRAM ISUMA UNCERTAINTIES conference*Florianópolis, SC, Brazil.

Wang, W., Deng, L., and Shao, X. (2016). "Number of stress cycles for fatigue design of simply-supported steel I-girder bridges considering the dynamic effect of vehicle loading." *Engineering Structures*, 110, 70-78.

Yang, J. P., and Lee, W.-C. (2018). "Damping effect of a passing vehicle for indirectly measuring bridge frequencies by EMD technique." *International Journal of Structural Stability and Dynamics*, 18(01), 1850008.

Yang, Y.-B., Yau, J., Yao, Z., and Wu, Y. (2004). *Vehicle-bridge interaction dynamics: with applications to high-speed railways*, World Scientific.

Yang, Y., and Lin, C. (2005). "Vehicle–bridge interaction dynamics and potential applications." *Journal of sound and vibration*, 284(1), 205-226.

Yang, Y. B., and Chang, K. C. (2009). "Extraction of bridge frequencies from the dynamic response of a passing vehicle enhanced by the EMD technique." *Journal of Sound and Vibration*, 322(4-5), 718-739.

Yang, Y. B., Li, Y. C., and Chang, K. C. (2014). "Constructing the mode shapes of a bridge from a passing vehicle: a theoretical study." *Smart Structures and Systems*, 13(5), 797-819.

Yang, Y. B., Lin, C. W., and Yau, J. D. (2004). "Extracting bridge frequencies from the dynamic response of a passing vehicle." *Journal of Sound and Vibration*, 272(3-5), 471-493.

Zhang, Y., Wang, L., and Xiang, Z. (2012). "Damage detection by mode shape squares extracted from a passing vehicle." *Journal of Sound and Vibration*, 331(2), 291-307.

STRUCTURAL HEALTH MONITORING OF BRIDGES – THE CONFLICTING CHALLENGES OF DETECTING GLOBAL AND LOCAL DAMAGE

by

CHENGJUN TAN
YAHYA M. MOHAMMED
NASIM UDDIN
EUGENE J. OBRIEN
PAUL C. FITZGERALD
PATRICK J MCGETRICK
CHUL-WOO KIM

Submitted to [or In preparation for] *Structural Health Monitoring*

Format adapted for dissertation

STRUCTURAL HEALTH MONITORING OF BRIDGES – THE CONFLICTING CHALLENGES OF DETECTING GLOBAL AND LOCAL DAMAGE

Abstract:

This paper uses extracted bridge mode shapes to detect bridge damage, including both local damage such as that due to a bridge strike and global damage such as that due to foundation scour. Typically, only one accelerometer is required, which is mounted on an instrumented vehicle passing over the test bridge. This concept is referred to as indirect measurement or "drive-by" bridge health monitoring. For a simple vehicle/bridge interaction (VBI) model, where the vehicle is represented as a moving sprung mass, a closed-form solution for the bridge mode shape is derived from the acceleration response of the instrumented vehicle. The validity of the proposed algorithm is numerically verified using a VBI model with a quarter-car. In addition, it is shown that the extracted mode shape can be used to assess the bridge condition. A damage index based on the extracted mode shape is proposed to find the location of damage when it is local and indicate the damage level. In the numerical study, the factors that affect the accuracy of the proposed algorithm are investigated, including the vehicle speed and measurement noise. Two laboratory experiments are conducted to validate the mode shape extraction and bridge damage detection processes for cases of both local and global damage. A road surface profile is allowed for in the laboratory tests.

Keywords: Structure health monitoring (SHM); bridge health monitoring; mode shape; indirect measurement; drive-by; damage detection; vehicle bridge interaction.

1. Introduction

Bridges play a significant role in the transportation network. Maintaining their condition is central to the efficient and safe operation of transportation facilities. Road owners and managers generally monitor structural condition – seeking to detect and locate possible damage – through periodic inspections and carry out repairs if necessary. Manual inspection is the conventional approach and is generally considered to be the most effective method for periodic monitoring. However, over the last two decades, there have been major advances in the concept of Structure Health Monitoring (SHM) using electronic sensors, as an alternative to manual inspection. Many SHM methods assess the bridge condition using modal parameters such as frequency, damping and mode shape [1-4].

Conventionally, bridge SHM uses sensors installed on the bridge structure directly, referred as to direct measurement. To obtain the bridge frequency or damping ratio in a short/medium span bridge, only one sensor is required to record the dynamic response through a simple vibration experiment. In contrast, quite a number of sensors are required on the bridge deck to obtain its mode shape. Clearly, the mode shape resolution is directly related to the number of sensors used [1, 5]. Thus, in practical terms, it is more difficult to obtain the bridge mode shape than the frequency or damping ratio. However, among these modal parameters, the mode shape is considered the best at determining the damage location.

Recently, there is increasing interest in using the response of a passing vehicle to extract the dynamic properties of a bridge, a process referred to as indirect measurement or "drive-by" bridge inspection [6-10]. Yang, et al. [11] first developed the idea of extracting bridge natural frequency from the acceleration response of an instrumented passing vehicle. They pointed out that the vehicle suspension system is excited by the bridge displacement as well as the surface profile through coupled vehicle/bridge vibration. As a result, the vehicle response contains information on the bridge properties. Yang and Lin [12] and Yang and Chang [13] verified the feasibility of extracting the bridge frequency from a passing vehicle response, numerically and experimentally respectively. Through this concept of indirect measurement, González, et al. [14] used a half-car VBI model to assess bridge damping by minimizing the sum of squared errors and hence estimate damping.

As another set of bridge modal parameters, mode shapes are important properties for many applications in bridge engineering, such as numerical modal calibration and updating [15, 16], bridge SHM and damage detection [2-4, 17]. The concept of indirect measurement is that the instrumented vehicle is sensitive to the vibration characteristics of each point as it passes over the entire bridge length, which generally offers much more spatial information, as well as higher resolution in mode shapes, in comparison with the direct measurement, where a limited number of sensors are installed on the bridge [18, 19]. A significant challenge is the short measurement window resulting from the length of time a highway-speed vehicle is in contact with a bridge.

Zhang, et al. [20] first attempted to implement an indirect approach to the extraction of mode shape-related characteristics of a bridge, and numerically and experimentally

verified its feasibility. In their approach, the instrumented vehicle is equipped with an additional controllable shaker, artificially applying a periodic force as the vehicle passes over the bridge. Oshima, et al. [21] propose a truck-trailer (multi-axle) convoy system to construct mode shapes and detect the bridge damage in an indirect approach. The vehicles with a small number (N) of trailers have two functions: exciting the bridge and measuring the responses at every contact point simultaneously. Therefore, there are N segments of bridge response measured at the same time for each vehicle location on the bridge. These synchronous responses can be applied to extract the mode shape vector by applying Singular Value Decomposition, but with low resolution. A novel algorithm using Short Time Frequency Domain Decomposition to estimate bridge mode shapes from indirect measurements is proposed by Malekjafarian and Obrien [22], and improved by Malekjafarian and Obrien [23], OBrien and Malekjafarian [24]. In addition, they showed that an extracted mode shape with high resolution can be used to detect the presence of bridge damage and its location. However, it has only been verified in numerical studies so far.

Yang, et al. [18] developed a single-input-single-output system approach to the construction of mode shapes from the acceleration response of a vehicle, where the bridge is only excited by one moving point under the wheel and the response is measured at the same point. This approach neglects bridge damping, which is found to have a non-negligible impact on the extracted mode shapes.

This paper describes an improved "drive-by" bridge mode shape extraction method [18] that takes account of bridge damping. The acceleration response is subjected to a band-pass filter and Hilbert Transform (HT) in succession to construct the mode shape of the

bridge. The extracted mode shape has high resolution and can be used to detect bridge damage. A damage index based on the extracted mode shape is applied to indicate the damage location and even reflect the damage level. A theoretical closed-form solution is derived, under the assumption of a simple VBI model, where the vehicle is represented by a moving sprung mass and is passing over a simply supported beam with constant speed. The validity of the proposed algorithm is numerically demonstrated using a VBI model with a quarter-car. The factors that affect the accuracy of the proposed algorithm are investigated, including the vehicle speed and measurement noise. Further, a laboratory experimental test is conducted to investigate the performance of the mode shape extraction and bridge damage detection processes. A road profile is included in the laboratory experiment.

2. Theoretical Background

Figure 1 shows the mathematical model of a simple vehicle and bridge dynamic interaction, where the vehicle is represented as a moving sprung mass m_v, supported by a spring of stiffness k_v, passing over a simply supported beam with constant speed v. The modeled beam of length L is assumed to have constant mass density $\bar{m}$ per unit length and constant bending rigidity EI. The following assumptions are adopted without losing the generality of the problem: [9, 19, 25-29]: (1) the beam is of Bernoulli–Euler type with constant cross section; (2) the vehicle mass is assumed to be small compared with that of the bridge; (3) the vehicle passes over the bridge at a constant speed; (4) the damping of the beam is Rayleigh type; (5) road roughness is ignored; (6) bridge damping is not

considered. Based on these assumptions, the vibration equations of motion for the bridge and vehicle are:

$$\bar{m}\ddot{u} + EIu'''' = f_c(t)\delta(x - vt) \quad (1)$$

$$m_v\ddot{q}_v + k_v(q_v - u|_{x=vt}) = 0 \quad (2)$$

where $u(x,t)$ represents the vertical displacement of the modeled beam; $q_v(t)$denotes the vertical displacement of the vehicle, measured from its static equilibrium position, and a dot and a prime represent the derivatives with respect to time *t* and with respect to the longitudinal coordinate *x*, respectively.

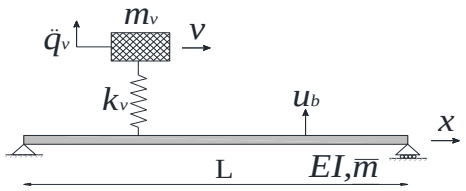

Figure 1. Numerical model of VBI system

Enhanced by the Hilbert Transform (HT), Yang, et al. [18] proposed that the HT instantaneous amplitude of the vehicle response includes the bridge mode shapes as:

$$A(t) = A_m \left| sin\frac{n\pi x}{L} \right| \quad (3)$$

where $A(t)$ represents the HT instantaneous amplitude and A_m is a constant non-time (or position)-related coefficient. Followed by this idea, Tan, et al. [30] showed that bridge damping affects the mode shape extracted with HT. The instantaneous amplitude of the vehicle acceleration is represented as

$$A(t) = A_m^* e^{-\varepsilon_{b,n}\omega_{b,n}t} \left| sin\frac{n\pi x}{L} \right| \quad (4)$$

where A_m^* is a constant coefficient similar to A_m; $\varepsilon_{b,n}$ and $\omega_{b,n}$ are bridge damping ratio and frequency of the n^{th} mode shape, respectively.

As Eq. (4) shows, the amplitude history $A(t)$ includes the mode shape function $sin\frac{n\pi x}{L}$ of the bridge (absolute value) multiplied by a constant coefficient, which is consistent with Eq. (3), where the bridge damping is not considered. However, the bridge damping appears to shift the mode shape in $A(t)$. To obtain greater accuracy in the mode shapes, the construction of the mode shape squares (MOSS) from the amplitude of the HT is reformulated as $MOSS_n = A(t)/e^{-\varepsilon_{b,n}\omega_{b,n}t}$ and normalized, which is feasible when the speed of the test vehicle is constant.

Bridge mode shapes have been used as an indicator of damage for many years. Fan and Qiao [31], Hadjileontiadis, et al. [32], Shi, et al. [33] use changes in the mode shapes for damage identification, and others [34, 35] use mode shape curvature that is more sensitive to local damage. Since the proposed method constructs mode shapes using data from a moving sensor (not fixed coordinates), the results are considered as approximate. Therefore, using the mode shape estimates, a damage index approach proposed by Zhang, et al. [20], is adopted. It is referred to here as the MOSS concept. As the mode shapes are normalized, a scaling factor α is introduced, representing the minimum distance between the damaged and undamaged mode shapes [20]:

$$\alpha = \frac{MOSS_n^d \cdot MOSS_n^u}{MOSS_n^d \cdot MOSS_n^d} \quad (5)$$

where $MOSS_n^d$ and $MOSS_n^u$ are the n^{th} MOSS values of the damaged and undamaged structures, respectively. Then the damage index is defined by calculating the discrepancy between the MOSS values of damaged and undamaged bridges as,

$$\Delta_n = MOSS_n^u - \alpha MOSS_n^d \quad (6)$$

When the damage location is not required, another damage indicator based on the sum of differences between the MOSSs for the damaged and undamaged bridges is defined by Obrien and Malekjafarian [36]:

$$DI_n^* = \frac{1}{n_{ss}} \sum_{j=1}^{n_{ss}} |MOSS_n^u(j) - \alpha MOSS_n^d(j)| \quad (7)$$

This paper proposes to detect the bridge damage using the extracted bridge mode shapes with drive-by data. The procedural steps can be summarized as follows [18]:

(1) Acquire the bridge frequency $\omega_{b,n}$ and damping ratio $\varepsilon_{b,n}$. In practice, they can be obtained from a current or previous simple vibration experiment, or design values.

(2) Calculate the corresponding instantaneous amplitudes, $A_n(t)$, with the target bridge natural frequency.

(3) Reformulate the amplitude history with $A_n(t)/e^{-\varepsilon_{b,n}\omega_{b,n}t}$, and then normalize it to output MOSS.

(4) Compare the output MOSS to that of the undamaged bridge and calculate the damage index.

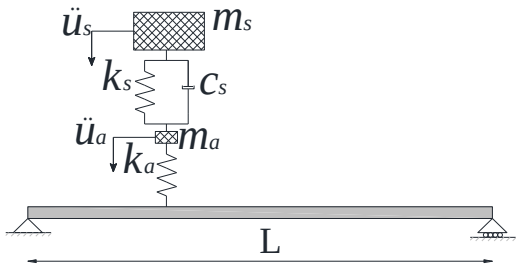

Figure 2. The VBI model used in simulations

3. Numerical Examples

Numerical simulations are used here to check the validity of the method proposed in section 2. A quarter-car model passing over a simply supported beam is adopted as shown in *Figure 2*, where the vehicle is again assumed to travel at constant speed. The vehicle and bridge properties are listed in *Table 1*. The vehicle frequencies are 0.58 Hz and 10.33 Hz. The first natural frequency of the bridge is 3.86 Hz. The road surface profile is not considered, and the time step is selected as 0.005 sec.

Table 1. Vehicle and bridge properties

Vehicle properties		Bridge properties	
m_s	14300 kg	Span	15 m
k_s	200 kN/m	Density	4800 kg/m^3
c_s	10 kNs/m	Width	4 m
m_a	700 kg	Depth	0.8 m
k_a	2750 kN/m	Modulus	2.75×10^{10} N/m^2
		Damping ratio	0.02

3.1 Extracting MOSS from vehicle acceleration

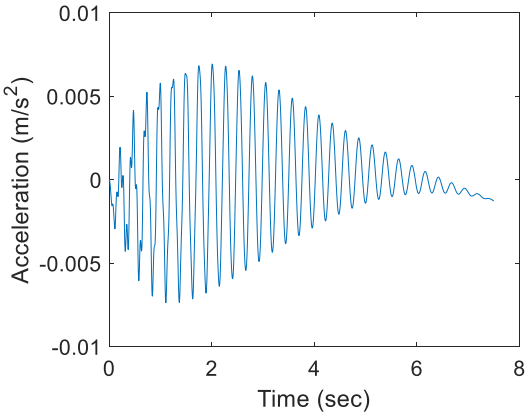

Figure 3. The vehicle acceleration response

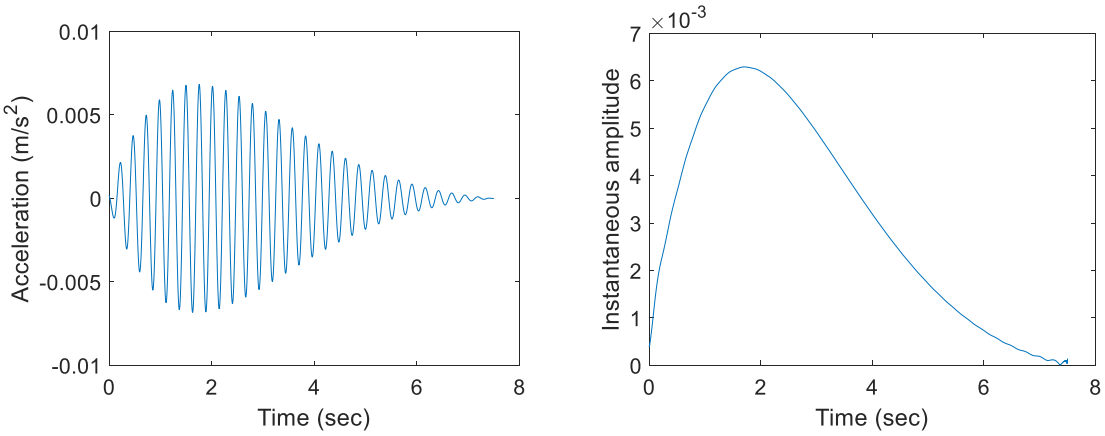

(a) (b)

Figure 4. Filtered vehicle response, (a) Acceleration; (b) Instantaneous amplitude $A(t)$

Figure 3 illustrates the vehicle acceleration response to passage over the bridge. In this case, the vehicle travels at a speed of just 2 m/s, in order to be sufficiently slow [18] for the assumption of the theoretical analysis in section 2. It is acknowledged that such a

low speed is unrealistic and may not even be enough to excite the bridge dynamically – higher speeds will be considered in the next subsection. The acceleration is processed by a suitable band-pass filter to distill out the single component associated with the bridge first natural frequency. The filtered signal is shown in *Figure 4* (a) and the resulting instantaneous amplitude in *Figure 4* (b). Yang, et al. [18] take a normalized version of this instantaneous amplitude to represent the relative mode shape of the bridge directly. However, it is observed that its shape in the figure has an apparent left-shift compared to that of the theoretical first bridge mode shape. This phenomenon happens due to the bridge damping effect as shown in Eq. (4), in comparison to Eq. (3). The revised process is applied to the instantaneous amplitude history, and the result is shown in *Figure 5* (a). Finally, the revised amplitude history is normalized to obtain the bridge MOSS as shown in *Figure 5* (b), where it is compared to the theoretical mode shape and that of Yang, et al. [18]. As can be seen, the extracted MOSS matches the theoretical one very well. Thus, it is concluded that the bridge damping effect is not negligible in the MOSS extracted using the HT method. The accuracy of the extracted mode shape is evaluated using the modal assurance criterion (MAC) as follows:

$$MAC = \frac{|\emptyset_e^T \emptyset_t|^2}{|\emptyset_e^T \emptyset_e||\emptyset_t^T \emptyset_t|} \quad (8)$$

where $\emptyset_e$ and $\emptyset_t$ denote the extracted and theoretical mode shapes, respectively. In this case, the MAC value is 0.9992.

3.2 The effect of vehicle speed

The effect of the vehicle speed on the proposed algorithm is studied, considering six different speeds: v = 2, 6, 10, 14, 18 and 22 m/s. The remaining properties of the VBI model are kept the same as above. Following the same procedure, the bridge MOSS is identified for each vehicle speed. The results show that the bridge MOSS can still be extracted well as vehicle speed increases. The MAC values are illustrated in *Figure 6*, which shows good values, even at higher speeds. While the MAC value decreases as vehicle speed increases (except for 2 m/s), all values are greater than 0.993.

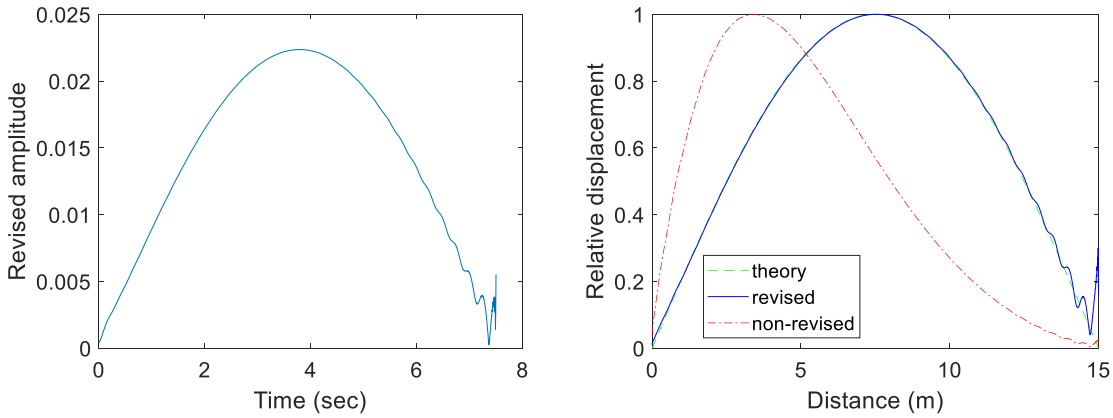

(a) (b)

Figure 5. Revised process results: (a) Instantaneous amplitude; (b) Extracted MOSS

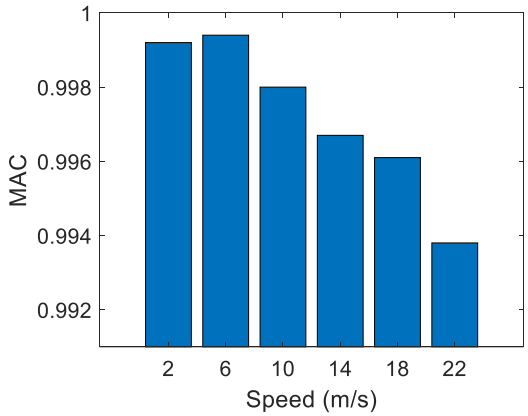

Figure 6. MAC values at different vehicle speeds

3.3 Damage detection using the extracted MOSS

In this section, local damage in the bridge is modeled using the damage model of Sinha, et al. [37], i.e. the stiffness loss is assumed to extend over a region of three times the beam depth. In this case, the element stiffness is taken to vary from a minimum value (maximum damage) at the crack location to full stiffness at a distance of 1.5 depths from the crack. The level of damage is defined by the ratio of the crack depth to the depth of the undamaged bridge. For example, a damage level of 10% means that the crack depth is 0.08 m for a 0.8 m deep bridge.

In this simulation, the damage is located at 6 m distance from left end, with three levels: 10%, 30% and 50%. The vehicle speed is 14 m/s. It is well known that damage changes the bridge natural frequency and, for concrete bridges, the damping ratio, which is the prerequisite of the proposed method. To detect bridge damage with the extracted MOSS, there is no necessity to update the current bridge frequency and damping ratio. That

is say, the healthy condition values of bridge frequency and damping ratio can be used to construct the MOSS. The damage, if present, will be reflected in the damage index anyway.

Figure 7 (a) shows the first MOSS for the three damage scenarios, compared to the healthy case. The MAC values are calculated as 0.9967, 0.9966, 0.9966 and 0.9965, corresponding to the bridge condition of 0%, 10%, 30% and 50% damage respectively. Based on Eq. (6), the damage index is calculated and is illustrated in *Figure 7* (b) for each damage level. A peak close to the damage location can be seen when the damage level is 30% or more. The results demonstrate the ability of the algorithm to detect and, to some extent, localize damage. The damage indicator DI^* defined in Eq. (7) is calculated for each of the damage scenarios and is shown in *Figure 8*. It is clear that DI^* is well-correlated with the level of damage.

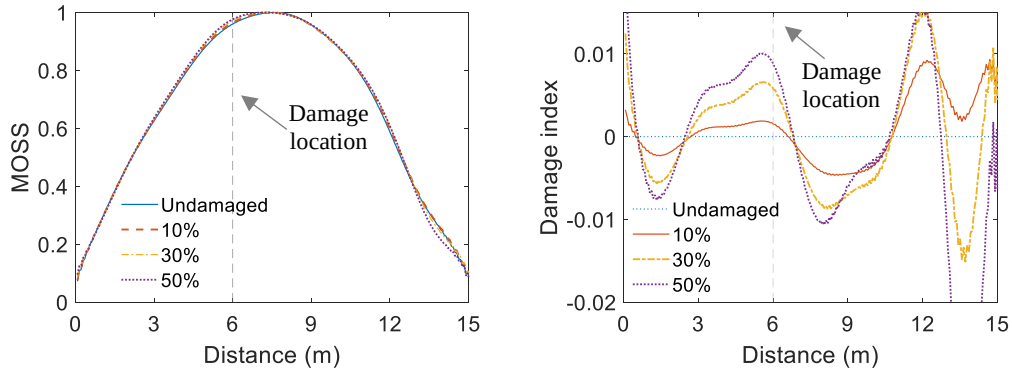

(a) (b)

Figure 7. Influence of Damage on MOSS: (a) Extracted MOSS for different damage levels; (b) Damage index

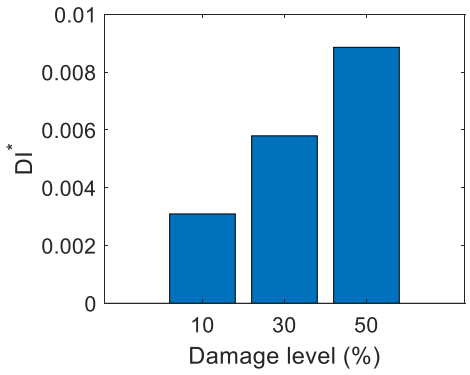

Figure 8. Damage index DI^* at different damage levels

3.4 Influence of Measurement Noise

To further investigate the feasibility of the proposed method, the effect of random noise in the measurements is investigated. Additive Gaussian white noise is combined in this section with the acceleration signal that is, according to [38], given by:

$$A_{poll} = A + E_{nse} \times N \quad (9)$$

where A_{poll} is the signal containing noise, A is the original signal containing no noise, N is a standard normal distribution vector with zero mean and unit standard deviation and E_{nse} is the energy in the noise. The term, E_{nse} is determined from the definition of SNR as follows:

$$SNR = 10log_{10}\frac{var(A)}{E_{nse}^2} \quad (10)$$

where SNR is the ratio of the power in the signal to the power in the noise and $var(A)$ is the variance of the signal.

Generally, noise with SNR level of 40 is considered for the acceleration measurement [36], which is added to the accelerations in this case. The results, shown in *Figure 9*, indicate that damage can still be detected from the index in the presence of noise. This is despite the fact that the band-pass filtering process in proposed algorithm reduces the impact of measurement noise, to some extent.

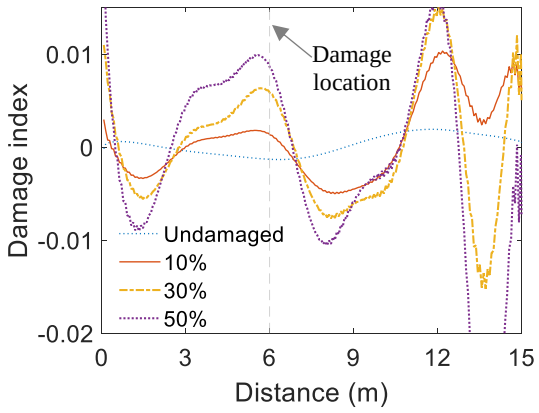

Figure 9. Damage index in presence of measurement noise

5. Experimental Study

5.1 Local Damage Detection

A scaled moving vehicle laboratory experiment is performed to investigate the feasibility of using indirect measurement for bridge health monitoring. The scaled bridge model used in the experiment is summarized in *Figure 10*. On either side of the 5.4 m simply supported test span, additional spans are used for vehicle acceleration and

deceleration. The beam properties, obtained from the manufacturer and from free vibration tests, are listed in *Table 2*. Track surface roughness is also considered in the experiment as shown in *Figure 10* (d). This profile was scaled using electrical tape on both wheel paths of the test vehicle at intervals of 100 mm, based on a real road profile measured on a 40.4 m road bridge in Japan (Kim, et al. [39]), which was categorized as very good (class A) according to the ISO 8608 [40]. This profile is intended to be representative of that expected on a typical highway bridge. However, there are some discrepancies with the measured profile since the scaled profile as a superposition of steps is formed using a simple construction method with layered tape and plastic strips [41].

(a)

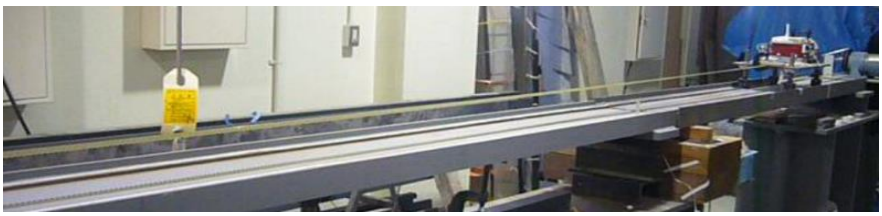

(b)

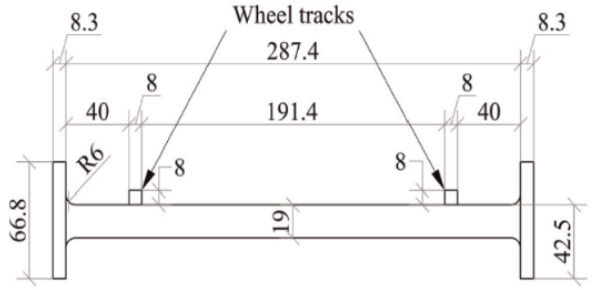

(c)

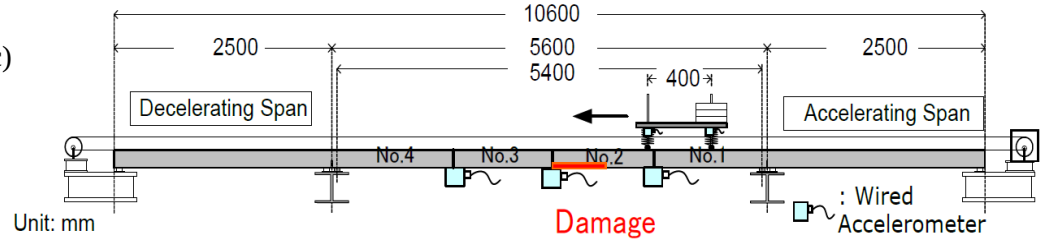

(d)

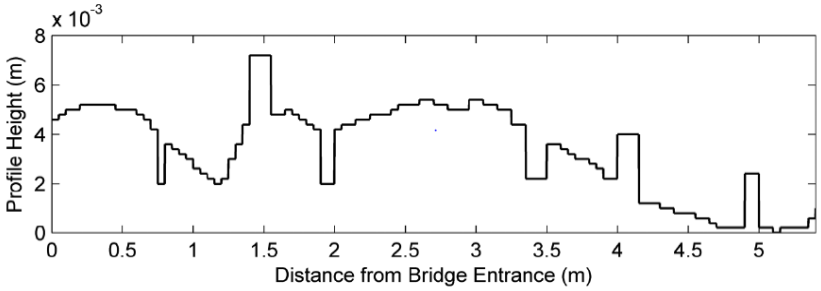

Figure 10. Scale model bridge: (a) Photograph of set-up, (b) Beam cross section (unit: mm), (c) Elevation, (d) Track profile.

Table 2. Structural properties of model girder

Span length L (m)	Material density (kg/m^3)	Cross sectional area, A (m^2)	1st natural frequency (Hz)	Damping ratio for 1st mode, ε	Second moment of area m^4
5.4	7800	6.7×10^{-3}	2.7	0.0016	5.77×10^{-7}

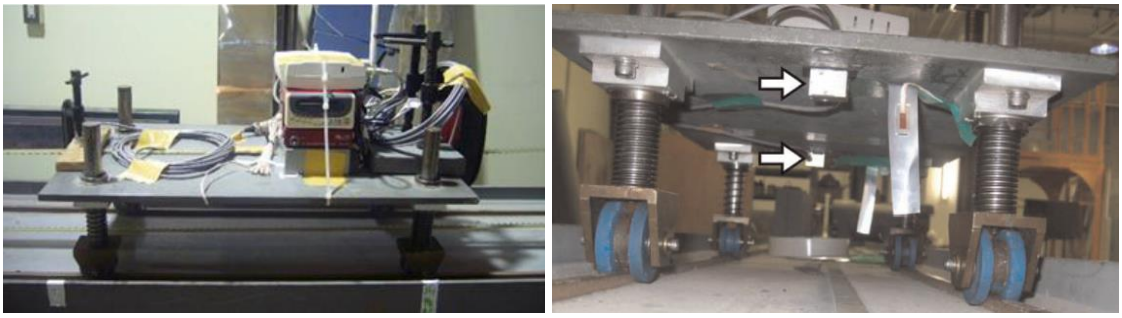

(a) (b)

Figure 11. Experimental vehicle: (a) Side view; (b) End view showing accelerometers.

Table 3. Vehicle model properties

	Mass (kg)	Suspension stiffness (N/m)	Suspension damping ($N \cdot s/m$)
Axle 1	7.9	2680	16.006
Axle 2	13.445	4570	27.762

A scaled two-axle vehicle model is instrumented for the experiments as shown in *Figure 11*. Two accelerometers were mounted at the centers of the front and rear axles respectively to monitor the vehicle motions. This instrumented vehicle also included a wireless router and data logger that allowed the axle acceleration data to be recorded remotely. The vehicle model configuration is given in *Table 3*. The axle spacing and track width are 0.4 and 0.2 m, respectively.

The test vehicle was propelled by a motor and pulley system. Its speed, therefore, was kept constant by an electronic controller as it passed over the bridge. The entry and exit of the vehicle to the beam were monitored using strain sensors in order to synchronize measurements: entry and exit points appeared as peaks in the strain signals. The scaled

vehicle speeds adopted for this experiment are 0.93, 1.16 and 1.63 m/s, represented here by *v1*, *v2* and *v3* respectively. The vehicle repeatedly crossed the bridge, five times at each speed. More details of this experiment are given in references [41-43].

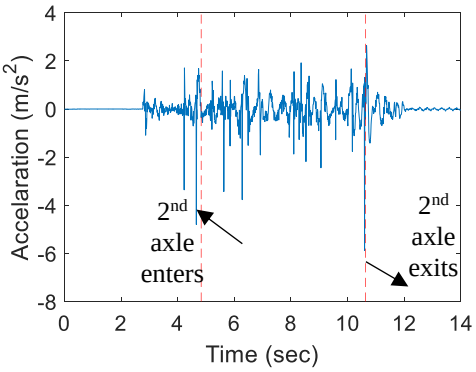

Figure 12. Rear axle acceleration

Figure 12 shows one of five recorded vehicle acceleration signals during its passage over the bridge at a speed of *v1*. A band-pass filter is applied to the signal and a revised process associated with the bridge damping ratio as $A_n(t)/e^{-\varepsilon_{b,n}\omega_{b,n}t}$. Then the process described in Section 3 is used to extract the bridge MOSS. The results are shown in *Figure 13*. Bridge damping has a significant effect on the mode shape inferred from the amplitude history of HT as can be seen by comparing Figure 13(b) and (c). The revised procedure provides a good match with the theoretical mode shape – Figure 13(d) – with a MAC value of 0.9971.

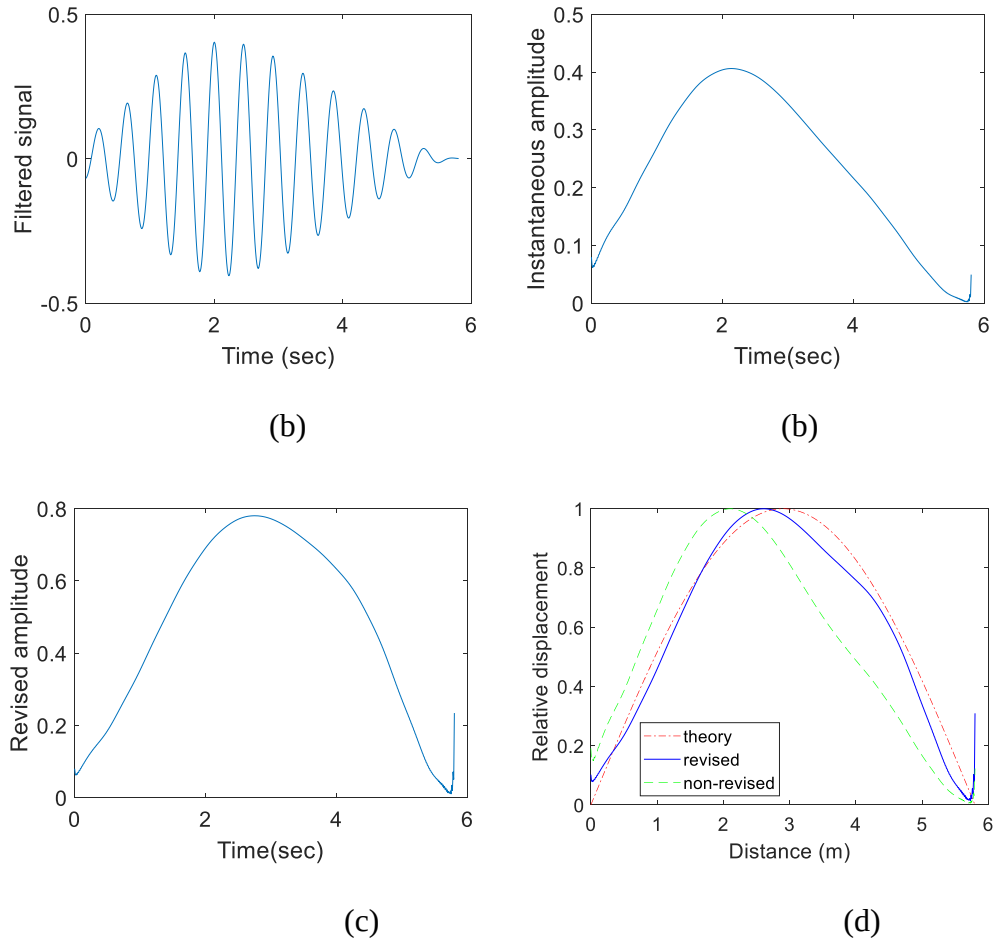

Figure 13. Extraction of MOSS for Test No. 1, speed of v1 (time measured from arrival of Axle 2): (a) filtered signal; (b) corresponding instantaneous amplitude of HT; (c) revised amplitude history; (d) extracted mode shape.

Similarly good results were found for five runs at speed *v*1. Consistent with the numerical results, the accuracy diminishes significantly as vehicle speed is increased, as can be seen from the MAC values plotted in *Figure 14*. The mean of the five MAC values for the speeds of *v1*, *v2* and *v3* are 0.995, 0.963 and 0.869 respectively.

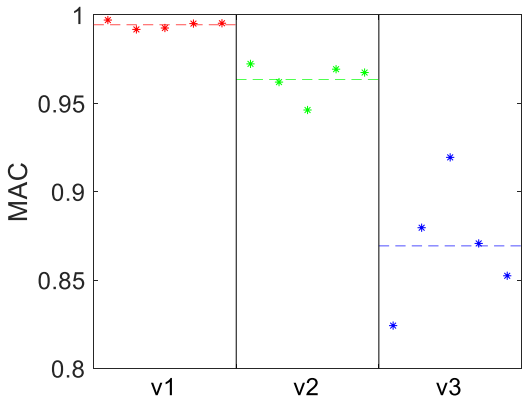

Figure 14. MAC values for different speeds (note: the dotted line represents the average value of five runs)

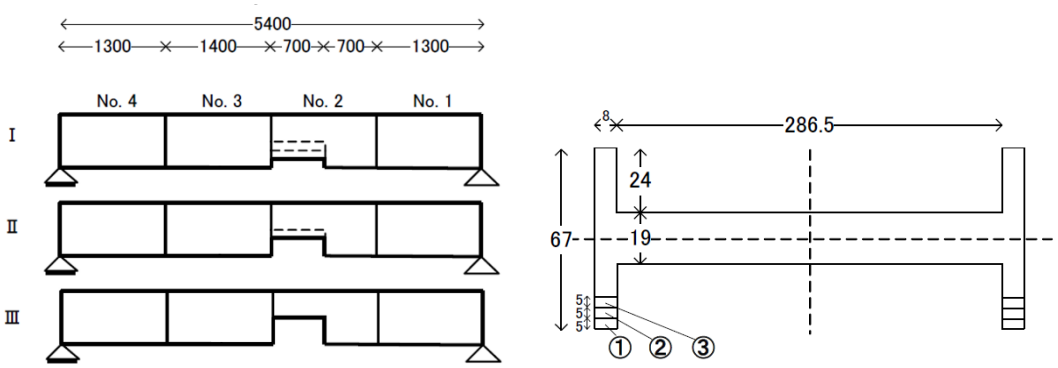

(a) (b)

Figure 15. Damage scenarios (dimensions in mm), (a) elevation, (b) beam cross section

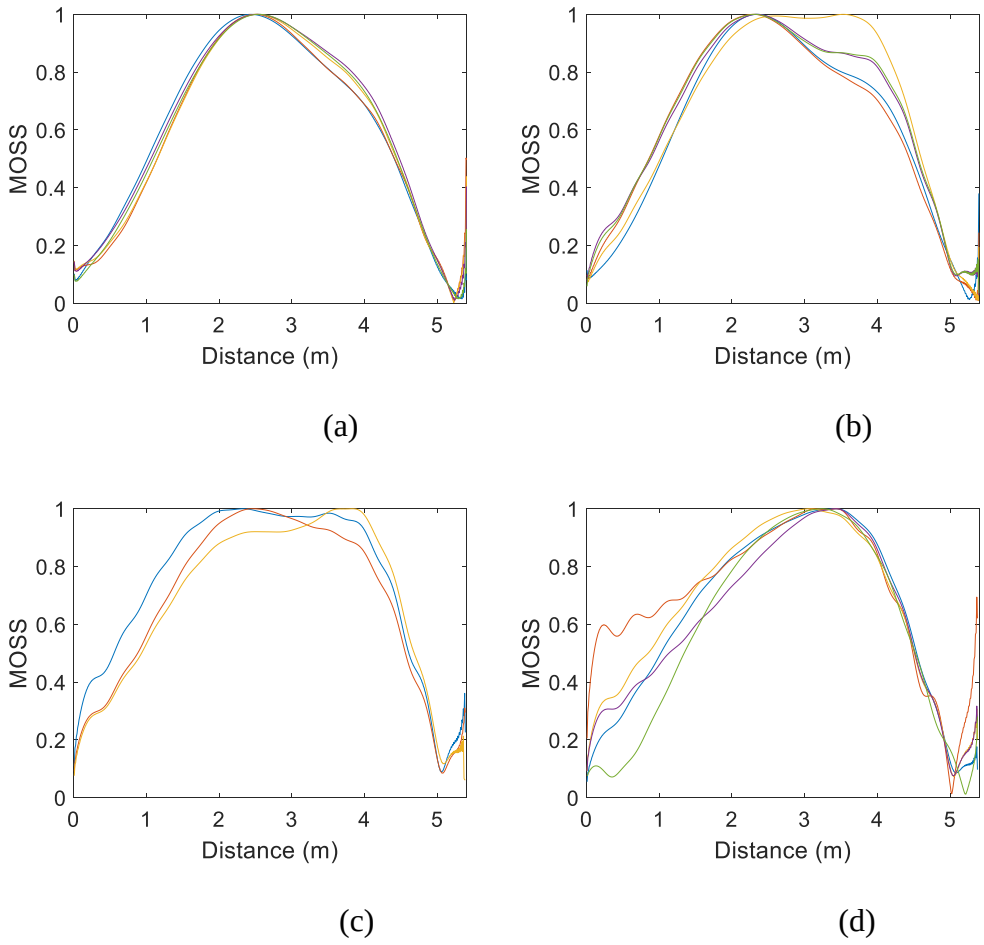

Figure 16. Extracted MOSS's for each scenario: (a) undamaged; (b) damage scenario D1; (c) scenario D2; (d) scenario D3. Note: two of the runs for scenario D2 are not shown here due to a sensor malfunction.

To investigate the feasibility of detecting damage, material in the cross-section of the model bridge was progressively removed and the tests repeated. This damage was applied over a 700 mm length in the left half of segment No. 2, illustrated in *Figure 15* (a). The damage was effected by removing equal parts of both flanges of the steel beam in the damage area as shown in *Figure 15*(b). There were three damage scenarios, D1, D2 and D3, corresponding to the removal of 5, 10 and 15 mm of flange respectively on each side.

The section 2nd moment of area for these damage scenarios was reduced by 13.6%, 27.2% and 39.4% respectively for D1, D2 and D3. The vehicle speed was maintained at 0.93 m/s for this damaged bridge experiment. The vehicle crossed the bridge repeatedly, five times for each scenario, at this speed.

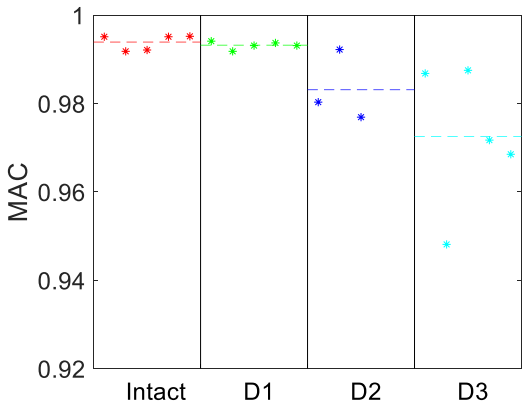

Figure 17. MAC values for different bridge conditions. Note: the dashed line represents the average value of five runs;

The bridge MOSS's were extracted from all of the recorded unsprung accelerations and are illustrated in *Figure 16*. The corresponding MAC values are shown in *Figure 17*. It is clear that, as the damage level increases, the average MAC values decrease. In addition, as seen in *Figure 16*, the results exhibit greater variability in MOSS between runs for the damaged scenarios, including for the lowest damage level, D1. The average MOSS from the five repeat runs for each damage scenario are shown in *Figure 18* (a). The damage indices defined by Eq. (6) are calculated based on the average MOSS results and illustrated in *Figure 18* (b). It can be seen from these experimental results that the damage index tends to increase with increasing damage and may also give an indication of damage location.

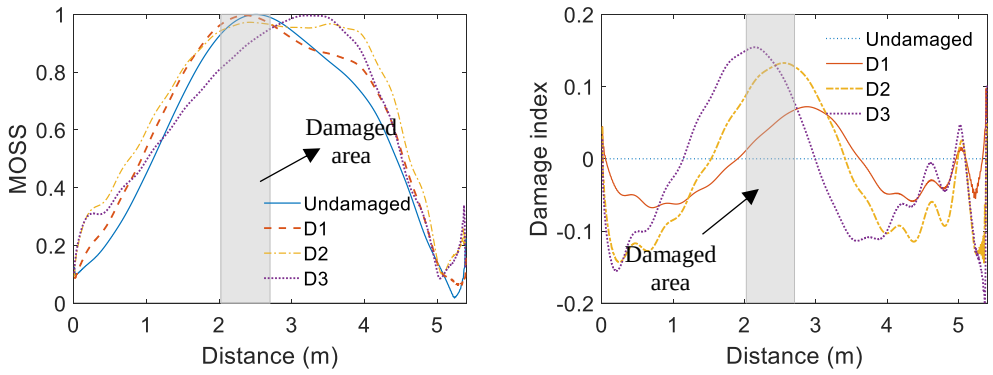

(a) (b)

Figure 18. Experimental results: (a) Average extracted MOSS for different damage levels; (b) Damage index based on MOSS

An alternative damage index, DI^* can be calculated based on the average MOSS for the bridge in its healthy state. This index exhibits a clear increase from damage scenario D1 to D2, but no significant additional change from scenario D2 to D3 (DI^*_{D1}=0.0409; DI^*_{D2}=0.0823; DI^*_{D3}=0.0828). *Figure 19* plots this damage index for the healthy state and scenario D1. The average MOSS of the five repeat runs for the undamaged scenario is set as the baseline, $MOSS^u_n$. The healthy bridge indices vary but not by much. For the lowest level of damage, D1, the index increases significantly and consistently for all five runs.

Figure 20 illustrates the variability in the damage index results for different runs and damage levels. For example, for one run at damage level D2, the peak value of the index is quite close to a run with damage level D1 while another is close to a run with damage level D3. Clearly, while the index is correlated with the level of damage, one run is insufficient to determine the damage level accurately. At this time, it is necessary to average the results from a number of runs to reduce the variability and provide a more accurate indication of damage level.

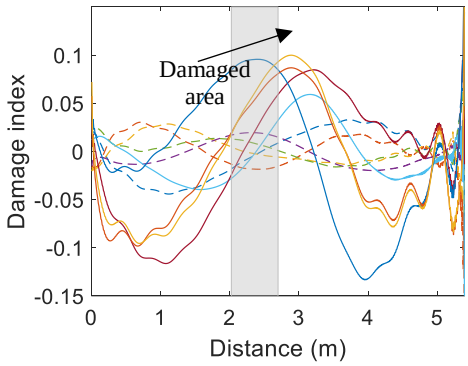

Figure 19. Extracted damage indices for undamaged scenario (dashed curves) and damage scenario D1 (solid curves).

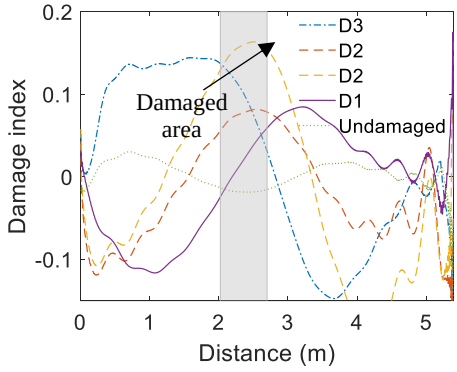

Figure 20. Particular cases where damage index is a poor indicator of damage level

5.2 Global Damage Detection

While local damage results in small changes in the mode shape, global damage, by its nature, affects the overall behavior of the structure and should be easier to detect from the extracted MOSS. *Figure 21* shows an experimental bridge constructed in the same laboratory at the University of Kyoto, to determine if global damage due to foundation scour can be detected by a moving vehicle. The model bridge had four simply supported

spans with the three internal piers supported on springs to represent the vertical stiffness provided by pad foundations. The starts and ends of the bridge had rigid supports. Approach and exit lengths were also present to allow the traversing vehicle to accelerate and decelerate. *Table 4* gives the properties of each span.

Table 4. Span details

Property	Unit	Value
Span length	mm	1300
Span width	mm	300
Span depth	mm	8.07
Second moment of area (rectangular cross section)	m^4	1.31×10^{-8}
Young's Modulus	$N\ m^{-2}$	2.05×10^{11}
Density	$kg\ m^{-3}$	7850

The combined stiffness of the four support springs representing each pier was 196 $N\ mm^{-1}$, which was verified from load-displacement tests. A static scaling criterion was used to calculate appropriate values for the support stiffness. Here, the support stiffness was selected so that the ratio of bridge mid-span deflection (for a unit load at mid-span) to foundation deflection (for a unit load directly above the support) was the same for both the experimental case and a full-scale benchmark case. The foundation stiffness for the full-scale benchmark was calculated using the approach of Adhikary, et al. [44] and assuming a pad foundation of dimensions 2 m × 4 m. To model scour, the springs were replaced with springs of lesser stiffness. Here, two scour cases were examined which equated to

24.5% and 44.9% stiffness loss from the healthy case (stiffness loss at pier 2 or pier 3 as shown in *Figure 21* (a)).

(a)

(b)

Figure 21. Four-span experimental bridge: (a) Elevation; (b) spring supports between spans.

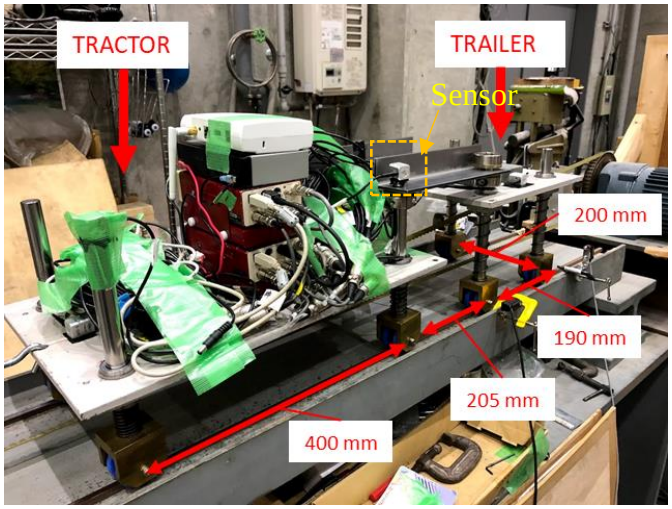

Figure 22. Experimental Vehicle

Figure 22 shows the experimental vehicle that was used which consisted of a tractor towing a trailer. Both the tractor and trailer had four sprung wheels with a steel plate resting on these springs. The tractor had a front and rear axle stiffnesses of 3066 N m^{-1} (i.e. 2×1533 N m^{-1} springs) and 3506 N m^{-1} (i.e. 2×1753 N m^{-1} springs) respectively. The trailer had equal stiffnesses in each axle of 16,928 N m^{-1} (i.e. 2×8464 N m^{-1}). The tractor and trailer had masses of 24.3 kg (of which 20.7 kg was sprung) and 13.7 kg (of which 10.1 kg was sprung) respectively. A vehicle velocity of 1.26 m/s was used in these experiments. The vehicle repeatedly crossed the bridge, 30 times for each scenario, at this speed.

In free vibration tests, it was found that the tractor had bounce and pitch frequencies of 3.1 Hz and 5.5 Hz respectively and the trailer had bounce and pitch frequencies of 6.6 Hz and 3.5 Hz respectively. Seven accelerometers were installed on the test bridge to obtain its modal parameters (one accelerometer at center of each span and one over each pier). Frequency Domain Decomposition (FDD) was applied to the bridge acceleration signals

in free vibration and the first five bridge frequencies determined as 9.8 Hz, 11.7 Hz, 14.1 Hz, 16.4 Hz and 21.9 Hz.

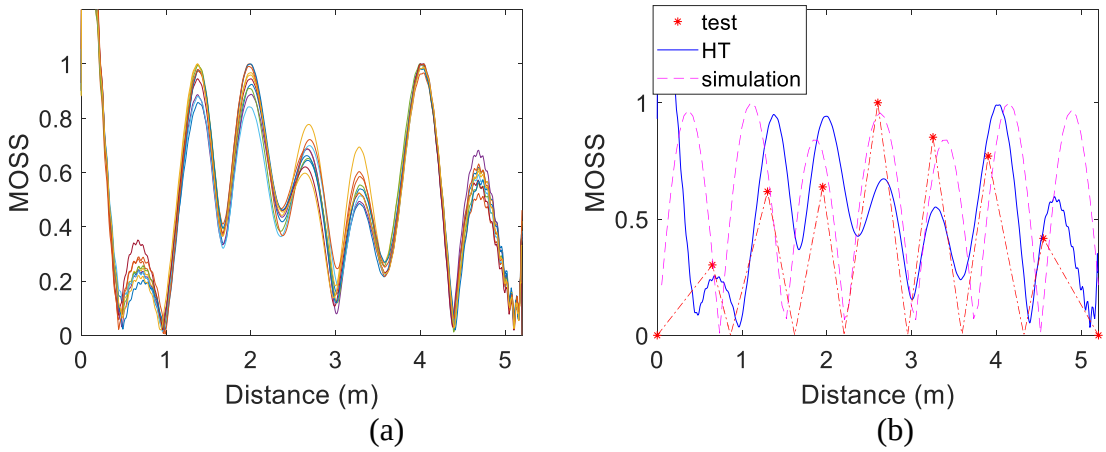

Figure 23. Experimental results: (a) Extracted MOSS for 10 repeat runs, (b) average MOSS

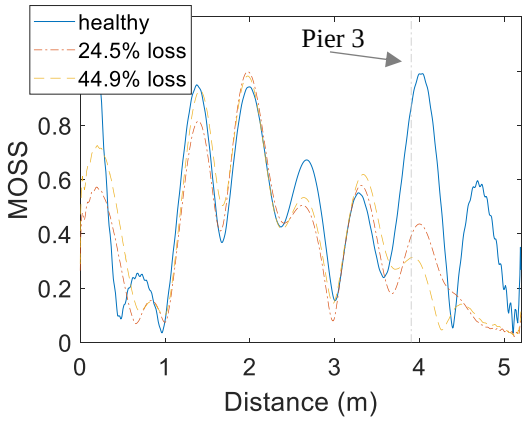

Figure 24. Experimental result with damage at pier 3

The proposed approach is applied on the recorded axle accelerations to extract the bridge mode shapes. However, it is found that in this case, this approach only performs excellently on extracting the 5th bridge mode shape, since the extracted results shows well

repeatability for repeat runs with bridge frequency of 21.9 Hz. For other bridge frequencies, there is no apparent repeatability of the extracted results for repeat runs. Hence, the 5^{th} bridge mode shape is extracted and used to assess the bridge conditions. Figure 23 (a) plots the extracted MOSS of ten successive-repeated runs when the test vehicle passes over the healthy bridge. The average MOSS from the ten runs is calculated and shown in Figure 23 (b), comparing to the simulation and test mode shape (here is MOSS with absolute value). The test mode shape is calculated based on the aforementioned seven accelerometers mounted on the bridge with free vibration. As Yang, et al. [18] pointed out, this proposed Hilbert-based approach is sensitive to the vicinity of nodal point of mode shapes, where shows clear error comparing to the theoretical one.

Similarly, 10 successive-repeated times experiment test at damaged conditions with pier 3 are randomly selected and analyzed, and the average MOSSs are illustrated in Figure 24. Based on the equation (6), the damage index are calculated using these average MOSSs, shown in Figure 25. In order to comparison, one extracted MOSS at undamaged condition is utilized to calculate the damage index, represented as healthy condition. As shown, the damage index value is smooth and small for the healthy condition. When the global damage happened, the damage index shows a great change and there is an apparent peak happened at the damaged location, increased by the damage severity. In addition, another damage index DI^* is calculated as well (undamaged=0.0309; 24.5% loss=0.1986; 44.9 % loss=0.2086).

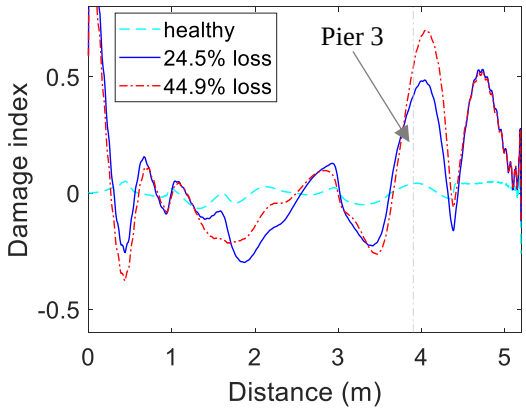

Figure 25. Damage index with pier 3

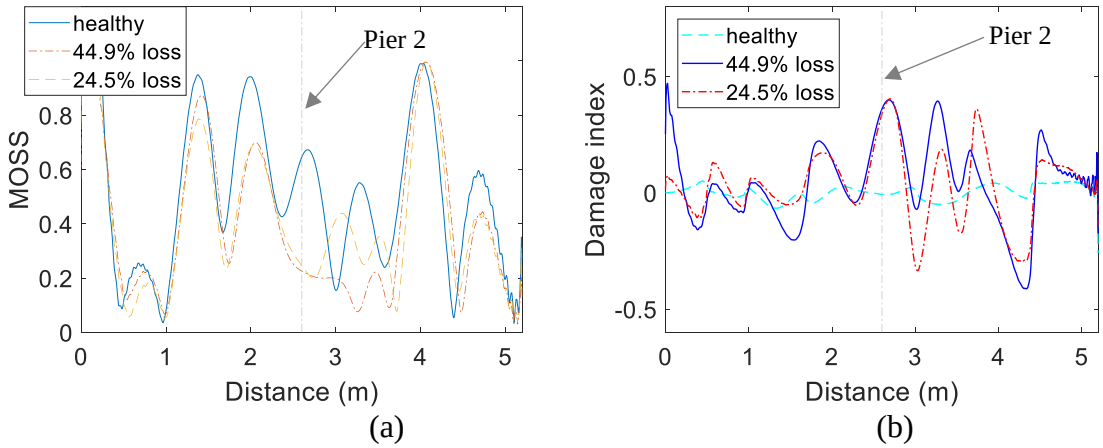

Figure 26. Experimental result with damage at pier 2; (a) the extracted average MOSSs, (b) damage index

Similarly, the proposed algorithm is used to investigate the global damage happened on pier 2. Ten successive-repeated times for three conditions (healthy, 24.5% loss and 44.9% loss) are calculated respectively, and the results are illustrated on Figure 26. The damage index can show a great difference between healthy and damage bridge conditions as well. The damage index DI^* is also calculated for this case (healthy=0.0310;

24.5% loss=0.1209; 44.9 % loss=0.1456). As shown, there is a great change from undamaged to 24.5 % loss condition, but a small change from 24.5 % loss to 44.9% condition.

6. CONCLUSIONS

This paper proposes an algorithm to detect bridge damage using the extracted mode shape from a passing vehicle. The mode shape is extracted using Hilbert Transform. The feasibility of the concept is established through theoretical analysis, numerical simulation and laboratory experiments. In both simulations and experiment, high vehicle speed is found to have a negative effect on the accuracy of the extracted mode shape. In the paper, different kinds of damage – local and global are investigated in the experiment, which are represented by decreasing the stiffness of beam or foundations, respectively. For any damage types, the used damage index, to some extent, can not only localize damage but also reflects the damage level. Besides, it is suggested that averaging several runs is necessary to localize damage and reflect damage level accurately.

ACKNOWLEDGMENT

The National Science Foundation of the United States (NSF-CNS- 1645863, and NSF-CSR- 1813949) sponsors this research. Any opinions, findings, conclusions or

recommendations expressed in this publication are those of the authors and do not necessarily reflect the view of the sponsors.

REFERENCE

[1] F. Magalhães, A. Cunha, and E. Caetano, "Vibration based structural health monitoring of an arch bridge: from automated OMA to damage detection," *Mechanical Systems and Signal Processing,* vol. 28, pp. 212-228, 2012.

[2] P. C. Chang, A. Flatau, and S. Liu, "Health monitoring of civil infrastructure," *Structural health monitoring,* vol. 2, no. 3, pp. 257-267, 2003.

[3] E. P. Carden, "Vibration Based Condition Monitoring: A Review," *Structural Health Monitoring,* vol. 3, no. 4, pp. 355-377, 2004.

[4] C. Z. Chrysostomou and A. Stassis, "Health-monitoring and system-identification of an ancient aqueduct," *Smart Structures and Systems,* vol. 4, no. 2, pp. 183-194, 2008.

[5] E. Grande and M. Imbimbo, "A multi-stage approach for damage detection in structural systems based on flexibility," *Mechanical Systems and Signal Processing,* vol. 76, pp. 455-475, 2016.

[6] X. Kong, C. Cai, and B. Kong, "Damage detection based on transmissibility of a vehicle and bridge coupled system," *Journal of Engineering Mechanics,* vol. 141, no. 1, p. 04014102, 2014.

[7] X. Kong, C. S. Cai, L. Deng, and W. Zhang, "Using Dynamic Responses of Moving Vehicles to Extract Bridge Modal Properties of a Field Bridge," *Journal of Bridge*

Engineering, vol. 22, no. 6, p. 04017018, 2017.

[8] J. P. Yang and W. C. Lee, "Damping effect of a passing vehicle for indirectly measuring bridge frequencies by EMD technique," *International Journal of Structural Stability and Dynamics,* vol. 18, no. 01, p. 1850008, 2018.

[9] X. Kong, C. Cai, and B. Kong, "Numerically extracting bridge modal properties from dynamic responses of moving vehicles," *Journal of Engineering Mechanics,* vol. 142, no. 6, p. 04016025, 2016.

[10] J. Marulanda, J. M. Caicedo, and P. Thomson, "Mode shapes identification under harmonic excitation using mobile sensors," *Ingeniería y Competitividad,* vol. 19, no. 1, pp. 140-145, 2017.

[11] Y. B. Yang, C. W. Lin, and J. D. Yau, "Extracting bridge frequencies from the dynamic response of a passing vehicle," *Journal of Sound and Vibration,* vol. 272, no. 3-5, pp. 471-493, 2004.

[12] Y. B. Yang and C. W. Lin, "Vehicle–bridge interaction dynamics and potential applications," *Journal of sound and vibration,* vol. 284, no. 1, pp. 205-226, 2005.

[13] Y. B. Yang and K. C. Chang, "Extraction of bridge frequencies from the dynamic response of a passing vehicle enhanced by the EMD technique," *Journal of Sound and Vibration,* vol. 322, no. 4-5, pp. 718-739, 2009.

[14] A. González, E. J. Obrien, and P. J. McGetrick, "Identification of damping in a bridge using a moving instrumented vehicle," *Journal of Sound and Vibration,* vol. 331, no. 18, pp. 4115-4131, 2012.

[15] J. M. Brownjohn, P.-Q. Xia, H. Hao, and Y. Xia, "Civil structure condition assessment by FE model updating:: methodology and case studies," *Finite elements*

in analysis and design, vol. 37, no. 10, pp. 761-775, 2001.

[16] B. Jaishi and W.-X. Ren, "Structural finite element model updating using ambient vibration test results," *Journal of Structural Engineering,* vol. 131, no. 4, pp. 617-628, 2005.

[17] S. W. Doebling, C. R. Farrar, and M. B. Prime, "A summary review of vibration-based damage identification methods," *Shock and vibration digest,* vol. 30, no. 2, pp. 91-105, 1998.

[18] Y. B. Yang, Y. C. Li, and K. C. Chang, "Constructing the mode shapes of a bridge from a passing vehicle: a theoretical study," *Smart Structures and Systems,* vol. 13, no. 5, pp. 797-819, 2014.

[19] L. Deng and C. Cai, "Identification of parameters of vehicles moving on bridges," *Engineering Structures,* vol. 31, no. 10, pp. 2474-2485, 2009.

[20] Y. Zhang, L. Wang, and Z. Xiang, "Damage detection by mode shape squares extracted from a passing vehicle," *Journal of Sound and Vibration,* vol. 331, no. 2, pp. 291-307, 2012.

[21] Y. Oshima, K. Yamamoto, and K. Sugiura, "Damage assessment of a bridge based on mode shapes estimated by responses of passing vehicles," *Smart Structures and Systems,* vol. 13, no. 5, pp. 731-753, 2014.

[22] A. Malekjafarian and E. J. Obrien, "Identification of bridge mode shapes using Short Time Frequency Domain Decomposition of the responses measured in a passing vehicle," *Engineering Structures,* vol. 81, pp. 386-397, 2014.

[23] A. Malekjafarian and E. J. Obrien, "On the use of a passing vehicle for the estimation of bridge mode shapes," *Journal of Sound and Vibration,* vol. 397, pp.

77-91, 2017.

[24] E. J. OBrien and A. Malekjafarian, "A mode shape-based damage detection approach using laser measurement from a vehicle crossing a simply supported bridge," *Structural Control and Health Monitoring,* vol. 23, no. 10, pp. 1273-1286, 2016.

[25] L. Frýba, *Vibration of solids and structures under moving loads*. Springer Science & Business Media, 2013.

[26] S. P. Brady, E. J. O'Brien, and A. Žnidarič, "Effect of vehicle velocity on the dynamic amplification of a vehicle crossing a simply supported bridge," *Journal of Bridge Engineering,* vol. 11, no. 2, pp. 241-249, 2006.

[27] S. P. Brady, E. J. O'Brien, and A. Znidaric, "The effect of vehicle velocity on the dynamic amplification of a," *Journal of Bridge Engineering,* vol. 11, no. 2, pp. 241-249.

[28] L. Deng and C. Cai, "Bridge model updating using response surface method and genetic algorithm," *Journal of Bridge Engineering,* vol. 15, no. 5, pp. 553-564, 2009.

[29] W. Wang, L. Deng, and X. Shao, "Number of stress cycles for fatigue design of simply-supported steel I-girder bridges considering the dynamic effect of vehicle loading," *Engineering Structures,* vol. 110, pp. 70-78, 2016.

[30] C. Tan, N. Uddin, E. J. OBrien, P. J. McGetrick, and C.-W. Kim, "Extraction of Bridge Modal Parameters Using Passing Vehicle Response," *Journal of Bridge Engineering,* vol. 24, no. 9, p. 04019087, 2019.

[31] W. Fan and P. Qiao, "A 2-D continuous wavelet transform of mode shape data for

damage detection of plate structures," *International Journal of Solids and Structures,* vol. 46, no. 25-26, pp. 4379-4395, 2009.

[32] L. Hadjileontiadis, E. Douka, and A. Trochidis, "Fractal dimension analysis for crack identification in beam structures," *Mechanical Systems and Signal Processing,* vol. 19, no. 3, pp. 659-674, 2005.

[33] Z. Shi, S. Law, and L. Zhang, "Damage localization by directly using incomplete mode shapes," *Journal of engineering mechanics,* vol. 126, no. 6, pp. 656-660, 2000.

[34] H. Li, C. He, J. Ji, H. Wang, and C. Hao, "Crack damage detection in beam-like structures using RBF neural networks with experimental validation," *International Journal of Innovative Computing Information and Control,* vol. 1, no. 4, pp. 625-634, 2005.

[35] A. Pandey, M. Biswas, and M. Samman, "Damage detection from changes in curvature mode shapes," *Journal of sound and vibration,* vol. 145, no. 2, pp. 321-332, 1991.

[36] E. J. Obrien and A. Malekjafarian, "A mode shape-based damage detection approach using laser measurement from a vehicle crossing a simply supported bridge," *Structural Control and Health Monitoring,* vol. 23, no. 10, pp. 1273-1286, 2016.

[37] J. K. Sinha, M. I. Friswell, and S. Edwards, "Simplified Models for the Location of Cracks in Beam Structures Using Measured Vibration Data," *Journal of Sound and Vibration,* vol. 251, no. 1, pp. 13-38, 2002.

[38] R. G. Lyons, *Understanding digital signal processing, 3/E*. Pearson Education India,

2011.

[39] C. W. Kim, M. Kawatani, and K. B. Kim, "Three-dimensional dynamic analysis for bridge–vehicle interaction with roadway roughness," *Computers & structures,* vol. 83, no. 19-20, pp. 1627-1645, 2005.

[40] ISO, "Mechanical vibration—Road surface profiles—Reporting of measured data," ed, 1995.

[41] P. J. McGetrick, C. W. Kim, A. González, and E. J. O. Brien, "Experimental validation of a drive-by stiffness identification method for bridge monitoring," *Structural Health Monitoring: An International Journal,* vol. 14, no. 4, pp. 317-331, 2015.

[42] C. W. Kim, R. Isemoto, T. Toshinami, M. Kawatani, P. McGetrick, and E. J. O'Brien, "Experimental investigation of drive-by bridge inspection," in *5th International Conference on Structural Health Monitoring of Intelligent Infrastructure (SHMII-5), Cancun, Mexico, 11-15 December, 2011*, 2011: Instituto de Ingeniería, UNAM.

[43] C. W. Kim, R. Isemoto, P. J. McGetrick, M. Kawatani, and E. J. Obrien, "Drive-by bridge inspection from three different approaches," *Smart Structures and Systems,* vol. 13, no. 5, pp. 775-796, 2014.

[44] S. Adhikary, Y. Singh, and D. Paul, "Modelling of soil-foundation-structure system," *Soil Dyn. Earthquake Eng,* vol. 61, pp. 13-28, 2014.

Wavelet-Entropy Approach for Detection of Bridge Damages using Direct and Indirect Bridge Records

by

CHENGJUN TAN
AHMED ELHATTAB
NASIM UDDIN

Submitted to [or In preparation for] *ASCE journal of infrastructure systems*
(Under 2nd review)
Format adapted for dissertation

WAVELET-ENTROPY APPROACH FOR DETECTION OF BRIDGE DAMAGES USING DIRECT AND INDIRECT BRIDGE RECORDS

Abstract

Bridges as a key component of road networks require periodic monitoring to detect structural degradation for early warning. Early detection of loci and extent for structural flaws is essential to maintain bridges functioning safely. The elegant properties of Continuous Wavelet Transform (CWT) in analyzing the signal in both time and frequency domains was the impetus to extensively employ this technique in Structural Health Monitoring applications. However, the faint signature of structural damages in the recorded bridge responses curtails the merits of employing this technique. Furthermore, the selection process for the optimal CWT parameters that could capture signal discontinuities due to structural damages is an arbitrary process, which adds another level of uncertainty to Wavelet Transforms. This paper investigates compiling Shannon entropy to CWT to infer the loci and extents of structural damages in bridges. Entropy is a measure used to evaluate the randomness of the data. The more stochastically the data, the higher the entropy. In this article, Shannon entropy is utilized to associates a proper probability density function for the used wavelet to measure the entropy of the wavelet function at different scales. Implementing this technique facilitates selecting the optimal CWT parameters to better depict the signal, and hence identifying signal discontinuities becomes viable. The paper numerically investigates the fidelity of the proposed approach to identify bridge damages

using mid-span bridge response as well as using indirect records from a vehicle passing over the bridge. An implicit Vehicle-Bridge Interaction (VBI) algorithm is utilized to mimic the vehicle bridge interaction dynamics for different scenarios.

Keywords: Bridge Health Monitoring, Shannon Entropy, Non-destructive evaluation, Wavelet Transform, Wavelet entropy, Drive-by Bridge Inspection.

1. Introduction

The wavelet transform is highly sensitive to discontinuities in signals, and for a long time has been utilized as a robust signal processing tool. Usually, it is used to identify sharp changes in continuous or discrete signals, which are often indicative of damage. Several studies have proven the robustness of wavelet based-algorithms in identifying the intensities and locations of structural damages, both numerically and utilizing scaled laboratory tests (Hou et al. 2000; Liew and Wang 1998; Lu and Hsu 2002). Rucka and Wilde (2006) utilized Gaussian wavelet and reverse biorthogonal wavelet to effectively detect the damage position of the one-dimensional beam and two-dimensional plate, respectively, without knowledge of neither the structure characteristics nor their mathematical model. In another field of study, Douka et al. (2003); Khorram et al. (2012) established a correlation between the crack size and the highest magnitude for the coefficient of the wavelet. Hester and González (2012) proposed a wavelet-based approach using wavelet energy content, instead of wavelet coefficient, which showed to be more sensitive to damages. In tandem with that, Poudel et al. (2007); Shahsavari et al. (2017) utilized wavelet analysis in extracting beam mode shapes as a metric to localize the damage.

Although the mode shapes (Poudel et al. 2007; Rucka and Wilde 2006; Shahsavari et al. 2017) or deflection (Douka et al. 2003; Nguyen and Tran 2010; Zhu and Law 2006) of a beam can be used as input signals for damage detection, on a bridge site, it may not be easy to measure them to the required level of accuracy and at high scanning frequencies (Hester and González 2012). Many kinds of research, therefore, investigated the use of bridge's acceleration as the input signal (Cantero and Basu 2015; Hester and González 2012; Hou et al. 2000; Kaloop and Hu 2015; Tan et al. 2017; Wang et al. 2016).

Recently, authors started to investigate invoking wavelet transform in the drive-by bridge inspection field. Drive-by bridge inspection is the science of utilizing indirect readings from a transit inspection vehicle to monitor the structural deterioration of bridges. This field of research has emerged when Yang et al. (Yang et al. 2004; Yang and Lin 2005) investigated the feasibility of extracting the fundamental bridge frequencies from the vehicle's response. The author found that for a smooth road profile, the vehicle axle acceleration spectrum is dominated by the bridge frequency. Further, for different bridge damping ratios, they observed an apparent drop in the signal power as the damping ratio increases. The latter observation illuminates the fidelity of utilizing indirect vehicle responses in monitoring the bridge health condition. Following Yang's work, Nguyen and Tran (2010) applied a Symlet wavelet transform to the displacement response of a moving vehicle to infer the severity and the location of bridge cracks. The authors theoretically simulated the vehicle bridge interaction dynamics utilizing a four degree-of-freedom half car and a cracked finite element beam. The study revealed that the algorithm sensitivity extensively dropped when the vehicle speed increased. In similar work, Khorram et al. (2012) performed a numerical investigation to compare the performance of direct and

indirect wavelet-based damage detection approach. The deflection response were applied as input signals. They pointed out that the indirect method showed more efficacy on damage detection than the direct method. The indirect method can even detect small cracks with a depth of 10% of beam depth. Although their method showed good performance, the vehicle is idealized as a moving force, neglecting the vehicle inertial component.

Acceleration responses of moving sensors can be also applied to detect the bridge damage (Cantero et al. 2019; Deng and Cai 2009; Fitzgerald et al. 2019; Tan et al. 2017; Xu and Wu 2007). Fitzgerald et al. (2019) numerically investigated the feasibility of using bogie acceleration measurements from a passing train with wavelet analysis to detect the presence of bridge scour. McGetrick and Kim (2014); McGetrick and Kim (2013) highlighted that damaged section used to induce a clear discontinuity in the acceleration response of the passing vehicle, which in return affects the wavelet coefficient. This feature allows damage to be identified and located, only if the vehicle traverses the bridge with considerably low driving speed (2.5m/s).

Successful utilization for wavelet transform requires proper selection for the wavelet scale. Wavelet scale plays an essential role, as it outlines the required frequency band to observe or analyze the objective signal. Wavelet transform can be calculated at every possible scale. A high scale associates to low frequency content, while a low scale corresponds to high frequency content (Hester and González 2012). The selection of appropriate/optimum scale has always been a challenge for users in the application of wavelet transform (Chatterjee et al. 2006; Chen et al. 2009). In most SHM applied with wavelet transforms, they aim to find and localize the discontinuity component of signals indicated by abnormal behavior of structures. It is well understood that not all the wavelet

coefficient give the desired results. Nguyen and Tran (2010) highlighted that only particular scale associated with wavelet coefficient can provide the identifiable result of damage. Up to date, there is no criterion for selecting the scale values, and the process is currently done arbitrarily and subjectively.

This paper introduces a Wavelet Entropy Theory (WET) to select the optimum scale that provides better detection of acceleration signal discontinuities. The article utilizes the signal Entropy as a metric in the scale selection process. Entropy is one of the fundamental notions of science, which generally refers to disorder or uncertain (de Oliveira 2015). Shannon (2001) proposed the concept of information entropy (Shannon entropy), which is defined as a measure of the average information content produced by a stochastic data as random events. The more stochastically the data, the higher the entropy. Therefore, Shannon entropy can be utilized to measure the energy distribution of the stochastic data. For Continuous Wavelet Transform, each wavelet shape can be associated with a probability density function that allows defining the entropy of the wavelet function (de Oliveira and de Souza 2006). The objective of this article is to compile Shannon Entropy with Wavelet Transform, to find the scale that has the lowest possible entropy for a particular signal. This scale will be the most representative scale to this signal, as it has the lowest entropy. In tandem with that, the wavelet of this scale will be very sensitive to any signal disorder, therefore damage detection becomes viable. This framework is what introduced as Wavelet Entropy Theory (WET).

2 Wavelet Entropy Theory Background

2.1 Wavelet transform

The wavelet analysis is a robust signal processing technique, which relies on the introduction of an appropriate basis and a characterization of the signal by the distribution of amplitude in the basis. If the wavelet is required to form a proper orthogonal basis, it has the advantage that an arbitrary function can be uniquely decomposed and the decomposition can be inverted (Rosso et al. 2001). The wavelet is a smooth and rapidly vanishing oscillation function with outstanding localization in both time and frequency domain. The continue wavelet transform (CWT) of a function $f(t)$ is defined as the integral transform of $f(t)$ with a family of wavelet functions $\Psi_{a,b}(t)$ for each a and b:

$$WT(a,b) = \int_{-\infty}^{+\infty} f(t)\,\Psi_{a,b}(t)dt \qquad (1) \qquad (1)$$

where

$$\Psi_{a,b}(t) = \frac{1}{\sqrt{a}}\Psi\left(\frac{(t-b)}{a}\right) \qquad (2) \qquad (2)$$

is called daughter wavelet derived from mother wavelet $\Psi(t)$, satisfies the properties of $\int_{-\infty}^{+\infty}\Psi(t)dt = 0$ and $\int_{-\infty}^{+\infty}|\Psi(t)dt| < \infty$; a and b are real-valued parameters, denoting the scale and translation parameters, respectively.

2.2 Shannon Entropy

In science, entropy is commonly associated with the amount of disorder/order; the higher the entropy the greater the disorder (Blackburn 2005). The random event or unpredictability, can be measured in terms of entropy. Claude Shannon, who is the father

of entropy theory, gives a useful criterion for analyzing and comparing probability distribution (Shannon 2001). It allows to measure the amount of information for any distribution using the concept of Shannon entropy. Assuming a discrete random variable X with possible values [x_1... x_n] and the probability distribution function P(X), such that $\sum_{i=1}^{n} P(x_i) = 1$, the entropy can explicitly be defined as:

$$E_{entropy}(X) = -\sum_{i=1}^{n} P(x_i) log_2 P(x_i) \qquad (3) \qquad (3)$$

where set $P(x_i) log_2 P(x_i) = 0$ when $P(x_i) = 0$.

It should be noted that $E_{entropy}(X)$ is a function of the probabilities of the random variable, P (X = x), in a sample (X) and not the random variable itself (x) (Bulusu and Plesniak 2015). This is in agreement with the fact that maximum entropy o f a discrete random variable is achieved by a uniform distribution (de Oliveira and de Souza 2006; Shannon 2001). Now considering the example of a coin toss, not necessarily fair, assume the probability of heads is represented by $P(h)$ while the probability of tails is $1 - P(h)$. Followed by the above equation, the entropy of this coin toss corresponding to $P(h)$ is plotted in Figure 1. The entropy of the unknown result of the next toss of the coin is maximized when the coin is fair (practically it is a uniform distribution). This is the situation of maximum uncertainty as it is most difficult to predict the outcome of the next toss. It is well understood that if the coin is not fair, there is less uncertainty, since one side is more likely to come up than the other; the more unfair the less uncertainty. Accordingly, the reduced uncertainty is quantified in a lower entropy. For instance, if $P(h)$ is 0.9, then the entropy of the coin toss becomes lower as 0.469. Extremely, a coin toss using a coin that has two heads and no tails ($P(h) = 1$) has zero entropy since the coin will always come up heads, and the outcome can be predicted perfectly. As it has shown, the Shannon

entropy is effective to measure the amount of uncertainty in the random data or event. It concluded once again that a system associated with the higher entropy has more uncertainty with greater information (Saviotti 1988). In contrast, a system associated with the lower entropy has the ordered state, consequently providing more stable, reliable or useful information to some extent.

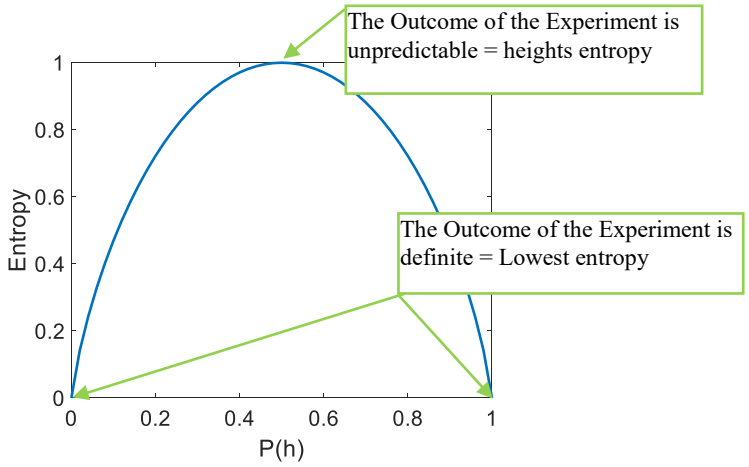

Figure 1. The entropy of coin toss experiment

2.3 Algorithm of Optimum Wavelet-Scale Search

As mentioned above, wavelet functions can be dilated into infinitely large or infinitesimally small scales (a). Therefore, a question that naturally arises by wavelet users is when or how to exit from the process of wavelet transformation; more specifically, what wavelet scale applies on the measured signal can effectively describe the interest of the user? For example, as shown in Figure 2, the interest of application on wavelet is to detect the abrupt in the contaminated sine function. Using the finer scale daughter wavelet to approximate the objective signal, that highlight the noise component, leads to a number of

redundant coefficients as noticeable distractions from the main results (Kailas and Narasimha 1999). While the greater scale daughter wavelet will dilute the wave shape, resulting in disability of detecting the partial changes of signals. How to select the optimal scale have always been the challenge in the application of wavelet transform. With the aid of Shannon entropy measure, optimal scale "a" (a_2) can be identified to depict signal discontinuity, which implies a presence of damage.

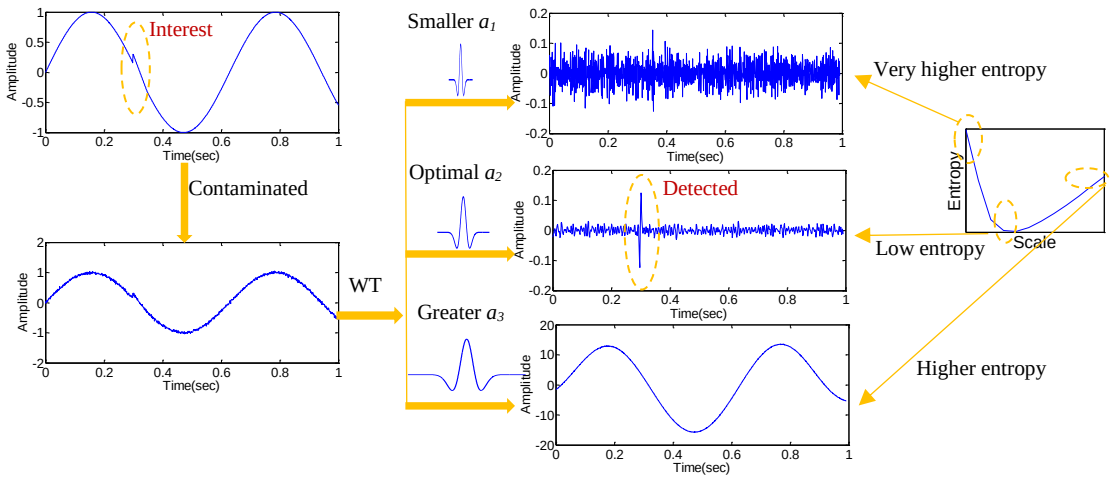

Figure 2. Schematic of WET technique application

The energy of the wavelet coefficients at particular scales a can be described as:

$$E_{energy}(a) = \sum_{i=1}^{N} |WT(a,b)|^2 \qquad (4) \qquad (4)$$

where N is the total number of wavelet coefficients.

The energy probability distribution of the wavelet coefficients is quantitatively described as:

$$p_i = \frac{|WT(a,b)|^2}{E_{energy}(a)} \; with \; \sum_{i=1}^{N} p_i = 1 \qquad (5) \qquad (5)$$

Therefore, the wavelet Shannon entropy at each scale associated with the energy

probability distribution can be calculated based on equation (3). Recall that the higher the entropy the greater the disorder, so the optimal scale of daughter wavelet to approximate the measured signal should have the lowest Shannon entropy value, which can provide the most ordered situation to observe or most effectively represent the original signal. In the same vein, this scale will be the most sensitive to any signal disorders. In fact, a very ordered process could be thought of as a periodic mono-frequency signal (signal with a narrow band spectrum). A wavelet representation of such a signal will be greatly resolved in one unique wavelet resolution level (particular scale a), which in consequence the Shannon entropy will be near zero or of a very low value (Ren and Sun 2008). However, in previous example the ideal ordered process is not exist. The optimal scale a_2 associated with lowest Shannon entropy provides the most ordered process in this case comparing to others.

From another perspective, a lower Shannon entropy value, which is attributed to lower signal uncertainty, translates to a higher concentration of the signal energy (Bulusu and Plesniak 2015). As it has shown in the example, the wavelet coefficients at both of the smaller scale (a_1) and greater scale (a_3) have the apparently dispersed energy distribution with higher Shannon entropy. Contrarily, the wavelet coefficients associated with lowest Shannon entropy greatly concentrate the energy at the position of the change happened. That is also the exact interest of detecting discontinuity or damage component from the measured signal in SHM applications.

The composition of Wavelet Transform, and Shannon Entropy can be summarized in the following steps:

(1) Acquisition of the measured data $X(t)$.

(2) Applying WT on $X(t)$ at series of scales from 1 to M with Eq. (1).

(3) Calculating the wavelet energies at each scale and their energy probability distribution using Eq. (4) and Eq. (5).

(4) Calculating wavelet Shannon entropy at each scale to select the scale which is associated with lowest entropy value as the optimal scale for damage detection with Eq. (3).

3 Numerically Investigating the Fidelity of WET

In order to investigate the fidelity and effectiveness of the proposed approach, a simple example is given as below. Consider a sinusoidal signal $X(t) = \sin(10t + 0.2)$ where; the sample size is 1000 and the sampling frequency is 1000Hz. The discontinuity presents at [300-350] sample window by adding a step function with 0.1 magnitudes. The signal has been contaminated by a White Gaussian Noise of 40dB noise intensity. Figure 3 shows the original and the corrupted signals.

Wavelet Analysis has been applied with mother wavelet of 'Gaussian2' to identify the signal discontinuity section, and the contour map is illustrated in Figure 4. In this plot, time and scale are represented by two mutually perpendicular horizontal axes, while wavelet coefficient is on the vertical axis. The variation of the signal power is depicted in the figure by the color intensity. As shown, it is difficult to directly identify the discontinuity section from Figure 4.

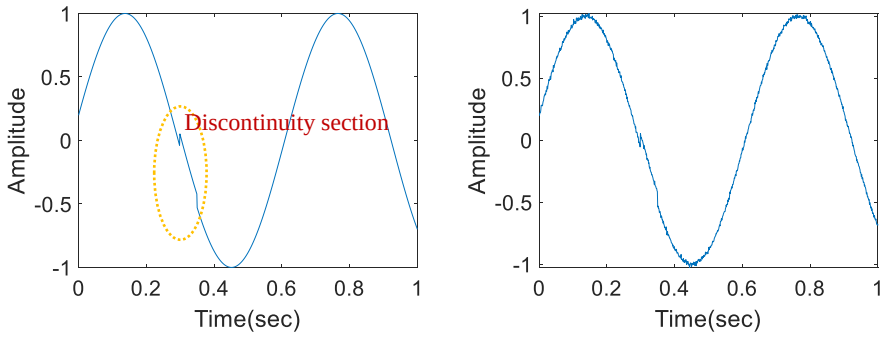

(a) (b)

Figure 3. Test signal, (a): The original signal with discontinuity; (b): The contaminated signal

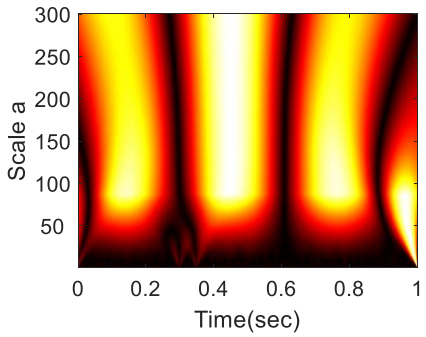

Figure 4. Wavelet transform of the signal from scale 1 to 300

To examine the proposed approach, first the wavelet coefficients energy at each scale from 1 to 300 are calculated using the Eq. (4). Then, the energy probability distribution of wavelet coefficients at each scale are obtained by applying the Eq. (5). Finally, the wavelet entropy at each scale is computed with the Eq. (3) and the results are shown in Figure 5. The minimum entropy presents at scale "*a*" of 4. The wavelet coefficient at scale 4 is taken out and illustrated in Figure 6 (b). It is evident in the figures that signal disorder has become clearly visible. The wavelet transform plot is rescaled as shown in

Figure 6 (a) for this scale, which shows two highlighted lines indicating the start and end points of signal discontinuity.

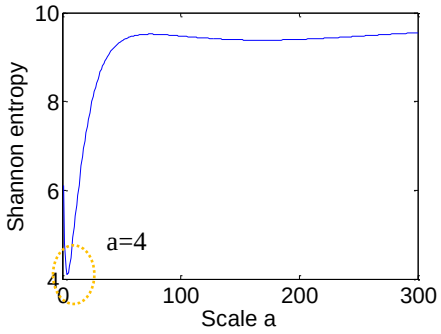

Figure 5. The Shannon entropy from scale 1 to 300

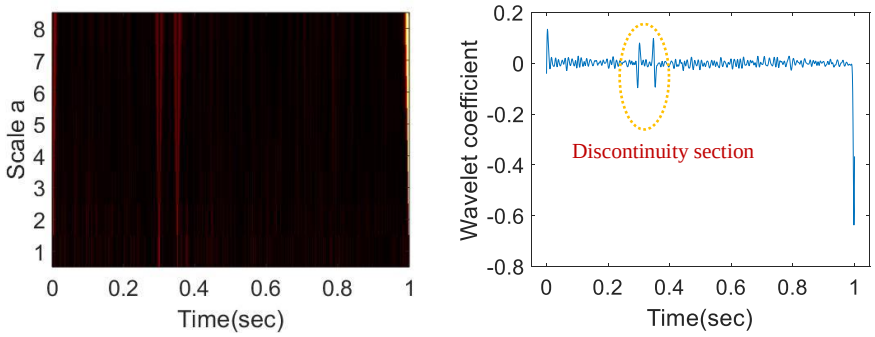

(a) (b)

Figure 6. Result of example (a): Wavelet transform of signal from scale 1 to 8; (b): The wavelet coefficient at scale 4

However, there are apparent edge effect happened, which is a common challenge in the field of wavelet-based application. The edge effect may interfere the decision of the damage detection. To avoid the edge effect, the ideal and simple way is to acquire much longer signal before and after the target component of signal, without introducing new

discontinuity. But that's not always possible. Alternately, the target signal can also be extended with some techniques to decrease edge effects, such as zero paddings, periodic extension, symmetric extension, and data windowing, and so on (Torrence and Compo 1998). Figure 7 plots the wavelet coefficient at scale 4 of the contaminated signal in Figure 3 (b) after using the zero paddings technique. As shown, there is no clear edge effect that may compete with the effect of damage.

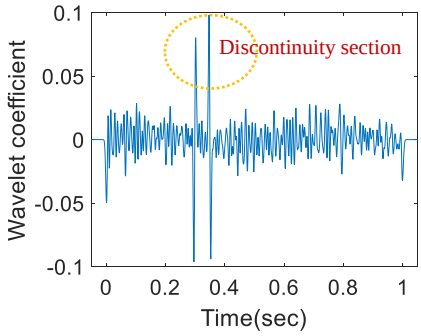

Figure 7. The wavelet coefficient at scale 4 after zero padding

Table 1.Vehicle and bridge properties

Vehicle properties		Bridge properties	
m_s	14300 kg	Span	20m
k_s	200 kN/m	Density	4800kg/m^3
c_s	10 kN s/m	Width	4m
m_a	700 kg	Depth	0.8m
k_a	2500 kN/m	Modulus	2.75×10^{10} N/m^2

4 Application of WET to VBI model

In this section, the feasibility of WET on localizing the bridge damage is investigated. Implicit Vehicle-Bridge Interaction (VBI) solver algorithm is utilized to mimic the vehicle bridge interaction dynamics (Elhattab et al. 2016; Tan et al. 2019). Then, both of responses of the bridge (direct Measurements) and the passing vehicle (indirect Measurements) are applied to the proposed algorithm to localize the bridge damage.

4.1 Application of WET to a quarter-car model

First, the vehicle is modeled as a quarter-car model crossing a 20-m approach distance followed by a 20-m simply supported bridge. The vehicle masses are represented using a sprung mass, m_s, and un-sprung mass, m_a, which are representing the vehicle axle mass and body mass respectively. The vehicle has axle mass bouncing degree of freedom "u_a" as well as sprung mass bouncing degree of freedom "u_s". The properties of the quarter-car are listed in Table 1 (Cebon 1999; Harris et al. 2007). The dynamic interaction between the vehicle and the bridge has been implemented in MATLAB. Unless otherwise mentioned, scanning frequency is set as 1000Hz. The bridge fundamental frequencies are 2.07Hz and 8.38Hz; whereas the vehicle frequencies are 0.57Hz and 10.33Hz, respectively. Structural damage is modeled utilizing the damage mode of Sinha et al. (2002). The damage level is defined as the ratio of the crack depth to the depth of the intact bridge. For instance, 0.1 or 10% damage level implies that a crack depth equals 0.08 m for a bridge with a depth of 0.8 m.

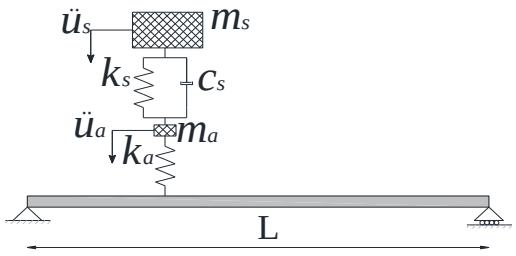

Figure 8. The VBI model

The vehicle is simulated by crossing the approach and the bridge with a constant speed of 2.5m/s. Figure 9(a) illustrates the mid-span acceleration response for the VBI model mentioned above. The x-axis shows the normalized position of the vehicle axle on the bridge with respect to the bridge length (L) (0 and 1 when the axle is at the start and end of the bridge, respectively). The bridge is damaged at 0.35L (L = bridge span) where the damage level is set to 0.5. The road surface profile is not considered in this case. In application of wavelet, the choice of wavelet is important. Different wavelets with different characteristic may give different results. Hester and González (2012) pointed out that Gaussian 2 and Mexican Hat were the most successful at identifying the type of damage investigated in their research, which is the same type to this paper. Therefore, Shannon entropy is computed for wavelet scales with Gaussian 2 and plotted as shown in Figure 9 (b). The optimal scale is found to be around 440; which will satisfy the minimal value of Shannon entropy. The wavelet coefficient at this particular scale is taken out and showed in Figure 9 (c). The plot shows an evident peak around the crack position.

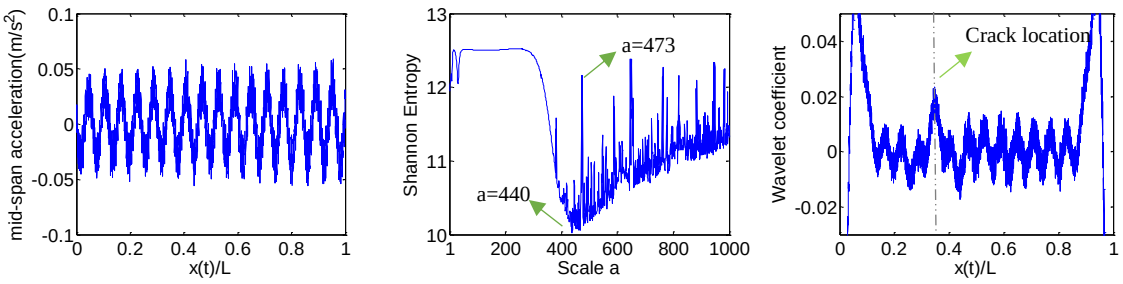

(a) (b) (c)

Figure 9: WET on direct measurement (a) bridge mid-span acceleration, (b) Shannon entropy, (c) wavelet coefficient

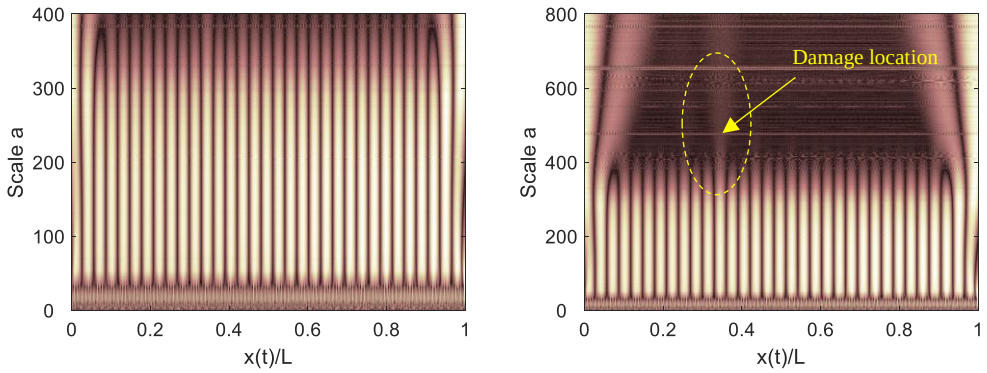

(a) (b)

Figure 10. Wavelet coefficients, (a) Scales from 1 to 400, (b) scales from 1 to 800

There are some traditional wavelet-based approaches for structural damage detection, who use CWT contour map to represent the damage location directly (Hou et al. 2000; Kim and Melhem 2004). In their approaches, no method was proposed to select the range of scales that can identify the damage. However, it is found that the range of scale is important for damage detection. For example, the contour map associated with this case, as shown in Figure 10 (a), scale from 1 to 400, is not able to indicate any damage

information. While the contour map as shown in Figure 10 (b), scale from 1 to 800 can show the difference happened at the bridge damage location, even it is not obvious. It is clearly observed that Figure 9 (c) shows a better result than Figure 10 (b) for damage detection.

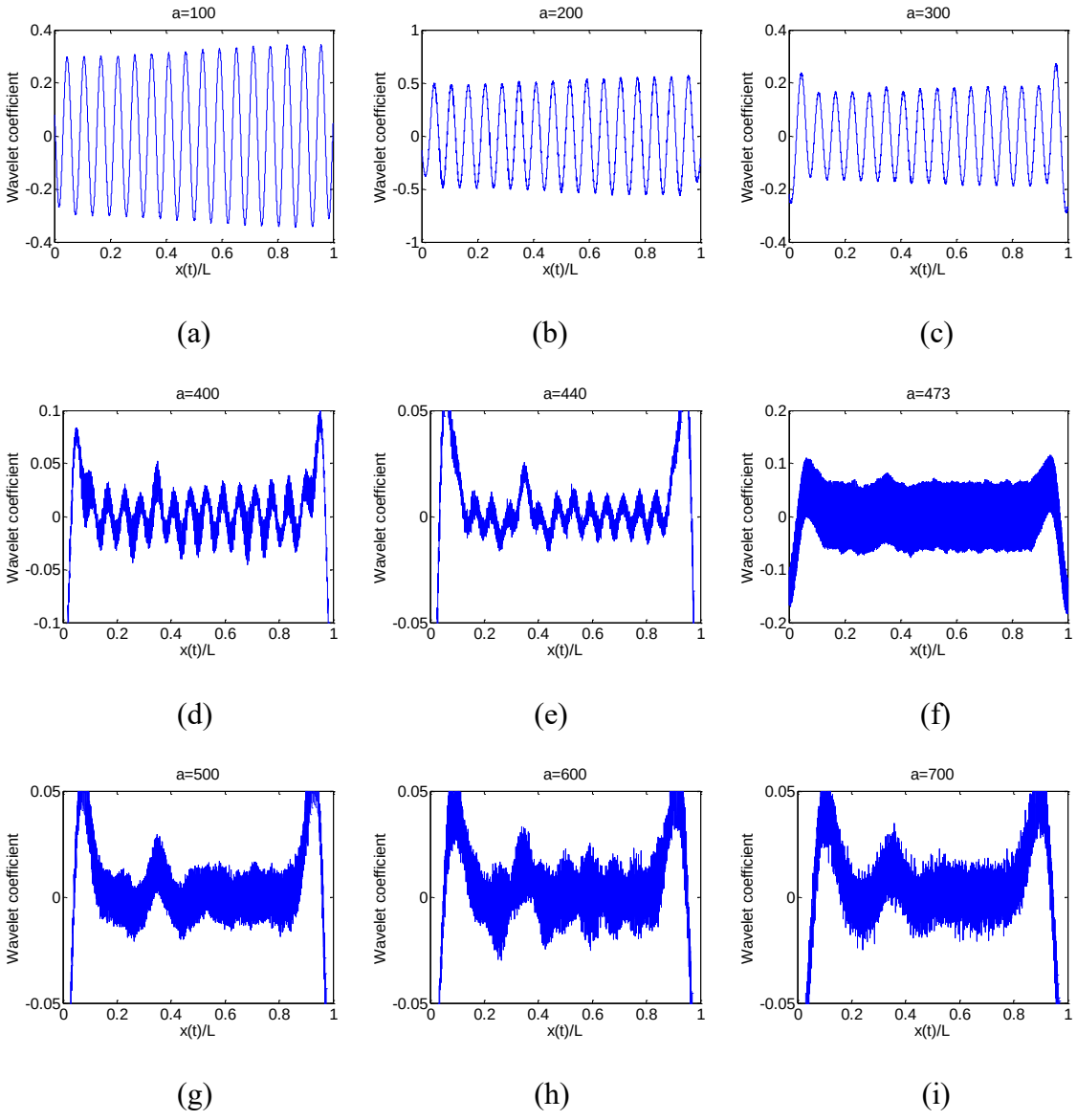

Figure 11. Wavelet coefficients at different scales

To further compare the proposed approach with the traditional approach, where CWT constants are randomly selected, in this case the wavelet coefficient with Gaussian 2, at different manually picked scales were presented in Figure 11. It is evident from the plots that the best scale that provides the best observation for the damage is where the Entropy of the Wavelet Energy is minimal (a=440). Lower scales (a =100 → 300) have the highest entropy (as depicted in Figure 9-b) therefore there is no sign of damage in their corresponding wavelet plots as presented in Figure 11 a-b-c. On the other hand, higher scales (500 → 700) have lower entropy, and therefore damage is representable in their corresponding wavelet coefficient plots. The figure points out that the optimal scale that has the highest sensitivity to the signal disorder (or the signal discontinuity due to bridge damage) is where Shannon entropy is minimal. This finding establishes the fidelity of the proposed technique in selecting the appropriate wavelet scale to identify signal discontinuities that present in the structure responses due to the existence of cracks or flaws. In addition, it is found that the wavelet coefficient with Mexican Hat can present similar result indicating crack location as well, where the optimal scale is 319.

Discrete wavelet transform (DWT) is another traditional approach used to detect structural damage existence and loci (Hou et al. 2000; Ovanesova and Suarez 2004). Generally, the details at level 1 from the DWT are used for indicating structural damage, based on its obvious discontinuity. Hence, this acceleration in Figure 9 (a) is applied with 5-level DWT to decompose and all the details for each level are illustrated in Figure 12. However, level 1 detail, as well as the other details show no sign for any damage information. In this case, it concludes that the bridge acceleration contains the damage information, but it is weak. It is difficult to extract the damage component information from

the recorded bridge acceleration response. The proposed approach shows more effectiveness to detect the damage than the one of DWT-based and contour map.

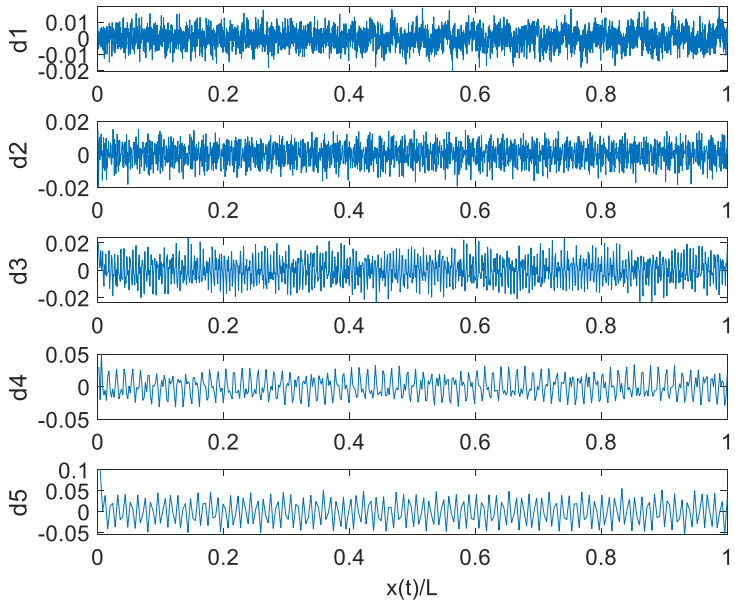

Figure 12. Details in wavelet decomposition of acceleration response at 5 levels

Then, with the same case, the application of WET to indirect measurements is also investigated. The vertical acceleration of the quarter-car axle mass is used as the source signal. The signal is presented in Figure 13(a). The acceleration response is analyzed with *Gaussian 2*. The wavelet scale that provides the minimum entropy has been utilized to plot the wavelet coefficient. The location of the damage is evident in the plot as shown in Figure 13(c). Furthermore, the plot shows a better identification (higher sensitivity) to structural damages when the vehicle response is used.

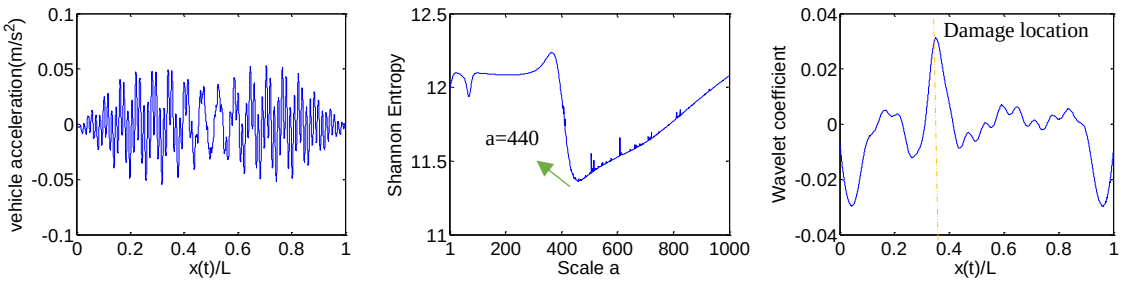

(a) (b) (c)

Figure 13. WET on indirect measurement (a) vehicle acceleration, (b) Shannon entropy, (c) wavelet coefficient.

4.2 Application of WET with random traffic

Then, the scenario of the two quarter-cars is simulated that another vehicle representing random traffic passes on the bridge. The traffic vehicle has the same characteristic with the test/instrumented vehicle, where the dynamic properties of m_s is 8300kg and others are kept same (the weight ratio of traffic vehicle to test vehicle is 0.6). In this case, the test vehicle and traffic vehicle with the same constant speed of 2.5m/s and the latter one moves in front with 5 meters space between them.

Followed by the proposed procedures, the results of applying WET to direct/indirect measurements are shown in Figure 14 and Figure 15, respectively. The x-axis shows the normalized position of the test vehicle on the bridge with respect to the bridge length. As shown, when the vehicle arrives/leaves the bridge, it introduces a discontinuity into bridge/vehicle acceleration response which is captured by the wavelet coefficient. Both direct and indirect results can still show a visible peak at the bridge damage location on its optimum wavelet coefficient. In addition, the indirect result shows

higher sensitivity to structural damages than the one of direct measurement.

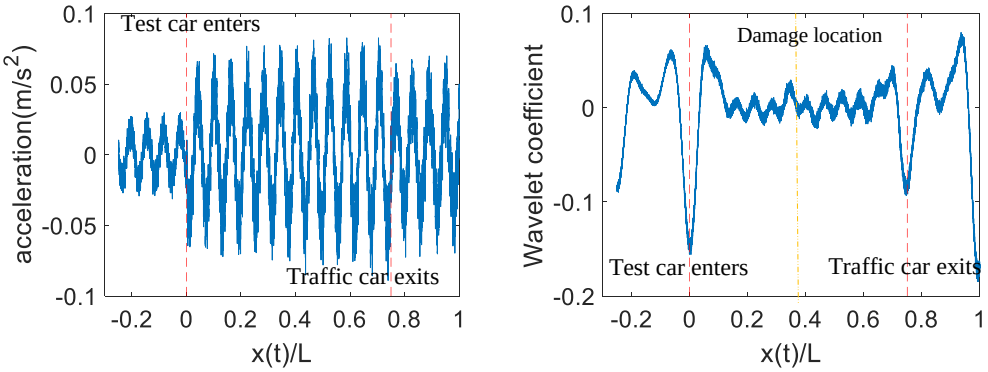

(a) (b)

Figure 14. WET on direct measurement with traffic. a) Bridge mid-span acceleration, (b) wavelet coefficient.

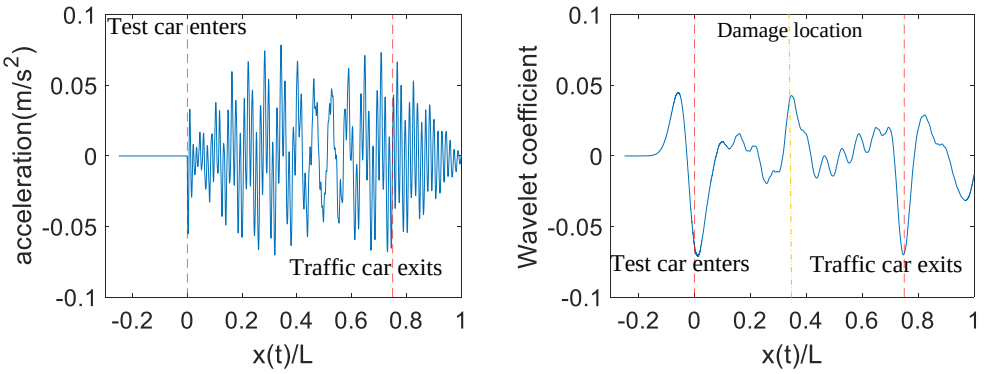

(a) (b)

Figure 15. WET on indirect measurement with traffic. a) Vehicle acceleration, (b) wavelet coefficient.

4.3 Application of WET to Half-car model

To further investigate the fidelity of the proposed WET on damage detection, a theoretical half-car model is adopted to represent the behavior of the vehicle as shown in Figure 16. This half-car model has four independent degrees of freedom, which correspond to vehicle body sprung mass bounce displacement, u_s, sprung mass pitch rotation, θ, and two tires displacement, u_{aR} and u_{aF}, respectively. The vehicle body mass is represented by the sprung mass, m_s and its moment of inertia is represented as, I_s. The vehicle body connects to the tire via a combination of spring of linear stiffness k_R or k_F and viscous dampers with damping coefficient, C_R or C_F. m_{aR} and m_{aF} represent tire mass of each axle and these masses contact to the road surface via springs of linear stiffness k_T. D1 and D2 represent the distance of each axle to the vehicle's center of gravity, respectively. All of those instrumented vehicle properties are listed in Table 2.

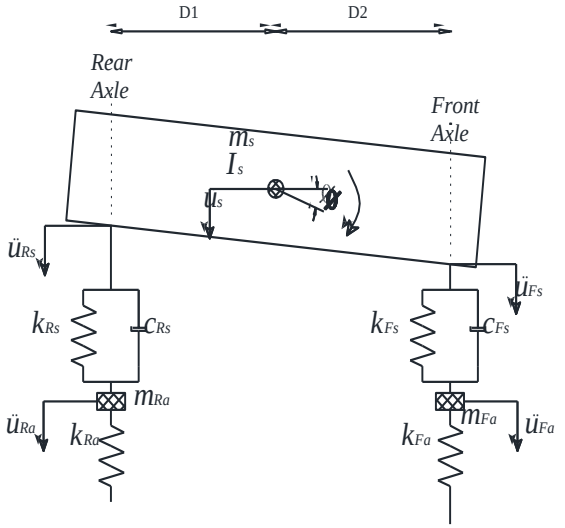

Figure 16. Half-car model

Table 2. Parameters of half vehicle model

Vehicle properties			
m_s	16600 kg	I_s	95765 kg m^2
k_R	400 kN/m	k_F	400 kN/m
c_R	8 kN s/m	c_F	8 kN s/m
m_{aR}	700 kg	m_{aF}	700 kg
k_T	1750 kN/m	k_F	1750 kN/m
D2	1.05m	D1	1.95m

The bridge properties are kept the same with the previous case, where the damage is still set at 0.35L at level 0.5. Figure 17 (a) shows the bridge mid-span acceleration when the half-car moved through the bridge with a constant speed of 2.5 m/s. The x-axis shows the normalized position of the vehicle rear axle on the bridge with respect to the bridge length. To detect the bridge damage, the proposed WET approach is applied to these signals. The optimum scale providing the minimum Shannon entropy value, is achieved as 438, and the corresponding wavelet coefficient is illustrated in Figure 17 (b). Similar to multiple vehicles, when vehicle axle arrives/leaves the bridge, it also introduces a discontinuity into bridge acceleration response. The wavelet coefficient still shows a small peak happened when the real axle passes over the bridge damage location. Principally, there are should be two peaks caused by two axles, when they are passing over the damaged area. The main reason may be that the weight of the front axle is much less than the rear one. Therefore,

one more case study is investigated, where let two axles have same the weight, namely D1=D2 in the half-car model. Here the bridge damage location is set at 0.6L with same damage level 0.5. Applying the same approach, the result is shown in Figure 18, where two similar small peaks are presented. One of them is located at 0.6L in the normalized x-axis, while another one is located around 0.45L, namely the locations when the corresponding axle passed over the damaged area.

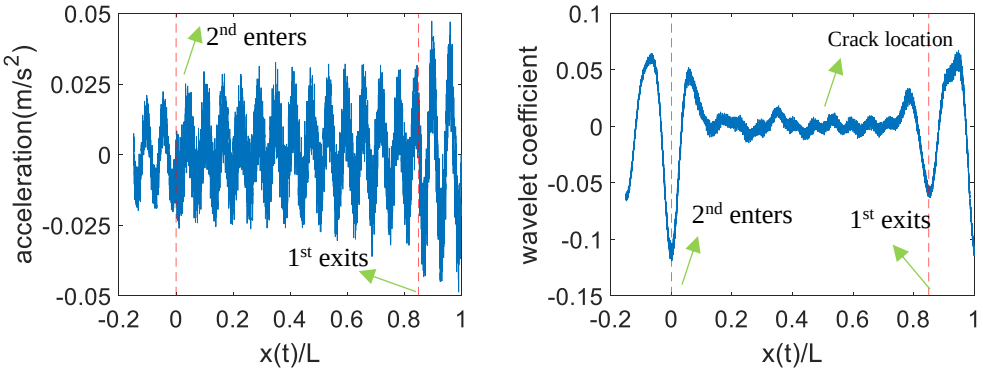

(a) (b)

Figure 17. WET on direct measurement with half-car, (a) bridge mid-span acceleration; (b) wavelet coefficient

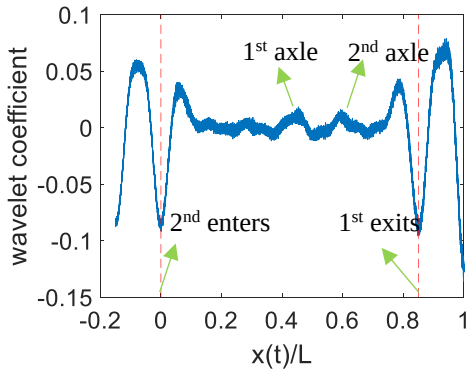

Figure 18. Wavelet coefficient with half-car

The same case of the half-car model with the bridge damage at 0.35L is studied using indirect measurements. The proposed approach is applied to both of two axle's accelerations, and the results are illustrated in Figure 19. The x-axis shows the normalized position of the corresponding axle on the bridge with respect to the bridge length. The optimum scales are 610 and 538 for front and rear axle respectively. Apparently, it is difficult to identify the bridge damage information from the front axle result. While the result of rear axle points out a clear peak at damage location. Therefore, it suggests using the rear axle (the more weight one) response as the input signal to detect bridge damage associated with 'drive-by' SHM. As same as the quarter-car result, the wavelet coefficient of axle present better identification, comparing to the one of direct measurement.

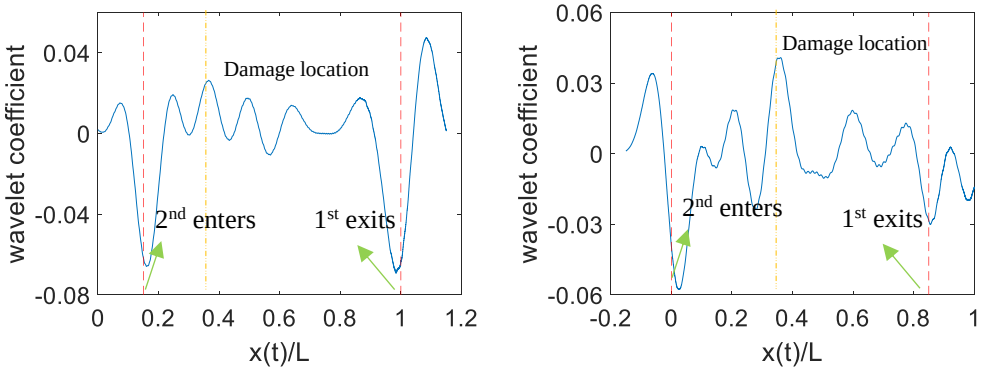

(a) (b)

Figure 19. Wavelet coefficient, (a) front axle, (b) rear axle

5 Parametric Investigation for the fidelity of using WET

To investigate the fidelity of WET, the effect of the vehicle velocity, signal noise,

damage loci and severity are investigated. Only the indirect measurement is utilized in this section. A quantitative indicator will be applied to evaluate the impact of each parameter on the approach sensitivity to damage detection. McGetrick and Kim (2014); Zhu and Law (2006) introduced a damage indicator as:

$$\alpha = \frac{log_2|WT(s,u_d)|}{log_2|WT_o(s,u_d)|} \qquad (6) \qquad (6)$$

Where u_d is the damage location; s_0 represents a particular scale and $WT(s,u_d)$ and $WT_o(s,u_d)$ are the wavelet coefficients for the responses of the damaged and intact states at location u_d, respectively.

This damage indicator needs to be modified for this study for two main reasons. First, in each case the particular scale might be different based on the entropy plot. Second, the peaks in wavelet coefficient plots do not usually present at the same position for each scale. Considering that there is only one major damage to the structure, a damage indicator can be defined as:

$$k = \frac{|WT(s_0,u_{d1})|}{|WT(s_0,u_{d2})|} \qquad (7) \qquad (7)$$

where u_{d1} is the loci of the highest peak location; u_{d2} is the loci of the lowest peak,s_0 represents the scale the provides minimum Shannon entropy, and $WT(s_0,u_{d1})$ and $WT(s_0,u_{d2})$ are their corresponding wavelet coefficients. Greater values for k reflects better identification for the damage.

5.1 Effect of vehicle speed

In this section, only the quarter car is simulated. The damage is kept at 0.35L with the damage level of 0.5. Three speeds are investigated 2.5 m/s 5m/s and 7.5m/s referring

to approximately 10km/h 20km/h and 30km/h. Figure 20 illustrates the optimal wavelet coefficient computed by the application of the proposed WET on axle acceleration records. The wavelet coefficient at the same scale for the undamaged response is also presented in the plots. Increasing the velocity decreases the predictability of the damage (k value). Figure 21 shows the calculated damage indicator "*k*" for different vehicle velocities. With the increase of vehicle velocity, the decreased interaction time causes less information of VBI model. That implies the "moving" sensor has lower resolution allowing damage detection to be located less accurately. It is found that it is difficult to detect damage information when the vehicle velocity is greater than 10 m/s. This conclusion is consistent with McGetrick and Kim (2014); McGetrick and Kim (2013).

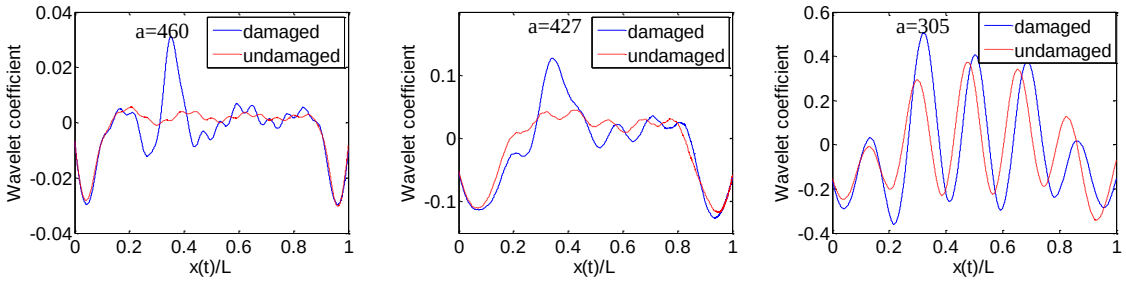

(a) (b) (c)

Figure 20. Particular scale wavelet coefficients of different velocities (a) 2.5m/s, (b) 5m/s, (c) 7.5m/s

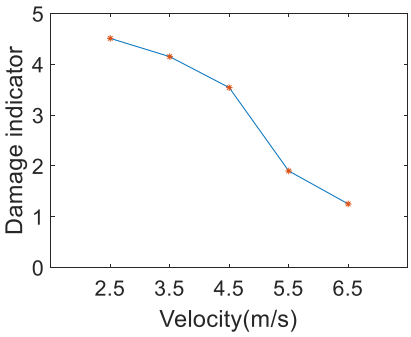

Figure 21. Damage indicator at different vehicle velocities

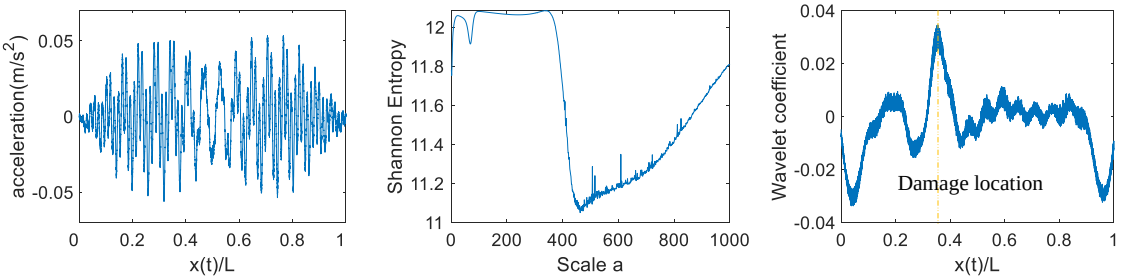

(a) (b) (c)

Figure 22. WET on indirect measurement with 60 dB noise level (a) polluted vehicle acceleration, (b) Shannon entropy, (c) wavelet coefficient.

5.2 Effect of noise

The impact of the noise is investigated by adding a white Gaussian noise to the vehicle responses. First, the signal of Figure 13 (a) was added to 60dB white Gaussian noise as shown in Figure 22 (a). By following the same procedure, the Shannon entropy and wavelet coefficient used to identify the bridge damage is computed and illustrated in Figure 22 (b) and Figure 22 (c), respectively. As it has shown, it still able to localize the bridge damage where it happens at 0.35L.

To further investigate the effect of noise, the signal of Figure 13 (a) has been reproduced by adding different noise intensities and the results are presented in Figure 23. The results reveal that the WET approach is insensitive to low noise contamination. The noise intensity has been increased from 75dB to 45dB with a step of 5dB. The damage indicator has been plotted in Figure 24. As noise intensity increases the approach becomes less sensitive to structural damage. It is found that it is not able to identify bridge damage when the noisy level reaches at 35dB.

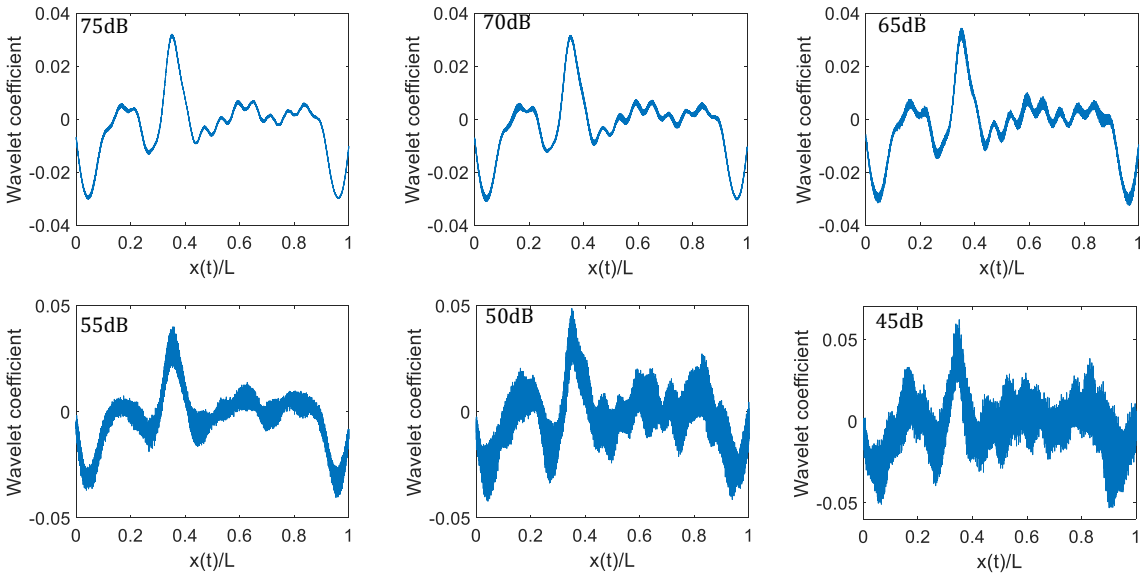

Figure 23. The wavelet coefficients at different noisy levels

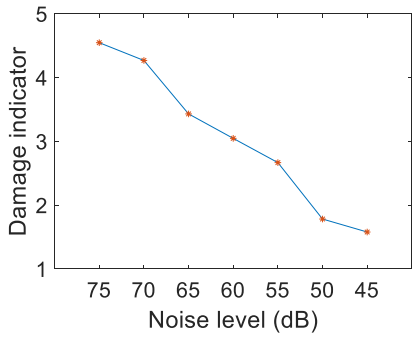

Figure 24. Damage indicator at different noise levels

5.3 Different damage loci and severity

Table 3 shows the values of the damage indicator for different damage locations and severities. The vehicle velocity is kept 5.5m/s for all cases. The damage index improves when the crack depth increases, as well as when the damage moves towards the bridge mid-span. Figure 25 shows wavelet coefficients for different severity levels, where damage is located at 0.4L. The peak of the wavelet coefficient is decreasing by decreasing of damage severity.

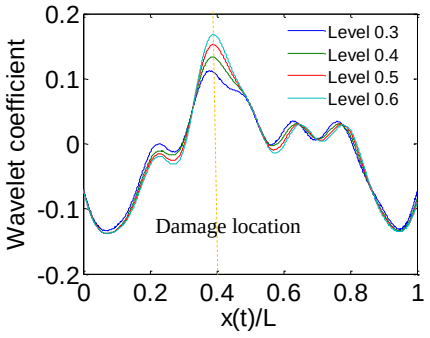

Figure 25. The wavelet coefficients with different damage levels

Table 3. The damage indicator identified at different loci and level

level / Damage loci	0.3	0.4	0.5	0.6
0.3L	1.87	2.26	2.50	2.94
0.35L	2.33	2.90	3.34	3.57
0.4L	3.19	4.33	5.04	5.64
0.45L	3.71	5.22	6.68	8.18

6 CONCLUSIONS

Recently, wavelet analysis has been frequently used to detect structural damage by depicting signal discontinuities from structural dynamic responses. However, there is one major dilemma that halts the merits of this approach, namely the selection of the appropriate wavelet scale. This paper introduces the Wavelet Entropy Theory (WET), which provides a methodology for selecting the optimal Wavelet scale by minimizing the wavelet entropy. The approach is a step towards enhancing many existing wavelet-based damage detection techniques, by introducing a methodology that can identify the wavelet scale that is most sensitive to structural damages. Entropy is referred to as the level of disorder/uncertainty of a set of random data. In the Wavelet Entropy Theory (WET), the entropy of the wavelet analysis at different scales is measured, where the scale that provides the least entropy is the most appropriate wavelet scale to represent the signal. Concurrently, the wavelet function at this scale will be the most sensitive function to any disorder in the signal, in other word structural damages. The measurement fidelity of the WET approach has been first verified using a simple sinusoidal signal. Afterward, the approach has been expanded to a numerical vehicle bridge interaction problem including a quarter-car model

and a half-car model, where the measurements are taken from the bridge (direct measurements), and from the vehicle (indirect measurements). The results reveal a successful identification for the structural damages for the two cases (the direct and the indirect monitoring testbeds), when the SNR values is less than 35dB. However, only smooth profile is investigated in this research work. Future studies might include the effect of the road roughness on the fidelity of the proposed WET method.

ACKNOWLEDGMENT

National Science of Foundation (NSF-CNS-1645863) sponsors this research. Any opinions, findings, and conclusions or recommendations expressed in this publication are those of the authors and do not necessarily reflect the view of the sponsors.

REFERENCES

Blackburn, S. (2005). *The Oxford dictionary of philosophy*, OUP Oxford.

Bulusu, K. V., and Plesniak, M. W. (2015). "Shannon entropy-based wavelet transform method for autonomous coherent structure identification in fluid flow field data." *Entropy*, 17(10), 6617-6642.

Cantero, D., and Basu, B. (2015). "Railway infrastructure damage detection using wavelet transformed acceleration response of traversing vehicle." *Structural Control and Health Monitoring*, 22(1), 62-70.

Cantero, D., McGetrick, P., Kim, C.-W., and OBrien, E. (2019). "Experimental monitoring

of bridge frequency evolution during the passage of vehicles with different suspension properties." *Engineering Structures*, 187, 209-219.

Cebon, D. (1999). *Handbook of vehicle-road interaction*.

Chatterjee, P., OBrien, E., Li, Y., and González, A. (2006). "Wavelet domain analysis for identification of vehicle axles from bridge measurements." *Computers & structures*, 84(28), 1792-1801.

Chen, S.-L., Liu, J.-J., and Lai, H.-C. (2009). "Wavelet analysis for identification of damping ratios and natural frequencies." *Journal of Sound and Vibration*, 323(1-2), 130-147.

de Oliveira, H. M. (2015). "Shannon and Renyi entropy of wavelets." *arXiv preprint arXiv:1502.01871*.

de Oliveira, H. M., and de Souza, D. "Wavelet analysis as an information processing technique." *Proc., Telecommunications Symposium, 2006 International*, IEEE, 7-12.

Deng, L., and Cai, C. (2009). "Bridge model updating using response surface method and genetic algorithm." *Journal of Bridge Engineering*, 15(5), 553-564.

Douka, E., Loutridis, S., and Trochidis, A. (2003). "Crack identification in beams using wavelet analysis." *International Journal of Solids and Structures*, 40(13-14), 3557-3569.

Elhattab, A., Uddin, N., and OBrien, E. (2016). "Drive-by bridge damage monitoring using Bridge Displacement Profile Difference." *Journal of Civil Structural Health Monitoring*, 6(5), 839-850.

Fitzgerald, P. C., Malekjafarian, A., Cantero, D., OBrien, E. J., and Prendergast, L. J. (2019).

"Drive-by scour monitoring of railway bridges using a wavelet-based approach." *Engineering Structures*, 191, 1-11.

Harris, N. K., OBrien, E. J., and González, A. (2007). "Reduction of bridge dynamic amplification through adjustment of vehicle suspension damping." *Journal of Sound and Vibration*, 302(3), 471-485.

Hester, D., and González, A. (2012). "A wavelet-based damage detection algorithm based on bridge acceleration response to a vehicle." *Mechanical Systems and Signal Processing*, 28, 145-166.

Hou, Z., Noori, M., and Amand, R. S. (2000). "Wavelet-based approach for structural damage detection." *Journal of Engineering mechanics*, 126(7), 677-683.

Kailas, S., and Narasimha, R. (1999). "The eduction of structures from flow imagery using wavelets Part I. The mixing layer." *Experiments in Fluids*, 27(2), 167-174.

Kaloop, M. R., and Hu, J. W. (2015). "Stayed-cable bridge damage detection and localization based on accelerometer health monitoring measurements." *Shock and Vibration*, 2015.

Khorram, A., Bakhtiari-Nejad, F., and Rezaeian, M. (2012). "Comparison studies between two wavelet based crack detection methods of a beam subjected to a moving load." *International Journal of Engineering Science*, 51, 204-215.

Kim, H., and Melhem, H. (2004). "Damage detection of structures by wavelet analysis." *Engineering Structures*, 26(3), 347-362.

Liew, K., and Wang, Q. (1998). "Application of wavelet theory for crack identification in structures." *Journal of engineering mechanics*, 124(2), 152-157.

Lu, C.-J., and Hsu, Y.-T. (2002). "Vibration analysis of an inhomogeneous string for

damage detection by wavelet transform." *International Journal of Mechanical Sciences*, 44(4), 745-754.

McGetrick, P., and Kim, C. "An indirect bridge inspection method incorporating a wavelet-based damage indicator and pattern recognition." *Proc., Proceedings of the 9th International Conference on Structural Dynamics (EURODYN'14)*.

McGetrick, P. J., and Kim, C. W. (2013). "A Parametric Study of a Drive by Bridge Inspection System Based on the Morlet Wavelet." *Key Engineering Materials*, 569-570, 262-269.

Nguyen, K. V., and Tran, H. T. (2010). "Multi-cracks detection of a beam-like structure based on the on-vehicle vibration signal and wavelet analysis." *Journal of Sound and Vibration*, 329(21), 4455-4465.

Ovanesova, A., and Suarez, L. E. (2004). "Applications of wavelet transforms to damage detection in frame structures." *Engineering structures*, 26(1), 39-49.

Poudel, U. P., Fu, G., and Ye, J. (2007). "Wavelet transformation of mode shape difference function for structural damage location identification." *Earthquake Engineering & Structural Dynamics*, 36(8), 1089-1107.

Ren, W.-X., and Sun, Z.-S. (2008). "Structural damage identification by using wavelet entropy." *Engineering Structures*, 30(10), 2840-2849.

Rosso, O. A., Blanco, S., Yordanova, J., Kolev, V., Figliola, A., Schürmann, M., and Başar, E. (2001). "Wavelet entropy: a new tool for analysis of short duration brain electrical signals." *Journal of neuroscience methods*, 105(1), 65-75.

Rucka, M., and Wilde, K. (2006). "Application of continuous wavelet transform in vibration based damage detection method for beams and plates." *Journal of Sound*

and Vibration, 297(3-5), 536-550.

Saviotti, P. P. (1988). "Information, variety and entropy in technoeconomic development." *Research Policy*, 17(2), 89-103.

Shahsavari, V., Chouinard, L., and Bastien, J. (2017). "Wavelet-based analysis of mode shapes for statistical detection and localization of damage in beams using likelihood ratio test." *Engineering Structures*, 132, 494-507.

Shannon, C. E. (2001). "A mathematical theory of communication." *ACM SIGMOBILE Mobile Computing and Communications Review*, 5(1), 3-55.

Sinha, J. K., Friswell, M. I., and Edwards, S. (2002). "Simplified Models for the Location of Cracks in Beam Structures Using Measured Vibration Data." *Journal of Sound and Vibration*, 251(1), 13-38.

Tan, C., Elhattab, A., and Uddin, N. (2017). "“Drive-by’’ bridge frequency-based monitoring utilizing wavelet transform." *Journal of Civil Structural Health Monitoring*, 7(5), 615-625.

Tan, C., Elhattab, A., and Uddin, N. "Wavelet Based Damage Assessment and Localization for Bridge Structures." *Proc., 26th ASNT Research Symposium*, 228-240.

Tan, C., Uddin, N., OBrien, E. J., McGetrick, P. J., and Kim, C.-W. (2019). "Extraction of Bridge Modal Parameters Using Passing Vehicle Response." *Journal of Bridge Engineering*, 24(9), 04019087.

Torrence, C., and Compo, G. P. (1998). "A practical guide to wavelet analysis." *Bulletin of the American Meteorological society*, 79(1), 61-78.

Wang, W., Deng, L., and Shao, X. (2016). "Number of stress cycles for fatigue design of simply-supported steel I-girder bridges considering the dynamic effect of vehicle

loading." *Engineering Structures*, 110, 70-78.

Xu, Z.-D., and Wu, Z. (2007). "Energy damage detection strategy based on acceleration responses for long-span bridge structures." *Engineering Structures*, 29(4), 609-617.

Yang, Y.-B., Lin, C., and Yau, J. (2004). "Extracting bridge frequencies from the dynamic response of a passing vehicle." *Journal of Sound and Vibration*, 272(3), 471-493.

Yang, Y. B., and Lin, C. W. (2005). "Vehicle–bridge interaction dynamics and potential applications." *Journal of sound and vibration*, 284(1), 205-226.

Zhu, X. Q., and Law, S. S. (2006). "Wavelet-based crack identification of bridge beam from operational deflection time history." *International Journal of Solids and Structures*, 43(7-8), 2299-2317.

DEVELOPING A REAL-TIME CRACK DETECTOR USING MASK R-CNN TECHNIQUE

by

CHENGJUN TAN
NASIM UDDIN

Submitted to [or In preparation for] *Frontiers of Structural and Civil Engineering*

Format adapted for dissertation

DEVELOPING A REAL-TIME CRACK DETECTOR USING MASK R-CNN TECHNIQUE

Abstract:

Cracks on civil infrastructure surface are one of the earliest indications of degradation of the structure, which is critical for maintenance. The prompt inspection of cracks is to prevent the continuous exposure avoiding the further damages to the environment. In last decades, image-processing techniques have been implemented for detecting cracks from images instead of human-conducted on-site inspections. With increasing size of image datasets and development of technology, machine/deep learning have become a potential method to improve crack detection. This study is to develop a detector using a state-of-the-art technique referred to as Mask R-CNN that can automatically detect cracks from images or videos, which is kind of deep learning. Mask R-CNN technique is a recently proposed algorithm not only for object detection and object localization but also for object instance segmentation of natural images. In this paper, we found that the current Mask-RCNN technique does not perform well on showing instance segmentation of long thin object directly such as cracks, although it works excellent on object detection and object localization. By appropriately adjusting parameters for the decision of instance segmentation, it is able to perform highly effective and efficient automatic segmentation of a wide range of images of cracks, in spite of a wider size of the shape. In addition, it was demonstrated that this proposed automatic detector could work on videos as well; indicating that this detector based on Mask R-CNN provides a robust and feasible ability on detecting cracks exist and their shapes in real time on-site.

Keyword: Deep Learning; Object Detection; Crack; Nondestructive Detection; Instance Segmentation;

1. Introduction

Cracks of civil infrastructures, including bridges, dams, roads, and skyscrapers, potentially reduce local stiffness and cause material discontinuities, so as to lose their designed functions and threaten the public safety (Budiansky and O'connell 1976, Kinra, Ganpatye, and Maslov 2006). This inevitable process signifier urgent maintenance issues. Early inspection and detection can take preventive measures to prevent damage and possible failure (Dhital and Lee 2012). Manual inspection is the most traditional approach for crack inspection, which highly depends on the specialist's knowledge and experience, lacking objectivity in the quantitative. In the manual inspection, the sketch of the crack is prepared manually and the conditions of the irregularities are noted, leading to labor-intensive, time-consuming and even dangerous (Mohan and Poobal 2017, Shi et al. 2016).

For fast and reliable surface defect detection, automatic detection is expected to develop instead of the slower and subjective traditional human inspection. Thereby there is increasing interest in vision-based crack detection using image-processing techniques (IPTs) for non-destructive inspection. IPTs has a significant advantage of that all superficial defects are almost likely identifiable (Cha, Choi, and Büyüköztürk 2017). In early studies, the cracks on a concrete surface generally are considered to possess two key properties i.e. it has low luminance and their structure shape is thinner and different with the other textural patterns (Sankarasrinivasan et al. 2015). According to these

considerations, many threshold-based approaches of IPTs have been proposed to find crack regions such as fast Haar transform, fast Fourier transform, Sobel edge detector, and Canny edge detector (Mohan and Poobal 2017). Fast Haar transform was defined as the best solution for detecting cracks and deterioration of a bridge in a field experiment (Abdel-Qader, Abudayyeh, and Kelly 2003), which was followed by an examination of modified edge detection problems (Nishikawa et al. 2012, Yamaguchi et al. 2008, Sinha and Fieguth 2006).

However, edge detection actually is an ill-posed problem, because the results are substantially affected by the noises with no optimal solution (Ziou and Tabbone 1998). Implementing the de-noising technique is one of an effective method to overcome it. Total variation de-noising (Rudin, Osher, and Fatemi 1992), a well-known de-noising approach, is able to reduce noises from images and improve edge detectability of images, which was applied to the study (Cha, You, and Choi 2016) conducted to detect loosened bolts from recorded images. Although this technique indeed improves the results of identification, the usage of such contextual (i.e. using prior knowledge) makes the feasibility limited (Cha, Choi, and Büyüköztürk 2017). In practice, random shape and irregular size of cracks and various noises such as irregularly illuminated condition, shading, blemishes and concrete spall in the acquired images under real-world lead to IPTs hardly adapted extensively.

One potential solution with more real-world adaptability is using machine/deep learning (LeCun et al. 1998). Several machine-learning based techniques have been proposed for detecting cracks from images (Jiang and Adeli 2007, Liu et al. 2002). With increasing size of image datasets and development of technology, machine-learning based methods have been becoming increasingly research focuses on detecting cracks from

images (Shi et al. 2016, Cha, Choi, and Büyüköztürk 2017, Lin, Nie, and Ma 2017, Yokoyama and Matsumoto 2017, Butcher et al. 2014, Cord and Chambon 2012, Lee and Lee 2004). Shi et al. (2016) applied a structured random tree to learn crack characteristic from a series of tokens learned from a manually labeled image database. They introduced a method to apply the integral channel features to redefine the tokens that constitute a crack and get a better representation of the cracks with intensity inhomogeneity. Then a structured random tree learn cracks characteristic from these redefined tokens and to be developed as an automatic detector, which shows advantages on detecting cracks than the threshold-valued based methods in the aspect of noises interference. However, it cannot work on video datasets so far.

Recently, image-processing algorithms based on convolutional neural networks (CNNs) have led to dramatic advances in computer vision for feature extraction (He et al. 2016). This feature extraction technique based on CNN have been adopted to learn the cracks features and then detect them (Yokoyama and Matsumoto 2017, Cha, Choi, and Büyüköztürk 2017). However, cracks in real-world situations vary extensively leading to learning hardly at the global view, meaning that both procedures of crack characteristic learning and detection are based on small tokens (small piece pixel) as mentioned above rather than a whole picture. The sliding window technique was applied to help detect cracks on the entire picture. Strictly speaking, these approaches only use CNN to classify crack or uncrack via every small piece pixel of a picture, rather than detect cracks location and the shape of recognized cracks directly at a global view.

In this study, we investigate to develop an automatic crack detector using state-of-the-art technique of Mask R-CNN to detect crack from image datasets. Mask R-CNN

technique is a recently proposed algorithm for object detection, object localization, and object instance segmentation of natural images (He et al. 2017). Not only can this technique detect the crack exist but also show out the crack location with a bound box. Furthermore, it is able to provide the shape of detected crack with a global view directly. In addition, this technique will be applied to video datasets to implement the task of detecting cracks. This research's content is described as follow. Section 2 presents the related work to proposal technique. Section 3 introduces the methodology of proposal technique. Section 4 presents the application including data preparation and results. Section 5 concludes this article and gives further work.

2. Related work

CNN: A convolution neural network is a typical machine learning method especially for image recognition. By convolution, it is possible to extract every feature of images. Figure 1 shows the key architectures of CNN, which mainly includes convolution layer, activate layer, pooling layer, fully connected layer and softmax layer. The convolution process performs the convolution of features. Patten in images is to be detected by the convolution of the feature, where is automatically acquired by training/learning. Output of each convolution process is called feature map. For more mechanisms of abovementioned layers, here refer readers to references (Yokoyama and Matsumoto 2017, Wu 2017). Recently, "very deep" CNNs have significantly improved image feature extraction and image classification (Krizhevsky, Sutskever, and Hinton 2012). For

example, the popular deep CNNs architectures ResNet-50 and 101 have shown the advantages in training speed and detection accuracy (He et al. 2016).

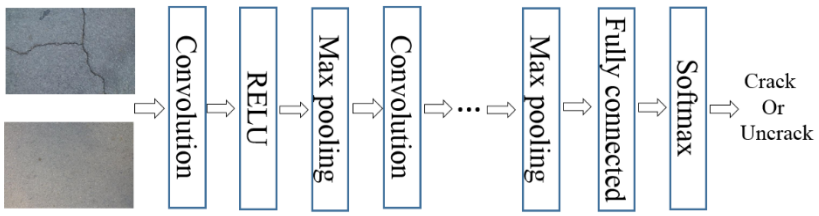

Figure 1. Convolution neural network

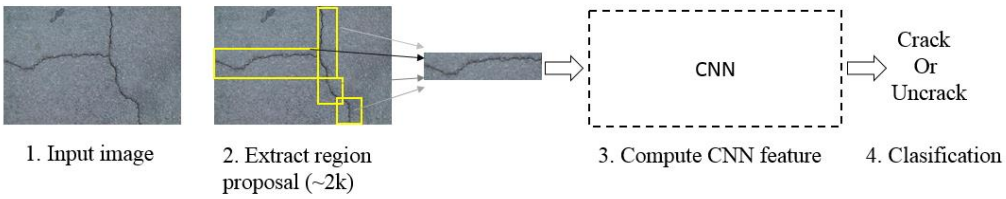

Figure 2. Conventional R-CNN system overview

R-CNN: In Comparison to image classification, object detection from images is a more challenging task that requires more complex methods to solve. R-CNN is one of the most basic models for implementing object detection (Girshick et al. 2014). Figure 2 illustrates the workflow chart of conventional R-CNN. A region proposal method such as *selective search (SS)* and *edge boxes(EB)* (Girshick et al. 2014, Uijlings et al. 2013) will be applied on input images to extract around 2000 bottom-up region proposals, and then each region of interest (ROI) is computed feature with CNN. Apparently, compared to CNN, the only change of R-CNN is to repeat the convolution on each ROI instead of the only input entire image. Therefore, conventional R-CNN has notable drawbacks: (1)

training is a multi-stage pipeline; (2) training is expensive in space and time; (3) object detection is slow (Girshick 2015).

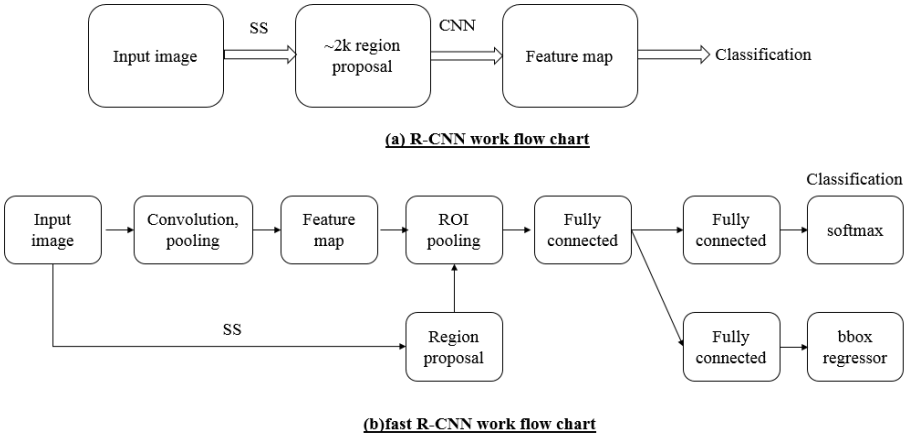

Figure 3. Workflow chart

Fast R-CNN: In order to overcome the drawbacks in conventional R-CNN for object detection, a fast R-CNN model was developed (Girshick 2015). The most important change compared to R-CNN is that fast R-CNN makes region proposal after obtaining feature map with CNN, which are connected each other by adopting a ROI pooling layer as shown on Figure 3. This eliminates the need for a separate CNN forward step for all areas of input images (Girshick 2015). In addition, fast R-CNN uses a multi-task loss function adding a loss function of the bound box (bbox), which is able to determine and refine the final bound for the detected object. The Fast RCNN method shows several advantages over conventional R-CNN: (1) no disk storage is required for feature caching; (2) higher detection quality; (3) training can update all network layers; (4) training is single-stage, using a multi-task loss (Girshick 2015).

RPN: Although fast R-CNN has made a breakthrough on object detection of images, it is also essential to use a region proposal method to extract ROI, exposing region proposal computation as a bottleneck. To solve this problem, a *Region Proposal Network* (RPN) that shares full-image convolutional features with the detection network, thus enabling nearly cost-free region proposals, was introduced by Ren et al. (2015). An RPN is a lightweight neural network that scans the image in a sliding-window fashion and finds areas that contain objects, which simultaneously predicts object bounds and object scores at each position. This is to say that RPNs are trained end-to-end to generate high-quality region proposals, which can be used by Fast R-CNN for object detection (Ren et al. 2015).

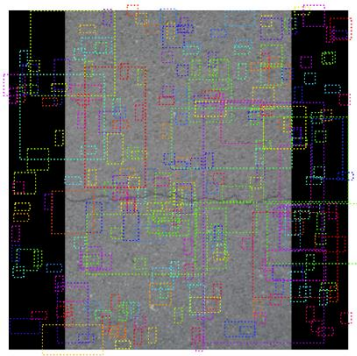

Figure 4. Simplified illustration randomly showing some anchor boxes

The regions that the RPN scans over are called *anchors*, which are boxes distributed over the image area, as shown in Figure 4. This is a simplified view. Practically, there are around 200K anchors of different sizes and aspect ratios that overlap to cover as much of the input image as possible. Each *anchor* is mapped to a lower-dimensional vector and this vector is fed into two sibling fully connected layers, corresponding to a bound box-regression layer (*reg*) and a box-classification layer (*cls*) respectively (Ren et al. 2015).

Although there are large numbers of anchors, the RPN can scan very fast. Since the sliding window is handled by the convolutional nature of the RPN, which allows it to scan all regions in parallel (on a GPU). Further, the RPN does not scan over the image directly. Instead, the RPN scans over the backbone feature map. This allows the RPN to reuse the extracted features efficiently and avoid duplicate calculations.

Bounding Box Refinement: A proposal anchor (also called positive anchor) might not be centered perfectly over the object. Therefore, the RPN will estimate a certain change in both directions of width and height to refine the anchor box to fit the object better. If several anchors overlap too much, only the one with the highest score of interest object is kept and others will be discarded. After that, the final *proposals* (regions of interest) is created that will be pass to the next stage. Figure 5 illustrates a simple example of bounding box refinement.

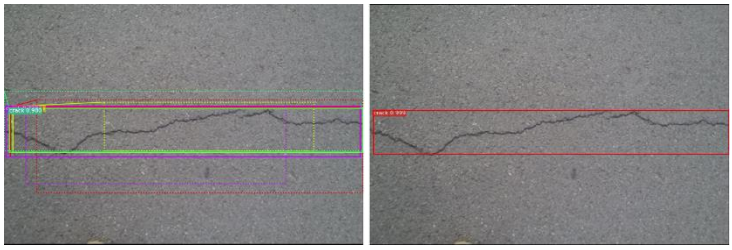

Figure 5. Example of bounding box refinement processing

FPN: fast R-CNN technique adding with RPN technique is referred as a faster R-CNN, which achieves state-of-the-art object detection accuracy and provides a real-time object detector (Ren et al. 2015). However, detecting objects in different scales is still challenging in particular for a small object. A pyramid of the same image at different scale can be utilized to detect object as shown in Figure 6(a). This approach has a notable

drawback that processing multiple scale images is extremely time-consuming and the memory demand is too high to be trained end-to-end simultaneously. Alternatively, a pyramid of feature map can be used for object detection as well, as shown in Figure 6(b). This approach improves the speed for learning and test in object detection to some extent, however, feature maps closer to the image layer composed of low-level structures that are not effective for accurate object detection.

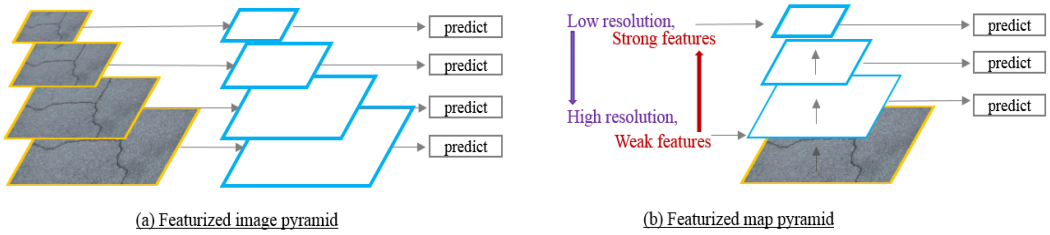

Figure 6. Predict models for object detection in different scales

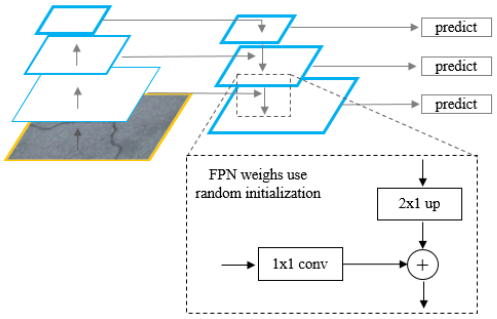

Figure 7. Feature pyramid network

To further improve accuracy and speed in object detection with faster R-CNN, Lin et al. (2017) have developed a feature pyramid network (FPN). FPN improves the standard feature extraction pyramid by adding a second pyramid that takes the high-level features from the first pyramid and passes them down to lower layers (Figure 7). Therefore, it allows

features at every level to have access to both, lower and higher level features. It has concluded that FPN is a practical and accurate solution to multi-scale object detection (Lin et al. 2017). Recently, the faster R-CNN that is a single, unified network for object detection, adds with RPN module performing as the 'attention' of this unified network.

3. Methodology

The Mask R-CNN Model: The Mask R-CNN model was developed by Facebook AI team in 2017 and significantly extends the Faster R-CNN model for object localization, semantic segmentation, and object instance segmentation of natural images (He et al. 2017). It is described as providing a 'simple, flexible and general framework for object instance segmentation' as shown in Figure 8 (Johnson 2018). Mask R-CNN follows the Faster R-CNN model of a feature extractor followed by abovementioned RPN, followed by an operation known as ROI-Pooling to produce standard-sized outputs suitable for input to a classifier, with three important modifications (Johnson 2018). (1) Mask R-CNN replaces the imprecise ROI-Pooling operation applied in Faster R-CNN to an ROIAlign operaion that allows very precise instance segmentation masks to be created. (2) Mask R-CNN adds a network head that is also a small fully convolutional neural network to produce the desired instance segmentations. (3) Mask and class predictions are decoupled, meaning that the mask network head predicts the mask independently from the network head predicting the class (Figure 8). Thereby this Mask R-CNN is to use of a multi-task loss function of $L = L_{cls} + L_{bbox} + L_{mask}$. For additional details, here refer interested readers to reference (He et al. 2017).

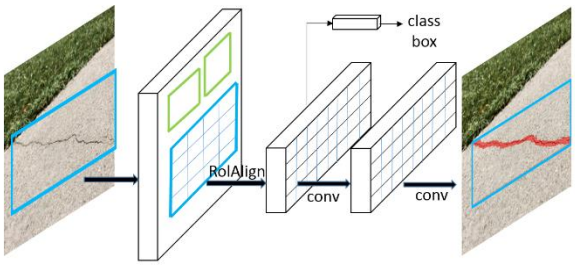

Figure 8. The Mask R-CNN framework for instance segmentation

Mask-RCNN is built on a backbone CNN architecture for feature extraction (Ren et al. 2015, Girshick 2015), which could be any CNN designed for images analysis in principle, such as ResNet-50 or ResNet-101 (He et al. 2016). However, it has been shown that using an FPN based on a network such as ResNet-50 or ResNet-101 as the Mask R-CNN backbone offers benefits in both accuracy and speed (He et al. 2017). Thus, the implementation of Mask R-CNN usually uses a ResNet-50 (or ResNet-101) + FPN as backbone.

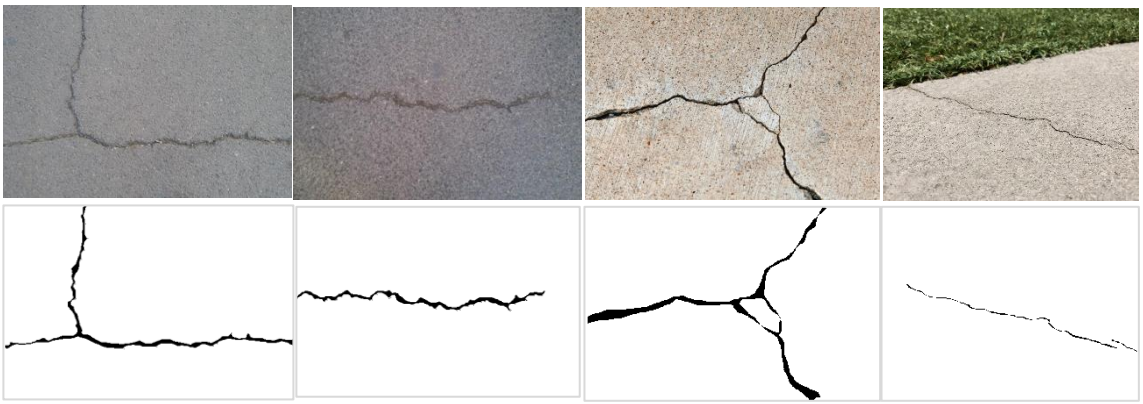

Figure 9. Examples of training images with crack ground truth

Mask R-CNN has been proofed to gain general-purpose object instance segmentation with a large of natural images (He et al. 2017). Although the properties of crack images will generally differ from these natural images, it is a reasonable candidate for use in the automated segmentation of crack images. Here, we investigate the efficacy of a Mask R-CNN model at detecting crack in different images.

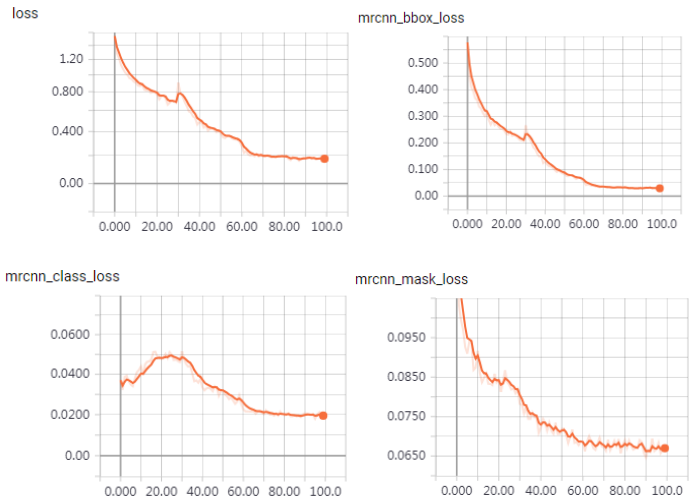

Figure 10. Loss function versus each epoch

4. Application

Dataset: The data used for these experiments consist of 352 crack images and corresponding annotations for crack in each image; 118 crack images and their crack ground truths are from the open resource in reference (Shi et al. 2016). The remaining crack images are randomly downloaded online and their crack ground truths are created manually with Matlab tools (2018b). Of these 352 images in the dataset, 286 images were used for

training; 36 images were used for validating the model and 30 images were held out for testing. Figure 9 illustrates the examples of training images with crack ground truth.

Training: The Mask R-CNN backbone applied in this paper uses a as a "very deep' CNN of ResNet-101 (He et al. 2016) adding with an FPN. The implementation used is based on an existing implementation by Matterport Inc. released under an MIT License, and which is itself based on the open-source libraries Keras and Tensorflow (2017, 2018c, 2018a). For this experiment, rather than training the network end-to-end from the start, we initialize the model using the known weights obtained from pre-training on the MSCOCO dataset (Lin et al. 2014). All CNN layers was trained in three stages: (1) training only the network heads, which are randomly initialized; (2) training the upper layers of the network (from stage 4 and up in the ResNet-101 model); (3) reducing the learning rate by a factor of 10 and training end to end. The total train epochs are 100 using stochastic gradient descent with the momentum of 0.9, starting with a learning rate of 0.001 and ending with a learning rate of 0.0001. We use a batch size of two on a single NVIDIA Tesla P100 16GB GPUs. Gradients are clipped to 5.0 and weights are decayed by 0.0001 for each epoch. To help avoid overfitting, the dataset was augmented using Gaussian blurring, random rotations, and random horizontal and vertical flips. The loss functions are illustrated in Figure 10.

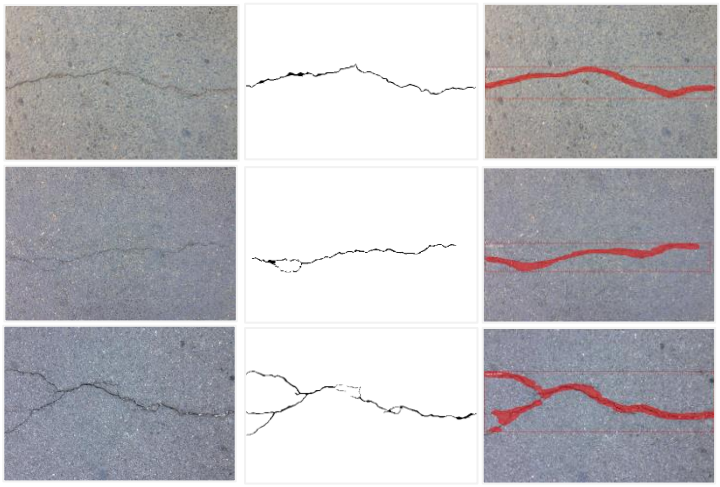

Figure 11. Examples of crack detection on validation images (left: original images; middle: ground truth; right: original images+ identified mask)

Results: We found that this state-of-the-art technique of Mask R-CNN is not able to offer precious instance segmentation with a long thin object such as cracks, although the bound box for object detection can be given accurately. In most cases, the mask (instance segmentation for cracks) was not shown in given model, even detecting the training images. In this proposed method, a threshold value (equal to 0.5) is applied to distinguish "background" (less than that) and "object" (no less than that). However, for the long thin object, it was observed that the computed values (by convolution) referred to its ground truth were usually small, which causes to show nothing on the mask if a high threshold value was still utilized. Therefore, we adjust a smaller threshold value to detect cracks.

After decreasing the threshold value (this paper uses 0.1), the previous training weight was used to detect crack from images. Figure 11 and Figure 12 show the examples of crack detection on validation images and test images, respectively. As they have shown, this technique not only detects the crack exists and location surrounding with a bound box,

but points out the shape of identified crack with a mask (instance segmentation). Although the identified crack mask are mostly fatter than its ground truth, leading to that an average mask intersection over union (IoU) on the validation dataset is very lower only around 0.22, it indeed provides to detect crack effectively and points out its shapes. Actually, the crack exists and location are identified accurately; the average bound box IoU are obtained as high as around 0.81 on the validation dataset. From the Figure 12, it is obvious that this machine/deep learning based crack detector is extremely effective to neglect nature noises of images such as dirt, oil spills, staining, shadow and other interferences. Furthermore, the trained Mask R-CNN model was applied to a video for crack detecting. As expected, it performs the excellent result as well, indicating that this automatic crack detector based on Mask R-CNN is feasible on detecting cracks exist and their shapes in real time on-site.

Figure 12. Examples of crack detection on test images

5. Conclusion & Future Work

In this paper, it was demonstrated that the Mask R-CNN model, while primarily designed with object detection, object localization, and instance segmentation of natural images in mind, can be used to produce high-quality results for the challenging task of crack recognition in widely varying images (videos) with very little modification and a little adjustment on parameter for mask decision. However, the current Mask R-CNN model cannot detect complicated crack well as shown in Figure 13 (top). In addition, as Figure 13 (bottom) shown, it might miss the recognition of certain parts of the image cracks. In this paper, we simply consider the crack as an integrated component of each image in training process, which means that one image possesses only one completely ground truth of integrity crack. Cracks in one image sometimes are even not connected to each other, which should better be separated, indicating that each image should have one or more corresponding ground truth of cracks. Future work will adopt separated crack of one image based on cracks characteristic to improve the efficacy and performance of Mask R-CNN-based models for automatic crack detection.

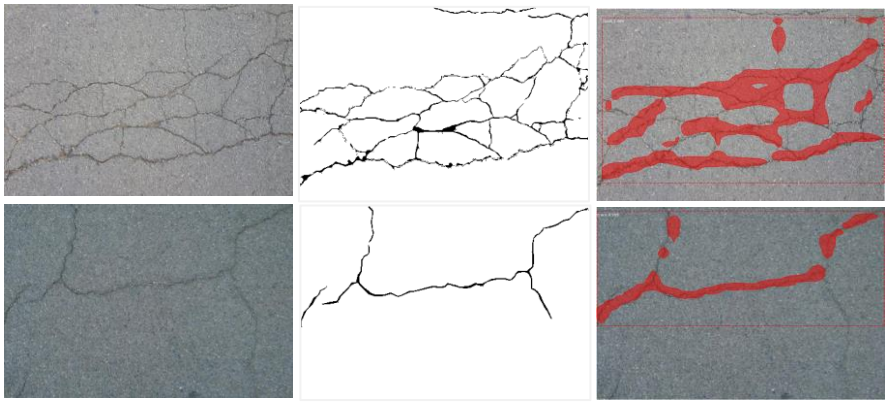

Figure 13. Examples of not very good crack detection (left: original images; middle: ground truth; right: original images+ identified mask)

Acknowledgment

National Science of Foundation (NSF-CNS-1645863) sponsors this research. Any opinions, findings, and conclusions or recommendations expressed in this publication are those of the authors and do not necessarily reflect the view of the sponsors.

REFERENCE

2017. "Mask RCNN." accessed 15 MAR. https://github.com/matterport/Mask_RCNN.

2018a. "Keras." https://github.com/keras-team/keras.

2018b. "Matlab ". https://www.mathworks.com/products/matlab.html.

2018c. "tensorflow ", accessed 15 Mar. https://github.com/tensorflow.

Abdel-Qader, Ikhlas, Osama Abudayyeh, and Michael E Kelly. 2003. "Analysis of edge-detection techniques for crack identification in bridges." *Journal of Computing in*

Civil Engineering 17 (4):255-263.

Budiansky, Bernard, and Richard J O'connell. 1976. "Elastic moduli of a cracked solid." *International journal of Solids and structures* 12 (2):81-97.

Butcher, John B, CR Day, JC Austin, PW Haycock, David Verstraeten, and Benjamin Schrauwen. 2014. "Defect detection in reinforced concrete using random neural architectures." *Computer-Aided Civil and Infrastructure Engineering* 29 (3):191-207.

Cha, Young-Jin, Wooram Choi, and Oral Büyüköztürk. 2017. "Deep Learning-Based Crack Damage Detection Using Convolutional Neural Networks." *Computer-Aided Civil and Infrastructure Engineering* 32 (5):361-378. doi: 10.1111/mice.12263.

Cha, Young-Jin, Kisung You, and Wooram Choi. 2016. "Vision-based detection of loosened bolts using the Hough transform and support vector machines." *Automation in Construction* 71:181-188.

Cord, Aurélien, and Sylvie Chambon. 2012. "Automatic road defect detection by textural pattern recognition based on AdaBoost." *Computer-Aided Civil and Infrastructure Engineering* 27 (4):244-259.

Dhital, D, and JR Lee. 2012. "A fully non-contact ultrasonic propagation imaging system for closed surface crack evaluation." *Experimental mechanics* 52 (8):1111-1122.

Girshick, Ross. 2015. "Fast r-cnn." *arXiv preprint arXiv:1504.08083*.

Girshick, Ross, Jeff Donahue, Trevor Darrell, and Jitendra Malik. 2014. "Rich feature hierarchies for accurate object detection and semantic segmentation." Proceedings of the IEEE conference on computer vision and pattern recognition.

He, Kaiming, Georgia Gkioxari, Piotr Dollár, and Ross Girshick. 2017. "Mask r-cnn."

Computer Vision (ICCV), 2017 IEEE International Conference on.

He, Kaiming, Xiangyu Zhang, Shaoqing Ren, and Jian Sun. 2016. "Deep residual learning for image recognition." Proceedings of the IEEE conference on computer vision and pattern recognition.

Jiang, Xiaomo, and Hojjat Adeli. 2007. "Pseudospectra, MUSIC, and dynamic wavelet neural network for damage detection of highrise buildings." *International Journal for Numerical Methods in Engineering* 71 (5):606-629.

Johnson, Jeremiah W. 2018. "Adapting Mask-RCNN for Automatic Nucleus Segmentation." *arXiv preprint arXiv:1805.00500*.

Kinra, Vikram K, Atul S Ganpatye, and Konstantin Maslov. 2006. "Ultrasonic ply-by-ply detection of matrix cracks in laminated composites." *Journal of Nondestructive Evaluation* 25 (1):37-49.

Krizhevsky, Alex, Ilya Sutskever, and Geoffrey E Hinton. 2012. "Imagenet classification with deep convolutional neural networks." Advances in neural information processing systems.

LeCun, Yann, Léon Bottou, Yoshua Bengio, and Patrick Haffner. 1998. "Gradient-based learning applied to document recognition." *Proceedings of the IEEE* 86 (11):2278-2324.

Lee, Byoung Jik, and Hosin Lee. 2004. "Position-Invariant Neural Network for Digital Pavement Crack Analysis." *Computer-Aided Civil and Infrastructure Engineering* 19 (2):105-118.

Lin, Tsung-Yi, Piotr Dollár, Ross Girshick, Kaiming He, Bharath Hariharan, and Serge Belongie. 2017. "Feature pyramid networks for object detection." CVPR.

Lin, Tsung-Yi, Michael Maire, Serge Belongie, James Hays, Pietro Perona, Deva Ramanan, Piotr Dollár, and C Lawrence Zitnick. 2014. "Microsoft coco: Common objects in context." European conference on computer vision.

Lin, Yi-zhou, Zhen-hua Nie, and Hong-wei Ma. 2017. "Structural Damage Detection with Automatic Feature-Extraction through Deep Learning." *Computer-Aided Civil and Infrastructure Engineering* 32 (12):1025-1046. doi: 10.1111/mice.12313.

Liu, Shaw-Wen, Jin H Huang, Jen-Chun Sung, and CC Lee. 2002. "Detection of cracks using neural networks and computational mechanics." *Computer methods in applied mechanics and engineering* 191 (25-26):2831-2845.

Mohan, Arun, and Sumathi Poobal. 2017. "Crack detection using image processing: A critical review and analysis." *Alexandria Engineering Journal*. doi: 10.1016/j.aej.2017.01.020.

Nishikawa, Takafumi, Junji Yoshida, Toshiyuki Sugiyama, and Yozo Fujino. 2012. "Concrete crack detection by multiple sequential image filtering." *Computer-Aided Civil and Infrastructure Engineering* 27 (1):29-47.

Ren, Shaoqing, Kaiming He, Ross Girshick, and Jian Sun. 2015. "Faster r-cnn: Towards real-time object detection with region proposal networks." Advances in neural information processing systems.

Rudin, Leonid I, Stanley Osher, and Emad Fatemi. 1992. "Nonlinear total variation based noise removal algorithms." *Physica D: nonlinear phenomena* 60 (1-4):259-268.

Sankarasrinivasan, S, E Balasubramanian, K Karthik, U Chandrasekar, and Rishi Gupta. 2015. "Health monitoring of civil structures with integrated UAV and image processing system." *Procedia Computer Science* 54:508-515.

Shi, Yong, Limeng Cui, Zhiquan Qi, Fan Meng, and Zhensong Chen. 2016. "Automatic road crack detection using random structured forests." *IEEE Transactions on Intelligent Transportation Systems* 17 (12):3434-3445.

Sinha, Sunil K, and Paul W Fieguth. 2006. "Automated detection of cracks in buried concrete pipe images." *Automation in Construction* 15 (1):58-72.

Uijlings, Jasper RR, Koen EA Van De Sande, Theo Gevers, and Arnold WM Smeulders. 2013. "Selective search for object recognition." *International journal of computer vision* 104 (2):154-171.

Wu, Jianxin. 2017. "Introduction to convolutional neural networks." *National Key Lab for Novel Software Technology. Nanjing University. China*.

Yamaguchi, Tomoyuki, Shingo Nakamura, Ryo Saegusa, and Shuji Hashimoto. 2008. "Image-Based Crack Detection for Real Concrete Surfaces." *IEEJ Transactions on Electrical and Electronic Engineering* 3 (1):128-135.

Yokoyama, Suguru, and Takashi Matsumoto. 2017. "Development of an Automatic Detector of Cracks in Concrete Using Machine Learning." *Procedia Engineering* 171:1250-1255. doi: 10.1016/j.proeng.2017.01.418.

Ziou, Djemel, and Salvatore Tabbone. 1998. "Edge detection techniques-an overview." *Pattern Recognition and Image Analysis C/C of Raspoznavaniye Obrazov I Analiz Izobrazhenii* 8:537-559.

CONCLUSION, CONTRIBUTION AND FUTURE WORK

Conclusion

This dissertation introduces a new method to extract the natural frequency of bridge from indirect measurements of a passing vehicle, based on wavelet analysis. In compare with FFT, the proposed approach is not restricted to the frequency resolution. The approach has been extended to point out to the frequency drop due to the structural damage. The extracted bridge frequencies using the proposed wavelet approach show a drop in its magnitude as the damage extent increases. However, the value of the extracted frequency did not show a good agreement with the theoretical bridge frequency. In contrast, FFT did not show any evidence for damage in the acceleration spectrum. The same results have been found for higher modes of vibrations (2^{nd} mode). The paper examined the sensitivity of the proposed approach to road roughness profile. In this regard, a Half-Car model with two axles has been utilized, and the signal of the axles have been subtracted with time lag to damp out the road roughness effect on the recorded signal. The subtracted acceleration has been processed using the proposed method and the results shows good agreement between the extracted and theoretical bridge frequencies. The approach has strong potential to provide a quick estimation for the bridge health condition.

This dissertation introduces a new approach combined with HT and band-pass filter technique to improve the bridge natural frequency identification from a passing vehicle. The proposed approach improves the identified frequency iteratively, where the initial value can be achieved by applying FFT directly. In contrast to FFT, the proposed approach is not restricted to the frequency resolution. Hence, this paper preliminarily found that the

proposed approach is able to detect the frequencies drop due to the bridge structural damage. In this regard, it is a promising way to estimate bridge conditions. However, the observed drop is very small in addition to the environment effect, which may limit the effectiveness of the proposed approach to structural damage detection. Nevertheless, it has shown improved identification of bridge frequencies over than FFT, without limitation to resolution. In addition, the proposed approach is not sensitive to vehicle velocity and signal noise.

This dissertation proposes an algorithm to extract bridge modal parameters, with a focus on damping ratio and mode shapes, using the dynamic response of a passing vehicle. The Hilbert Transform is applied to the filtered signals. The feasibility of the concept is established through theoretical analysis, numerical simulation and laboratory experiments. It is demonstrated that the proposed algorithm is greatly improves the extracted mode shape over the algorithm presented by Yang et al. A key limitation of the proposed algorithm at this time is a requirement for the vehicle to have a low and constant speed. Besides, the high bridge damping generates a strong edge-effect of the extracted mode shapes, negatively affecting the accuracy of the proposed algorithm. In the simulations, it is found that an increase in vehicle speed decreases the precision of the extracted results. The proposed algorithm is also shown to be capable of extracting the modal parameters of the second mode shape with relatively good precision. In addition, it is found that although the band-pass filter can partially remove the random vibration caused by the road roughness, the road roughness with Class A, i.e., roughness condition of ‘very good’ has negative impact on the proposed algorithm, especially for the higher modes. The laboratory experiments provide further evidence of the potential of the proposed algorithm. It

accurately identifies the bridge damping so as to detect the first increase of that, only using one sensor installed on instrumented vehicle. It is concluded that the proposed algorithm is able to detect the change of bridge damping ratio and higher accuracy mode shapes, and has potential for application in the use of indirect measurement to monitor bridge health.

Recently, wavelet analysis has been frequently used to detect structural damage by depicting signal discontinuities from structural dynamic responses. However, there is one major dilemma that halts the merits of this approach, namely the selection of the appropriate wavelet scale. This paper introduces the Wavelet Entropy Theory (WET), which provides a methodology for selecting the optimal Wavelet scale by minimizing the wavelet entropy. The approach is a step towards enhancing many existing wavelet-based damage detection techniques, by introducing a methodology that can identify the wavelet scale that is most sensitive to structural damages. Entropy is referred to as the level of disorder/uncertainty of a set of random data. In the Wavelet Entropy Theory (WET), the entropy of the wavelet analysis at different scales is measured, where the scale that provides the least entropy is the most appropriate wavelet scale to represent the signal. Concurrently, the wavelet function at this scale will be the most sensitive function to any disorder in the signal, in other word structural damages. The measurement fidelity of the WET approach has been first verified using a simple sinusoidal signal. Afterward, the approach has been expanded to a numerical vehicle bridge interaction problem including a quarter-car model and a half-car model, where the measurements are taken from the bridge (direct measurements), and from the vehicle (indirect measurements). The results reveal a successful identification for the structural damages for the two cases (the direct and the indirect monitoring testbeds), when the SNR values is less than 35dB. However, only

smooth profile is investigated in this research work. Future studies might include the effect of the road roughness on the fidelity of the proposed WET method.

This dissertation proposes an algorithm to detect bridge damage using the extracted mode shape from a passing vehicle. The mode shape is extracted using Hilbert Transform. The feasibility of the concept is established through theoretical analysis, numerical simulation and laboratory experiments. In both simulations and experiment, high vehicle speed is found to have a negative effect on the accuracy of the extracted mode shape. In the paper, different kinds of damage – local and global are investigated in the experiment, which are represented by decreasing the stiffness of beam or foundations, respectively. For any damage types, the used damage index, to some extent, can not only localize damage but also reflects the damage level. Besides, it is suggested that averaging several runs is necessary to localize damage and reflect damage level accurately.

In this dissertation, we developed an effective and fast automatic crack detector based on Mask R-CNN, which can suppress noises efficiently by learning inherent feature of cracks from a 'very deep' CNN. Comparing to only CNN based method working on small batch of images, it can detect the crack of images in a global view providing a bound box for the crack exist and location. Moreover, This Mask R-CNN based crack detector outputs mask for predicted cracks simultaneously displaying the shape of cracks. Because Mask R-CNN can compute very fast on GPUs, the proposed crack detector performs excellent on video dataset, which make it feasibility to become a real-time crack detector on site equipped to the advanced UAVs. Furthermore, the comparative studies give evidence on that machine/deep learning based method is more effective to extract the

feature of images in suppressing nature noises of images. In these studies, the proposed method yields state-of-the-art accuracy.

Contribution

(1) Develop a new way of bridge frequency identification based on wavelet coefficients energy in 'drive-by' inspection, which is not restricted to frequency resolution, so as to detect the bridge frequency drop caused by any damages.

(2) Propose an algorithm identifying bridge frequency iteratively removing the effect of vehicle velocity, utilizing HT and band-pass filter technique.

(3) Propose an algorithm to extract bridge modal parameters, with a focus on damping ratio and mode shapes, using the dynamic response of a passing vehicle.

(4) Consider the bridge damping effect on the 'drive-by' bridge inspection, and derive the single component of bridge frequency mode shape from a vehicle acceleration.

(5) Detect the bridge damage with different kinds of damage – local and global, using the extracted mode shape from a passing vehicle.

(6) Conduct lab experiments to verify the feasibility of bridge damage detection algorithms.

(7) Propose Wavelet Entropy Theory (WET) to provide a methodology for selecting the optimal Wavelet scale by minimizing the wavelet entropy, in the application of bridge damage detection with both direct and indirect measurements.

(8) Develop an effective and fast automatic crack detector based on Mask R-CNN, which can suppress noises efficiently by learning inherent feature of cracks from a

'very deep' CNN.

Future work

(1) Develop an algorithm to detect the bridge global damage based on wavelet analysis.

(2) Compare different techniques to extract the bridge single component mode shape information from a passing vehicle acceleration, such as band-pass filter, singular spectrum analysis, stochastic resonance and wavelet analysis.

(3) Develop CNN-based algorithm to detect the global damage using the 'drive-by' inspection, based on the lab experiment data.

(4) Find the best sensor location for 'drive-by' inspection (installed on axle or vehicle body).

(5) Further investigate the road roughness effect on 'drive-by' inspection through lab experiment.

(6) In this dissertation, we simply consider cracks as an integrated component of each image in the training process, which means that one image possesses only one completely ground truth of integrity crack. Cracks in one image sometimes are even not connected to each other, which should better be separated, indicating that each image should have one or more corresponding ground truth of cracks. Future work will adopt separated crack of one image based on cracks characteristic to improve the efficacy and performance of Mask R-CNN based automatic crack detection.

ACKNOWLEDGMENTS

I would like to express my deepest gratitude to Professor Nasim Uddin, my Super advisor and Committee Chair, who has always supported my career goals and actively provided me with guaranteed academic time to achieve these goals. I am grateful to all of my Dissertation committee members, Dr. Hosch, Dr. Waldron, Dr. Haider and Dr. Ashraf, who have provided me with a wide range of personal and professional guidance and taught me a lot about scientific research and life. In addition, thanks to Professor Eugene J. OBrien of the University of Dublin, Ireland, who provided me with laboratory experimental data and reviewed my published journal articles.

Nobody has been more important to me in the pursuit of this project than the members of my family. I would like to thank my parents, whose love and guidance are with me in whatever I pursue. They are the ultimate role models. Most importantly, I wish to thank my loving and supportive wife, Yihua Wen, who provide unending inspiration.